An Investigation of the Destabilization, Aggregation, and Deposition of Asphaltenes

by

Cláudio Vilas Bôas Fávero

A dissertation submitted in partial fulfillment
of the requirements for the degree of
Doctor of Philosophy
(Chemical Engineering)
in The University of Michigan
2018

Doctoral Committee:

Professor H. Scott Fogler, Chair
Professor Joerg Lahann
Professor Ronald G. Larson
Professor Margaret Wooldridge

Cláudio Vilas Bôas Fávero

cfavero@umich.edu

ORCID iD: 0000-0001-9708-3401

To the memory of my grandmother Maria, my godmother Fátima, and my uncle Roberto

Acknowledgment

First and foremost, I would like to thank my advisor Professor H. Scott Fogler for the opportunity to work with him and to pursue my graduate studies in his research group. With Professor Fogler I learned how to be precise, how to be concise, and how to think critically. These skills were essential for me to write this dissertation, interact with research sponsors, teach, to name a few things, and it will surely make a difference in my professional life after graduating. As a member of Professor Fogler's research group, I was not only given the opportunity to conduct the research to write this dissertation but also, I was given the opportunity to acquire skills that go beyond those that are required to obtain a doctorate degree. I cannot thank Professor Fogler enough for all the learning opportunities that he has provided to me these years.

I also would like to thank the members of my doctoral committee, Professor Joerg Lahann, Professor Ronald Larson, and Professor Margaret Wooldridge for their contributions in my dissertation. In special I would like to thank Professor Larson. I had the opportunity to have Professor Larson as Instructor for a fluid dynamics course in my first year of graduate school. His class taught me more than fluid dynamics. In his class, I learned how to combine imagination and physical reasoning to tackle the problem at hand. I am very thankful for having acquired this skill early in my PhD.

When conducting the research presented in this dissertation, I had the opportunity to work a number of students in the Fogler group. Each student contributed to my growth, personal or professional, and I will be always thankful for it.

During my graduate studies I also had the chance to work with my colleagues from the department. It started with the core courses in my first year in graduate school and the long nights at the library to work on homework and class projects, then with organizing recruitment events, starting the peer mentoring program for incoming students, and so on. These situations created memories and established friendships for life.

My parents, my family, and my friends I thank for supporting me on my choices in life. Particularly, I want to mention my grandmother Maria, my godmother Fatima, and my uncle Roberto. This dissertation is dedicated to their memory. I like to think that somehow, they can experience through me everything they have missed in their way-too-short life.

And finally, I thank my partner Zhilin. It is his smile that I look forward to seeing after a long day of work. Life in graduate school can be great, but with him it is splendid. In him I find my best friend and my partner for life.

Cláudio Vilas Bôas Fávero

Ann Arbor, 2018

Table of Contents

List of Tables

List of Figures

List of Appendices

Abstract

Asphaltenes are a class of molecules in crude oil that are soluble in aromatic solvents, such as toluene, and insoluble in n-alkanes, such as heptane. The amount of asphaltenes that is destabilized and the rate of aggregation of the destabilized asphaltenes increases as the volume fraction of n-alkane in oil increases. In the oil field, as pressure of oil decreases there is an increase in the volume fraction of n-alkane, such as methane, causing asphaltenes to destabilize and deposit in the pore space of reservoir and on the walls of pipelines and production equipment. In this dissertation, a mechanistic study of asphaltene deposition as well as investigation on asphaltene destabilization and aggregation are presented. For the first time, experimental results of asphaltene deposition from crude oil of different origins and different chemical compositions were obtained and used to validate the diffusion-limited deposition model. The effect amphiphilic molecules on asphaltene destabilization and deposition was also investigated. The dissolution of solid asphaltenes in solvents were measured and results are briefly discussed.

In the study of asphaltene deposition, a new apparatus was designed and built to measure rates of asphaltene deposition. This apparatus consists of a glass column packed with stainless steel beads over which oil-heptane mixture is flown. It was found that only the unstable asphaltenes can form a multi-layer deposit on the surface of the beads. As asphaltene precipitate and grow in size from nano to micro-meter, the micro-meter sized particles tend to flow through the packed bed without depositing. For the case of unstable asphaltenes in the nano-meter size in oil-heptane mixture under Stokes flow, a single deposition mechanism, a diffusion-limited process, is able to explain the deposition of asphaltenes from crude oils of different origins. The validity of deposition

mechanism was not verified for other geometries, such as a pipe geometry. Additionally, the diffusion-limited deposition mechanism cannot explain the deposition process observed for inertial flow regime (Re > 1), when the deposition rate decreases as fluid flow velocity increases. Addition of amphiphilic compounds, namely dodecylbenzene sulfonic acid and dodecylphenol, to oil can result in either an increase or decrease of amount of asphaltenes depositing, depending on the crude oil and on the functional group of the amphiphile.

The stability of asphaltenes extracted from different crude oils to form model oils was investigated using measurements of asphaltene detection times. The experimental results show that when asphaltenes from different crude oils are fractionated under same conditions, i.e., same heptane concentration and oil-heptane contact time, the model oil of these fractions will have identical detection times curves. These fractions of same detection time curves were found to have different chemical composition in terms of hydrogen, carbon, and nitrogen content. Further characterization of these fractions could help relate asphaltene stability to asphaltene molecular properties and perhaps reveal the mechanism of asphaltene destabilization by n-alkanes. This study of asphaltene destabilization, aggregation and deposition reinforces the concept that there is no such thing as an "onset concentration" of asphaltene precipitation.

CHAPTER I

Introduction

Production of crude oil petroleum is often hindered by fouling of pipelines caused by asphaltenes[1]. Asphaltenes are molecules in crude oil that can be dissolved in aromatic solvents, such as toluene, and that will precipitate in presence of n-alkanes, such as methane and n-heptane[2], [3]. They have a moderately high molecular weight containing both aliphatic and aromatic carbons [4] and associate into nanometer-sized colloidal particles and clusters [5].

The process by which asphaltenes destabilizes is not fully understood. There is evidence that indicates that asphaltene clusters are stabilized by steric repulsion forces[6], [7] that exist due to the alkyl chains that stick out of the asphaltene clusters. These alkyl chains contract when immersed in n-alkanes, resulting in a decrease of repulsion forces between asphaltenes leading to asphaltene destabilization and aggregation. Once destabilized, asphaltenes can grow in size and they can also form multi-layered deposits on surfaces [8]. Assessing the risk of asphaltene deposition for a given crude oil at given production condition has central role in flow assurance engineering[3].

The main goal of the investigations presented is to understand the process of asphaltene destabilization and aggregation in oil-heptane mixtures and to reveal the mechanism by which asphaltenes deposit on surfaces. The findings of this research are presented in five chapters and a brief description of the content of each chapter can be found below.

Chapter II. This chapter synthesizes the work in our and other laboratories on the kinetics of asphaltene destabilization and aggregation. The content of this chapter was published in the journal of Advances in Colloid and Interface Science [9]. Four different experimental techniques

were used to study asphaltenes undergoing aggregation process in crude oils and model oils. The techniques are (1) detection time of asphaltene aggregation, (2) centrifugation of asphaltenes, (3) small angle neutron scattering, and (4) asphaltene deposition in capillaries. The asphaltenes were destabilized by different n-alkanes and a geometric population balance with the Smoluchowski collision kernel was used to model the asphaltene aggregation process. Additionally, by postulating a relation between the aggregation collision efficiency and the solubility parameter of asphaltenes and the solution, a unified model of asphaltene aggregation model was developed. When the aggregation model is applied to the experimental data obtained from several different crude oil and model oils, the detection time curves collapsed onto a universal single line, indicating that the model successfully captures the underlying physics of the observed process.

Chapter III. This chapter investigates the stability of asphaltenes and fractions of asphaltenes. The stability is measured using the detection time of asphaltene destabilization. It is shown that when asphaltenes from different crude oils are fractionated under same conditions, i.e., heptane concentration and oil-heptane contact time, the model oil of these fractions will have identical detection time curves. Important implications of these findings on the behavior of asphaltenes in solution are discussed in this chapter.

Chapter IV. This chapter describes our research on the rate of dissolution of solid asphaltenes in solvents. It was found that the dissolution rate of asphaltenes depends both on the origin of asphaltenes and on the solvent in which asphaltenes are dissolving. A discussion on the relationship between the rate of dissolution and the solubility parameter of asphaltenes is provided.

Chapter V. This chapter is reproduced from our article in Energy and Fuels [8] and describes a mechanistic investigation of asphaltene deposition. For this investigation, a new deposition apparatus was designed and constructed to investigate asphaltene deposition. The

apparatus consists of a packed bed of stainless steel beads over which a mixture of oil and heptane is passed at a specified flow rate and run-time. The asphaltene deposition rate and the mass of deposit can be obtained along the packed bed. The dependency of the asphaltene deposition rate on concentration of unstable asphaltenes and on fluid flow velocity was studied. An analysis of the experimental results is presented, showing that a diffusion-limited deposition model can explain the asphaltene deposition of nanometer-sized unstable asphaltenes in the viscous flow regime.

Chapter VI. This chapter discusses the effect of amphiphilic molecules on the kinetics of asphaltene destabilization, aggregation, and deposition. The effect of the functional group, length of alkyl chain, and number of repeating units was studied. Experimental results are discussed, showing that the effect of these amphiphilic molecules on asphaltene destabilization, aggregation and deposition strongly dependent on the crude oil and on the functional group of the amphiphilic molecule.

Chapter VII. The conclusions of the research discussed in Chapters II through VI are presented in this chapter. In addition, the implication of these findings in the research field of flow assurance are discussed.

Chapter VIII. The research findings of this dissertation led to new research questions that presented in this chapter. An approach to answer each of these questions is proposed.

References

[1] J. L. Creek, "Freedom of action in the state of asphaltenes: Escape from conventional wisdom," *Energy Fuels*, vol. 19, no. 4, pp. 1212–1224, 2005.

[2] K. Kraiwattanawong, H. S. Fogler, S. G. Gharfeh, P. Singh, W. H. Thomason, and S.

Chavadej, “Thermodynamic Solubility Models to Predict Asphaltene Instability in Live Crude Oils †,” *Energy Fuels*, vol. 21, no. 3, pp. 1248–1255, May 2007.

[3] J. Creek, J. Wang, and J. Buckley, “Verification of Asphaltene-Instability-Trend (ASIST) Predictions for Low-Molecular-Weight Alkanes,” *SPE Prod. Oper.*, vol. 24, no. 2, pp. 5–8, 2009.

[4] K. H. Altgelt and M. M. Boduszynski, *Composition and Analysis of Heavy Petroleum Fractions*, 1st Editio. CRC Press, 1993.

[5] M. P. Hoepfner, C. Vilas Boas Favero, N. Haji-Akbari, and H. S. Fogler, “The fractal aggregation of asphaltenes,” *Langmuir*, vol. 29, no. 28, pp. 8799–8808, 2013.

[6] S. Wang, J. Liu, L. Zhang, Z. Xu, and J. Masliyah, “Colloidal Interactions between Asphaltene Surfaces in Toluene,” *Energy Fuels*, vol. 23, no. 2, pp. 862–869, Feb. 2009.

[7] S. Wang, J. Liu, L. Zhang, J. Masliyah, and Z. Xu, “Interaction forces between asphaltene surfaces in organic solvents.,” *Langmuir*, vol. 26, no. 1, pp. 183–90, Jan. 2010.

[8] C. Vilas Bôas Fávero, A. Hanpan, P. Phichphimok, K. Binabdullah, and H. S. Fogler, “Mechanistic Investigation of Asphaltene Deposition,” *Energy Fuels*, vol. 30, no. 11, pp. 8915–8921, Nov. 2016.

[9] C. Vilas Bôas Fávero, T. Maqbool, M. Hoepfner, N. Haji-Akbari, and H. S. Fogler, “Revisiting the flocculation kinetics of destabilized asphaltenes,” *Adv. Colloid Interface Sci.*, 2016.

CHAPTER II

Asphaltene Destabilization and Aggregation Kinetics

Published at *Adv. Colloid Interface Sci.,* 2017, vol. 244, pp. 267–280

2.1. Introduction

Production of crude oil petroleum is often hindered by fouling of pipelines caused by asphaltenes. Therefore, it is of industrial interest to be able to predict if asphaltenes from a given oil field will deposits in pipelines.

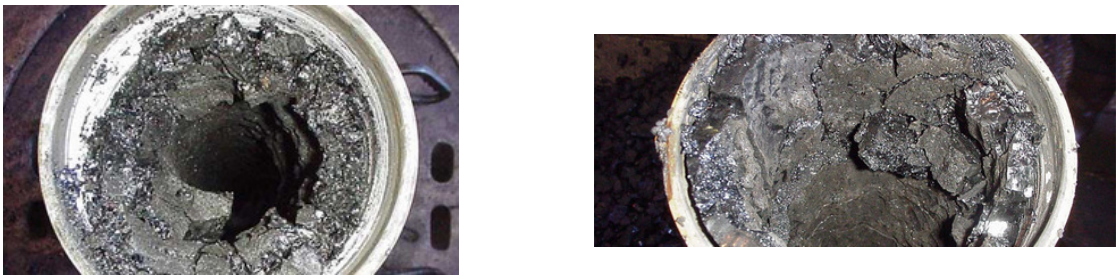

Figure 2.1 – Asphaltene deposits in a pipeline [1]

Asphaltenes are defined as the molecules in crude oil that can be dissolved in aromatic solvents, such as toluene, and that will precipitate in presence of n-alkanes, such as heptane. Asphaltene molecules have a moderately high molecular weight [2] and contains both aliphatic and aromatic carbons [3]. In its natural state, asphaltenes are associated into nanometer-sized colloidal particles and clusters [4].

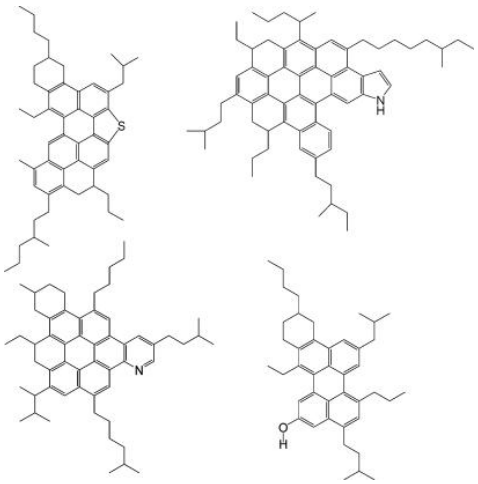

Figure 2.2 – Hypothetical asphaltene molecules [5]

Asphaltenes clusters can be either stable or unstable [4]. Stable clusters are the clusters that will not aggregate upon contact, whereas unstable clusters can aggregate upon contact. The process by which asphaltenes clusters go from a stable to an unstable state is referred to destabilization or precipitation. The process of growth is called flocculation or aggregation. Stable and unstable clusters are also referred to as soluble and insoluble, respectively. The mechanism of asphaltene destabilization is not fully understood. There is evidence that indicates that asphaltene clusters are stabilized by steric repulsion forces that exist due to the alkyl chains that stick out of the asphaltene clusters [6], [7]. These alkyl chains would change their conformation depending on the media they are immersed. In n-alkanes, the alkyl chains would be compressed resulting in low repulsion forces between clusters and therefore maximum aggregation. In toluene, the alkyl chains would be sticking out providing maximum repulsion between clusters and therefore preventing cluster from aggregating.

Asphaltene destabilization is a precursor of asphaltene deposition. Therefore, to assess the risk of deposition in a pipeline one needs to predict if asphaltene destabilization will occur in a pipeline. Asphaltene destabilization occurs as the volume fraction of light n-alkane (e.g., methane

in natural gas) in oil increases in oil depressurization. As the volume fraction of n-alkane in oil increases, the quantity of asphaltenes that precipitates also increases. Further depressurization can lead to light n-alkanes to escape the liquid phase and form a gas phase, resulting in decrease of the volume fraction of n-alkane in the liquid phase and redissolution of asphaltenes.

Risk assessment of asphaltene deposition has been commonly based on the measurements of the lowest volume fraction of n-alkane in oil that asphaltene precipitation can be detected. This lowest volume fraction is often called *onset point*. For volume fractions below the onset point, asphaltenes were assumed to be inheritably stable and therefore would not cause deposition issues. Figure 2.3 shows two examples of *onset point* measurement.

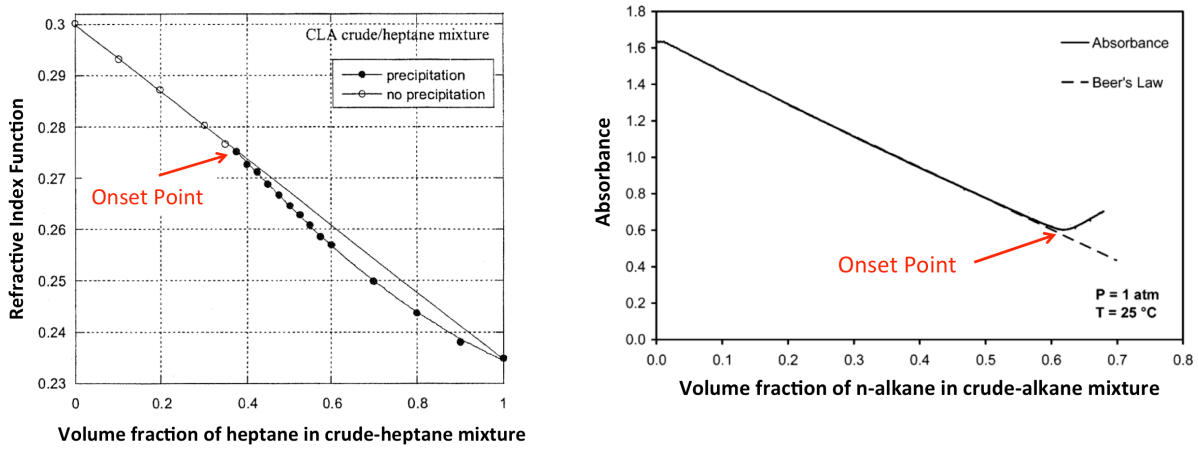

Figure 2.3 – Experimental determination of "onset point" of asphaltene precipitation using (left) the refractive index technique [8] and (right) the UV-Vis absorbance technique [9]

In these tests to measure onset point, heptane is continuously titrated into crude oil while a physical property of the mixture that can indicate a phase transition is monitored. The refractive index and light absorbance are the properties monitored in Figure 2.3 (left) and 4 (right), respectively. The point at which a departure from a linear trend on refractive index or absorbance is observed indicates the onset point. This value was then used to calculate parameters such as solubility blending and insolubility numbers [10] critical refractive index of precipitation [11] to

make risk assessment of asphaltene deposition. However, it has now been shown that if one gives enough time for n-alkane and oil to interact at a volume fraction below the so-called onset point, asphaltene precipitation will be detected [12]. This time delay in detecting asphaltene precipitation shows that *there is no such thing as an onset point*. Much attention has been given to the kinetics of asphaltene destabilization and aggregation since then. In this chapter a review [13] of the investigations of destabilization and aggregation kinetics of asphaltenes will be presented.

2.2. Measuring the Kinetics of Asphaltene Destabilization and Flocculation

2.2.1. Detection Time Experiments

In this experiment, heptane is added to crude oil at a controlled flow rate while keeping the oil well mixed. When the desired volume fraction of heptane in the oil-heptane mixture is reached, the flask is sealed, and mixture is kept stirred. Aliquots are then withdrawn as time elapses and examined under the microscope for presence of detectable particles as shown in Figure 2.4.

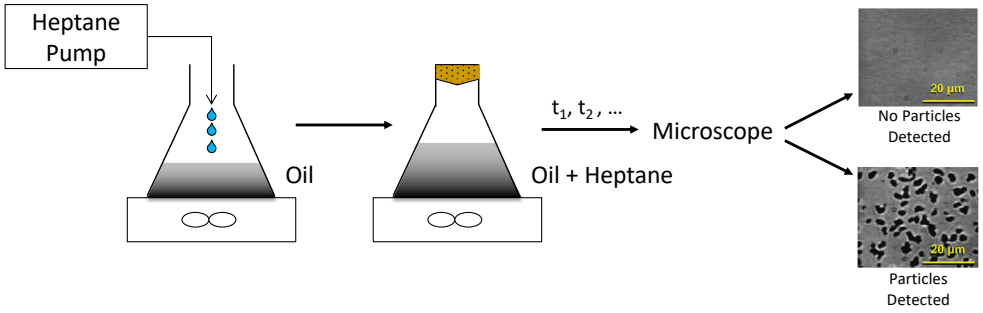

Figure 2.4 – Schematics of detection time experiments

Sampling is continued until particles are detected in micrographs as shown in Figure 2.5.

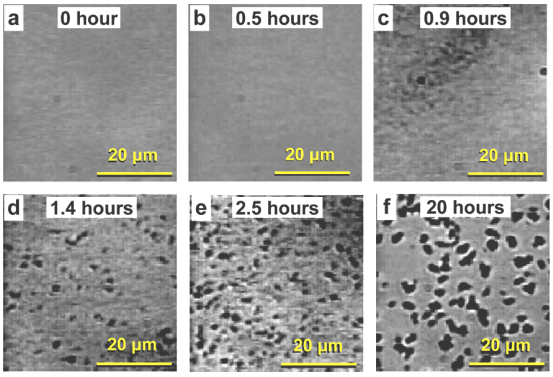

Figure 2.5 – Microscopy pictures taken of a crude oil-heptane mixture as a function of time. Detection time of precipitation is between 0.9 and 1.4 hours. [12]

The *detection time* is defined as the time required for asphaltene particles reach a size of 0.5 µm where they could be clearly observed under the microscope. This procedure was repeated for different volume fractions of heptane in oil-heptane and the detection times recorded for different oils. A plot of the detection time as a function of the volume percent of heptane in the oil-heptane mixture is shown in Figure 2.6. One observes a linear line in a semi log plot of detection time versus heptane concentration for the three oils investigated. The slope of line and the intercept at detection time of 0.1h for each of the oils is different.

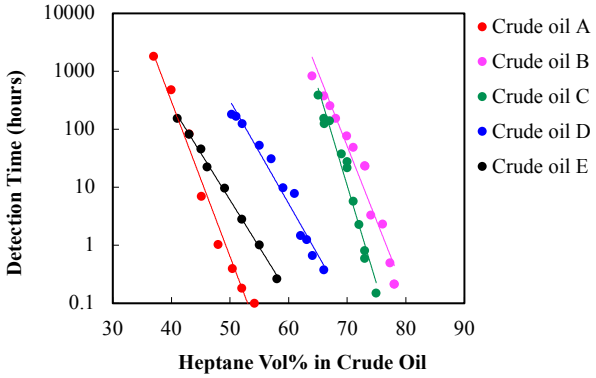

Figure 2.6 – The detection time of asphaltene precipitation as a function of initial heptane concentration (vol%) for crude oils A, B, C, D, and E. Data extracted from [14]

The detection time curve for model oils was also investigated. Model oils consists of asphaltenes extracted from crude oil and re-dissolved in pure solvents, in this case toluene and 1-methylnaphtalene. By varying the initial concentration of heptane in model oil-heptane mixture, the detection time-concentration curves for model oils were determined in an identical fashion to that for crude oil. Figure 2.7. shows the detection time-concentration curves for both crude oils and model oils as a function of the initial heptane concentration. One observes that in all cases the semi-log plot of detection time as a function of heptane concentration is linear, but with different slopes and different intercepts at 0.1h of detection time for the different model oils and different crude oils. The underlying physics of the detection time curve that explains the slope and intercept will be discussed in Section 5.

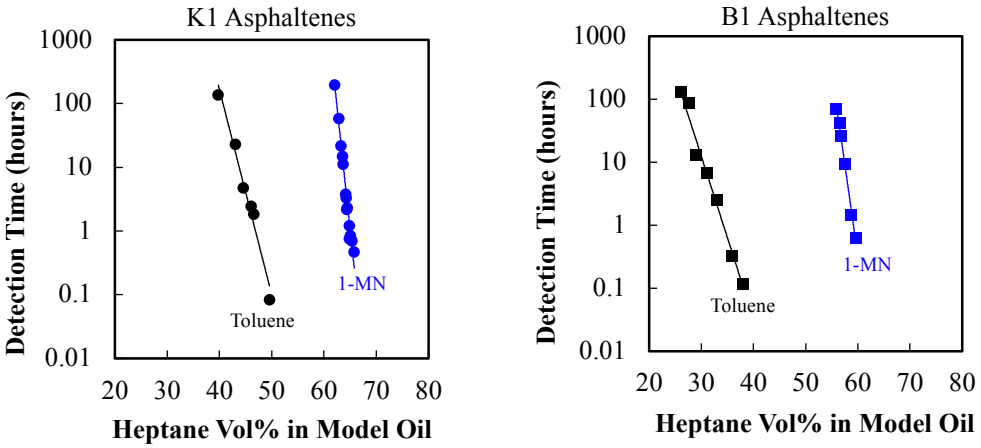

Figure 2.7 – The detection time of asphaltene precipitation as a function of heptane concentration for model oils with (left) K1 asphaltenes and (right) B1 asphaltenes [14]

2.2.2. Centrifugation Experiments

In addition to the detection time, the amount of asphaltenes that can be removed by centrifugation was measured as a function of time for different volume fractions of heptane in oil-heptane mixture. The procedure is shown schematically in Figure 2.8. The separation of asphaltenes from oil-heptane mixture is primarily based on asphaltene particle sizes. The size of

particle that can be separated from the mixture is a function of fluid properties and centrifugation conditions. For the experiments presented here, it is estimated that asphaltene particles larger than 200 nm are removed from oil-heptane mixture to form a centrifugation cake.

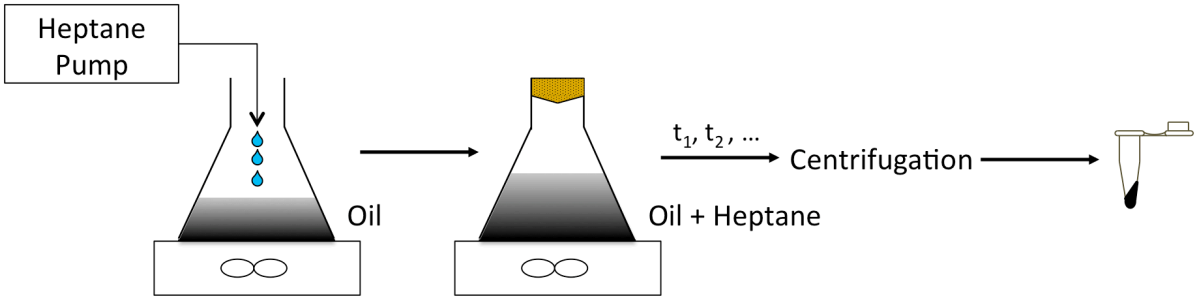

Figure 2.8 – Schematics of the centrifugation experiment

Figure 2.9. shows the amount of asphaltenes that are larger than ~ 200nm as a function of time after destabilization of a mixture of 46.5% heptane in crude oil K1. The asphaltene concentration was continually measured until no further change in asphaltene concentration was observed as can be seen in the plateau region in Figures 2.9. The plateau region for 46.5% heptane begins at approximately 400 hours. The precipitated asphaltene concentration – time curves were repeated for different initial heptane concentrations and shown in Figure 2.9.

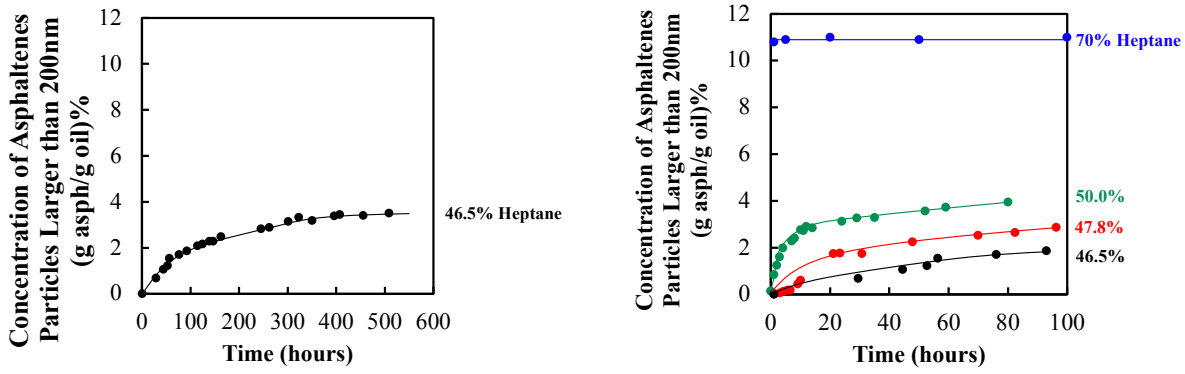

Figure 2.9 – Centrifugation experiment results for K1 crude oil at different heptane concentration [12]

One observes different values of the plateau concentration for the different initial heptane concentrations in oil-heptane mixture. From these plateau values, one can determine the amount of asphaltene precipitated as well as that remaining in solution as a function of heptane concentration. Using Figure 2.9 we can construct the solubility curve in terms of (grams remaining in solution/gram crude oil) as a function of percentage heptane for a given oil as shown in Figure 2.10 for crude oil K1. One observes that the time required to accurately measure the solubility of asphaltenes is a strong function of the heptane concentration and the importance of considering kinetic effects is most pronounced at low heptane concentrations.

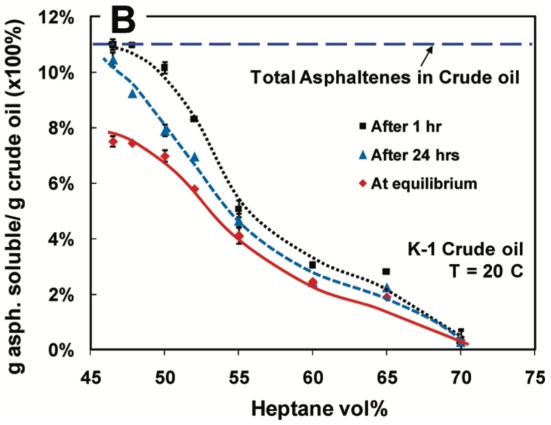

Figure 2.10 – Asphaltene solubility in K1 crude oil as a function of heptane concentration in crude oil–heptane mixtures. [12]

It has been suggested that the long-term kinetics of asphaltene destabilization and aggregation is an experimental artifact related to oxidization of oil molecules with oxygen from air [15]. Centrifugation experiments were performed in air and in nitrogen environment with crude oil. Experimental results are presented in Appendix B. No detectable effect of oxygen from air on the kinetics of asphaltene destabilization and aggregation was observed. The experimental results of aggregation kinetics presented in Beck et al [15] are for bitumen, while the ones studied here

are for crude oils. It is possible that bitumens are more susceptible oxidation than crude oils, which would explain why the kinetics of asphaltene aggregation are affected by the oxygen from air.

2.2.3. Small Angle X-ray and Neutron Scattering

Because the microscope can only measure particles sizes of 0.5 μm or above, X-ray and neutron scattering [4] (see Figure 2.11) was used to measure changes in asphaltene particle size in the nanometer size. The scattering curves of heptane-diluted crude oil, Oil A, at 0, 10, and 20% heptane after mixing for 1 day and 6 months after destabilization by heptane addition to crude oil are shown in Figure 2.12.

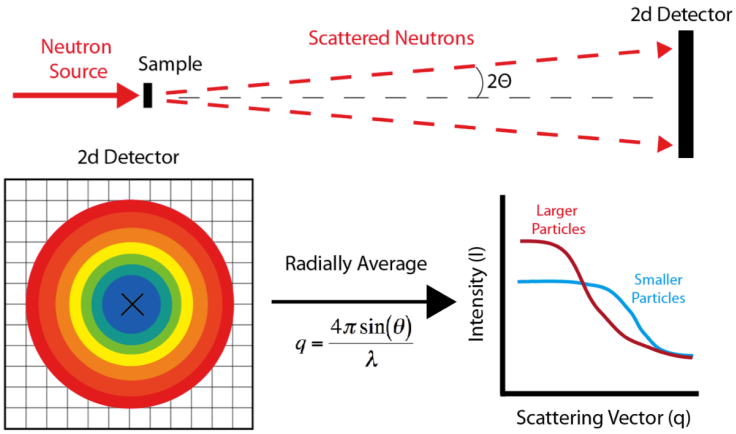

Figure 2.11 – Schematic of small angle neutron scattering technique [16]

The scattering curves were normalized by the scattering contrast ($\Delta\rho^2$) and the asphaltene volume fraction (Φ), to visualize the effect of heptane on asphaltene size and fractal dimension. The increase in scattering intensity at low angles is an indication of an increase in the size of asphaltene clusters, which is due to the formation and aggregation of unstable asphaltene particles. These measurements are consistent with the trends in the detection time curves reported in Section 4.1 and 4.2.

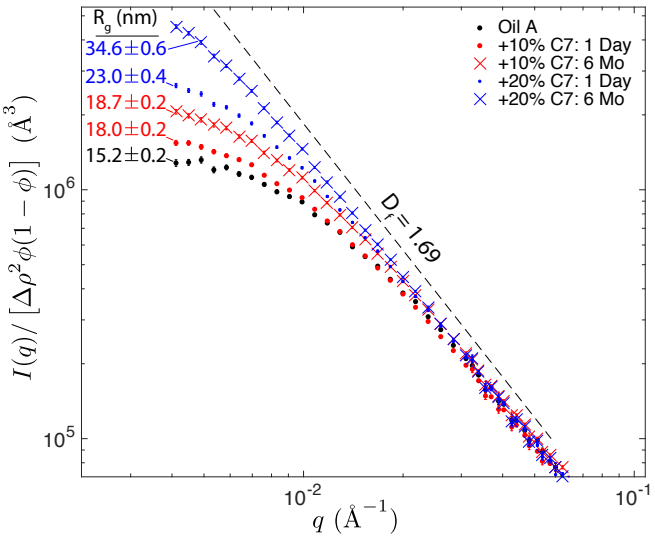

Figure 2.12 – Small angle neutron scattering profiles of pure oil A, 10 and 20vol% heptane in oil A of 1 day and 6 months after heptane addition to oil A. Unpublished data from the author [4]

Another important finding from scattering was the discovery of differences in fractal dimension, Df, of stable and unstable asphaltene clusters. The fractal dimension here is defined as the scaling factor between scattering intensity, I, and scattering angle, q, determined at the linear region at high angle, i.e., $I \sim q^{-Df}$. The fractal dimension of combined stable and unstable and the fractal dimension of stable clusters only can be measured experimentally. The fractal dimension of unstable cluster is then calculated invoking the superposition property of scattering:

$$[I(q)]_{Combined} = [I(q)]_{Stable} + [I(q)]_{Unstable} \quad (1)$$

where $[I(q)]_{Combined}$ is the scattering of the mixed sample. Subtracting the scattering intensity of a centrifuged sample that only contains only stable asphaltenes ($[I(q)]_{Stable}$) from $[I(q)]_{Combined}$ will isolate the scattering from the unstable asphaltenes ($[I(q)]_{Unstable}$). For Oil A, we see from Figure 2.13 that the stable clusters have a fractal dimension of 1.69 whereas the unstable clusters have a fractal dimension of 2.12. The lower fractal dimension of stable indicates that they have a more open and solvent-swollen structure when compared to unstable cluster. The increase in

fractal dimension upon asphaltene destabilization reveals a fundamental change in the way that asphaltenes interact with itself depending on their surrounding environment.

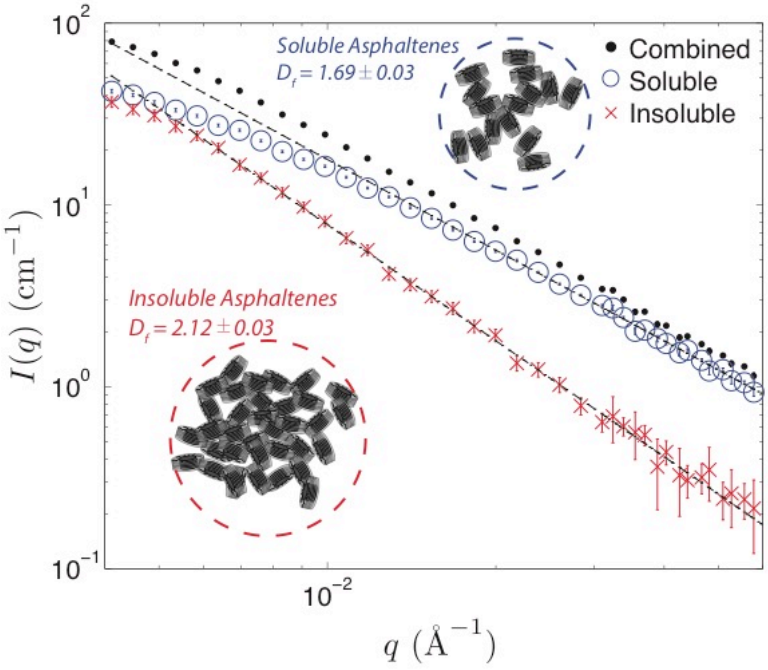

Figure 2.13 – Small angle neutron scattering profile of soluble asphaltenes (shown in blue), precipitating asphaltenes (shown in red), and combined soluble and precipitating (shown in black). The slope of the lines in this q-range gives the fractal dimension of the structures. Adapted from [4]

Using the differences in fractal dimension, a schematic of the stable and unstable asphaltenes can be visualized in Figure 2.14. When heptane is added to crude oil, two phenomena occur. First, asphaltenes that will remain stable will have the same fractal dimension ($D_f^{Soluble} = D_f^0$) but their radius of gyration will increase ($R_g^{Soluble} > R_g^0$) compared to their size and fractal dimension in the undiluted oil. Second, a fraction of asphaltenes may destabilize, depending on the quantity of heptane added. These unstable asphaltenes will have a higher fractal dimension ($D_f^{Insoluble} > D_f^0$) and their radius of gyration will increase to a macroscopic size ($R_g^{Insoluble} \rightarrow \infty$) and eventually can be detected in optical microscopy.

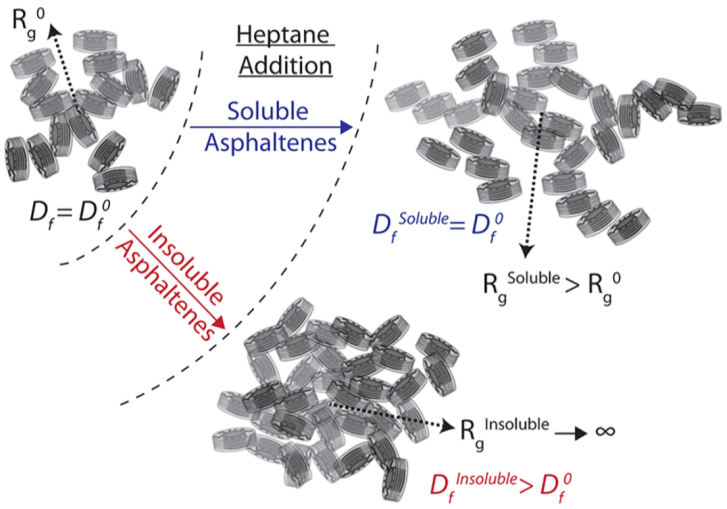

Figure 2.14 – Schematic of the asphaltene precipitation process upon addition of heptane to crude oil or model oils. [4]

2.2.4. Asphaltene Deposition Experiments

The deposition of asphaltenes from crude oil when destabilized by heptane addition was also investigated. The schematic of the deposition apparatus is shown in Figure 2.15.

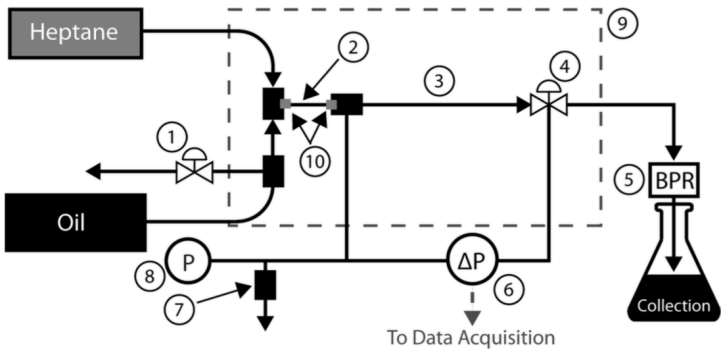

Figure 2.15 – Schematics of the asphaltene deposition apparatus. 1: Valve, 2: Mixing capillary, 3: Test section, 4: Splitter valve, 5: Back pressure regulator, 6: Differential pressure transducer, 7: Relief valve, 8: Pressure gauge, 9: Constant temperature water bath, 10: porous frits. [17], [18]

In this investigation, crude oil and heptane are continuously mixed at constant flow rates immediately before entering a capillary tube whose differential pressure drop is recorded as a function of time. The experimental results are presented in Figure 2.16 in terms of the measured differential pressure (ΔP) shifted by the differential pressure before any deposit formed (ΔP_0). The

increase in pressure drop in Figure 2.16 characterizes the asphaltene deposit on the capillary wall, constricting the flow and thus increasing the pressure drop.

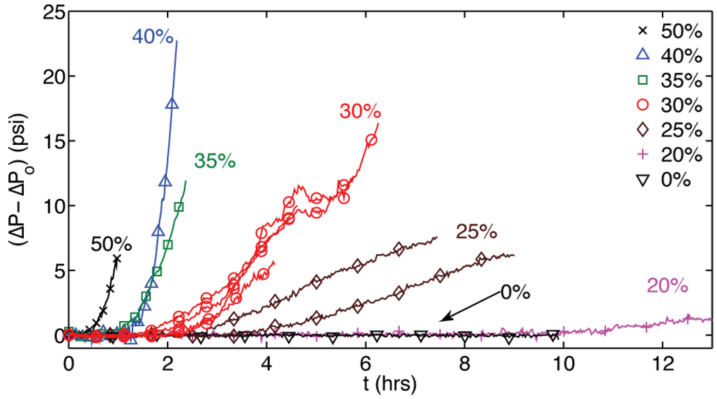

Figure 2.16 – Pressure drop across the capillary test section as function of run time at various concentration of heptane in the oil-heptane mixture. [19]

These experiments were carried out using crude oil-heptane mixtures with different heptane concentrations entering to the capillary tube. The higher heptane concentration causes the pressure drop to increase faster than the lower heptane concentrations. The "onset point" of this oil was measured to be 40vol% of heptane and yet deposits were formed at heptane concentrations as low as 20% heptane. This result is one more evidence that *there is no such thing as an onset point*. Arterial deposits were also visualized, and SEM images of the capillary inlet and outlet for a 30% heptane deposition experiment are shown in Figure 2.17.

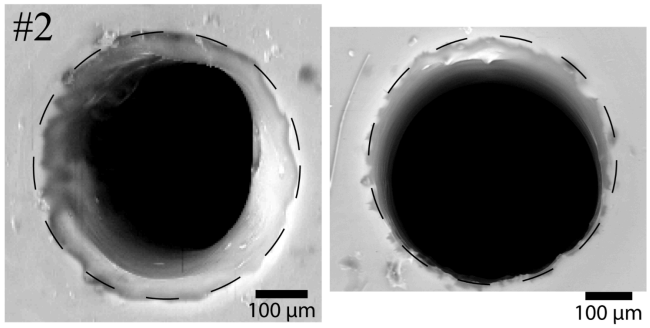

Figure 2.17 – Microscopy image of capillary inlet (left) and outlet (right) after running a mixture of 30 vol% of heptane in Oil A. Dashed lines indicate the inner capillary wall edge. [19]

In Chapter III a new technique to study asphaltene deposition will be introduced and discussed, a packed bed of stainless steel beads.

2.3. Mathematical Modeling of Asphaltene Destabilization and Aggregation

2.3.1. Asphaltene Molecules, Nanoparticles and Clusters

Asphaltenes exist in crude oil and model oils in an aggregated state as nanoaggregates and cluster of nanoaggregates, as shown in Figure 2.18. Nanoparticles, or nanoaggregates, are stacked layers of asphaltene molecules, which contain an aromatic core with alkyl chains.

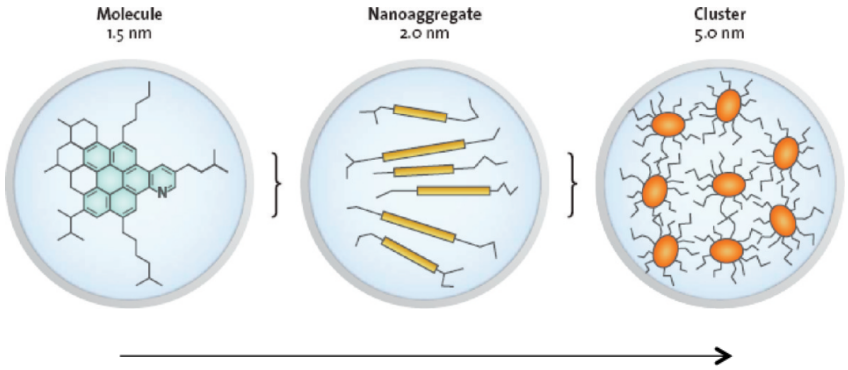

Figure 2.18 – Asphaltenes natural state. Adapted from [2]

When modeling the asphaltene aggregation [20], it will be assumed that a fraction of asphaltenes are destabilized immediately at the time of n-alkane to crude oil to form an initial concentration unstable nanoparticles (nanoaggregate), $C_1(0)$, of size d_1. The fraction of asphaltenes that destabilizes is a function of the concentration of n-alkane in oil-alkane mixture. This fraction taken to be the plateau value of the centrifugation plot at the heptane concentration of interest.

2.3.2. Population Balance and the Smoluchowski Collision Kernel

Once destabilized by a precipitant, the unstable nanoparticles begin to aggregate. The population balance model can be used to keep track of the number of particles of each size as a

function of time and the Smoluchowski collision kernel gives the rate constant of particle aggregation [21], [22].

$$\frac{dC_k}{dt} = \frac{1}{2}\sum_{i+j=k} K_{ij} C_i C_j - C_k \sum_{i\geq 1} K_{ik} C_i \tag{2}$$

where C_k = concentration of k-th species, $K_{i,j}$ = collision kernel between i-j species, and t = time. The collision kernel, K_{ij},

$$K_{ij} = \frac{2R_g T}{3\mu} \frac{\left(d_i + d_j\right)^2}{d_i d_j} \beta \tag{3}$$

Where T = Temperature (K), μ = Viscosity (Pa.s), R_g is the universal gas constant (J K^{-1} mol^{-1}), β is the collision efficiency, and d_i is the diameter of particle undergoing aggregation. A derivation of the collision kernel can be found in the Appendix. When β = 1, the aggregation process is diffusion-limited. For aggregation processes that are reaction-limited, β is lower than 1 and equal to the inverse of the Fuchs stability ratio[23]. The collision efficiency can also be interpreted as the ratio between the number of collisions that result in aggregation and the total number of collisions. The word collision in collision efficiency might lead one to think that asphaltene particles behave like billiard balls that can bounce on and off of each other. However, in the asphaltene aggregation process the particles are undergoing Brownian motion where concentration gradients will drive particles to encounter and aggregate. In an aggregation process where β is lower than unity, the concentration gradient that drives particles to encounter is lower than the gradient in a diffusion-limited process. Therefore, particles do not "bounce off" of each other. Instead, there is a reduction on the rate of encounter of particles.

2.3.3. Coarse-Grained Population Balance – Geometric Form

It is assumed that all asphaltene nanoaggregates that destabilize upon heptane addition are spheres of 2.5nm diameter. These 2.5nm spheres are the monomer of the aggregation process. Two monomers can aggregate forming a dimer, two dimers can aggregate forming a tetramer and so on, as shown schematically in Figure 2.19. Only two-body encounters are considered in this model.

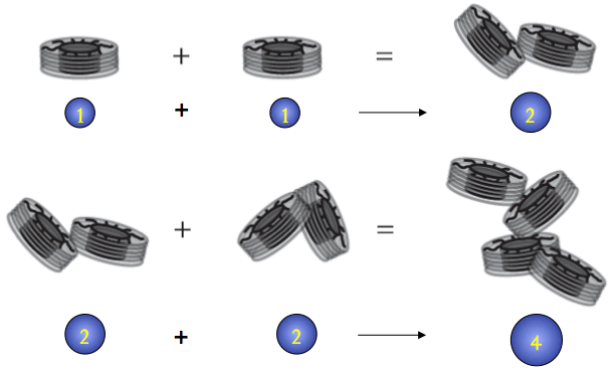

Figure 2.19 – Schematics of the asphaltene aggregation that is modeled with the population balance equations.[13]

When two particles aggregate, they take the shape of a larger sphere. The diameter of the new larger particle is calculated by assuming that the volume of the two smaller particles that aggregated to form the new larger particle is conserved.

Experimental observation indicates that asphaltene particle can grow up to tens of microns in diameter. The relationship between particle diameter and number of monomers in a k-mer is given by $d_k = d_1 k^{1/3}$ where d_1 is the diameter of monomer, d_k is the diameter of the k-mer and k is the number of monomers in the k-mer. Given that the monomers have 2.5nm in diameter, a particle of 10um will contain 6.4×10^{10} monomers. In the population balance model, one ordinary differential equation (Equation 2) is required for each k-mer in the system. Consequently, to model the aggregation process of asphaltenes, which has particles containing up to 6.4×10^{10} k-mers, 6.4×10^{10} coupled ordinary differential equation would need to be solved. This number assumes that

one would take into account all k-mers, k being integer numbers, between 1 and 6.4 x 10^{10}. Solving this many coupled ordinary differential equations is prohibitive. In order to circumvent this problem, the population balance must be coarse-grained by lumping a range of k-mers into a single average particle size. This lumping is done by using a geometric progression with scaling factor R. In this way, only k-mers of $k = R^{i-1}$ will be computed in the model, with *i* being integers greater than 1. Finally, with the geometric progression used to coarse-grain the population balance only 37 particle sizes will have to be taken into account to model particle aggregation and comprehend particle distribution between 2.5nm and 10um. Note that this population balance does not take particle breakage into account. When lumping the particles using the geometric progression, Equation 2 is re-written as

$$\frac{dC_i}{dt} = \frac{K_{i-1,i-1}}{R} C_{i-1}^2 + C_{i-1} \sum_{j=1}^{i-2} K_{i-1,j} \frac{R^{j-1}}{R^{i-1} - R^{i-2}} C_j - C_i \sum_{j=1}^{i-1} K_{i,j} \frac{R^{j-1}}{R^i - R^{i-1}} C_j - C_i \sum_{j=i}^{N-1} K_{i,j} C_j \qquad (4)$$

These population balance equations were solved numerically to predict the change in the particle size distribution with time as shown in Figure 2.20. First, we note that the rate of increase in particle size is higher for 50% heptane than 46.5% heptane. It is also observed that the mean particle size increases and that the kurtosis of the distribution remains as particles grow larger. The time for a detectible number of particles to reach 500 nm is also shown on these plots. These times matched with the detection time curve shown on the right of Figure 2.20. In Figure 22 (c) we note that the model predicts the same linear relation in a semi logarythmic plot of detection time as a function of heptane concentration as that introduced in Figure 2.6.

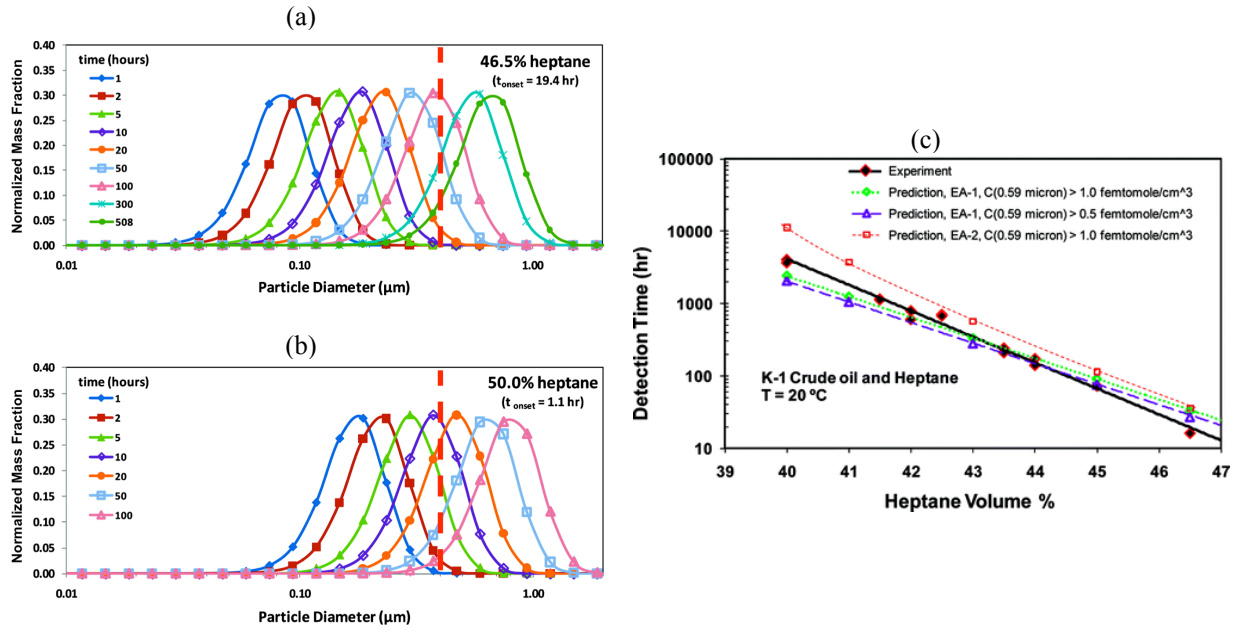

Figure 2.20 – The asphaltene cluster size distribution as a function at different times after heptane addition as predicted by the population balance model (a) [20]; Experimental and predicted detection time for K1 crude oil as a function of heptane concentration (b) [20]

The equations were also solved to predict the weight in grams of asphaltene that be centrifuged out of mixture per gram of crude oil as a function of time and compared with the experimental measurements in Figure 2.20 (c). One readily observes there is an excellent fit between the model and the experimental data.

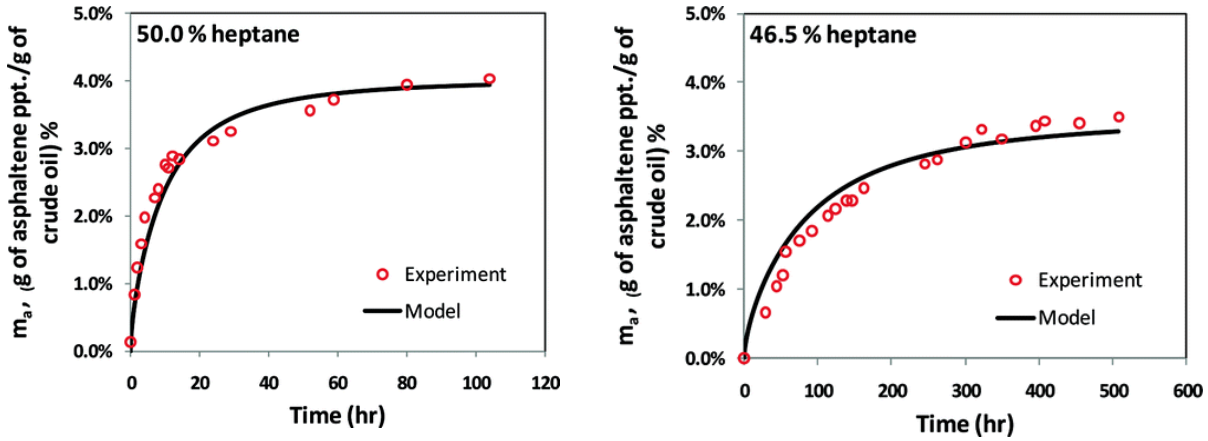

Figure 2.21 – Experimental and modeling results of asphaltene aggregation as a function of time for K1 crude oil at 50 and 46.6vol% heptane [20]

There was one fitting parameter used in matching the asphaltene precipitant-time curves and that parameter was collision efficiency, β, in the flocculation kernel, $K_{i,j}$. The collision efficiency β is shown as a function of the heptane concentration in Figure 2.22. One observes that as heptane concentration is increased, the collisions efficiency also increases.

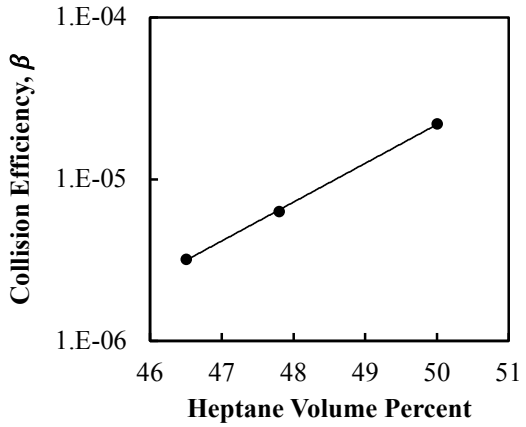

Figure 2.22 – Collision efficiency as a function of heptane concentration in oil-heptane mixture [20]

2.3.4. Steric Stabilization of Asphaltene Clusters

In modeling asphaltene flocculation, we have shown that the geometric population can successfully predict the changes in particle size distribution and the amount of asphaltenes precipitated as a function of time for a given crude oil [20]. The only fitting parameter is the collision efficiency. The collision efficiency is the inverse of the Fuchs stability ratio

$$\beta = \frac{1}{2a}\int_{2a}^{\infty} \exp\left[-\frac{U}{k_B T}\right]\frac{dD}{(D+2a)^2} \tag{5}$$

Where a is the diameter of asphaltene particles, U is the particle-particle interaction energy, k_B is the Boltzmann constant, T is the temperature, and D is the surface-to-surface separation distance between particle. The interaction energy between asphaltenes has been measured experimentally using atomic force microscope. It was found that the repulsion forces between

asphaltene clusters can be explained by a polymer brush, where thickness of the brush is affected by solvent in which asphaltenes is immersed into, as shown in Figure 2.23.

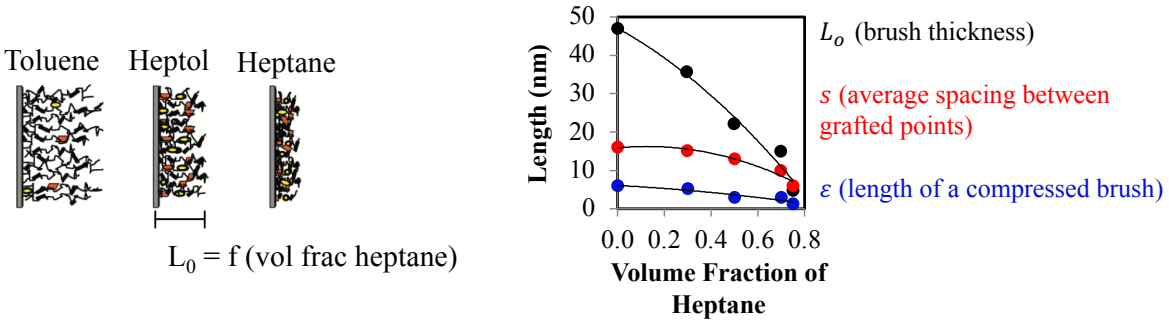

Figure 2.23 – Repulsion forces between asphaltenes[7], [6]

The repulsion forces between asphaltene particles due to the steric repulsion of polymer brush is given by[24]

$$\frac{F_S}{a} = \frac{16\pi k_B T L_0}{35 s^3}\left[7\left(\frac{D+2\varepsilon}{2L_0}\right)^{-\frac{5}{4}} + 5\left(\frac{D+2\varepsilon}{2L_0}\right)^{\frac{7}{4}} - 12\right] \tag{6}$$

The attractive forces between asphaltene particles can be computed using the sphere-sphere van der Walls forces with the appropriate value of Hamaker constant for asphaltenes[24].

$$\frac{F_{vdW}}{a} = \frac{d}{dD}\frac{A_{eff}}{6}\left[\frac{2a^2}{R^2-4a^2} + \frac{2a^2}{R^2} + \ln\left(1-\frac{4a}{R^2}\right)\right] \tag{7}$$

Where R is the distance between center of particles, and A_{eff} is the effective Hamaker constant. The effective Hamaker is calculated as follows

$$A_{eff} = \left(\sqrt{A_{heptol}} - \sqrt{A_{asphaltenes}}\right)^2 \tag{8}$$

The Hamaker constant of asphaltenes is ~ 6 x 10^{-20} J. The asphaltene-asphaltene interaction energy as a function of surface-to-surface separation distance can be calculated by superimposing the attractive and repulsion forces from Equation 6 and 7, respectively. A plot of the interaction energy versus separation distance for different heptane volume fractions is shown below.

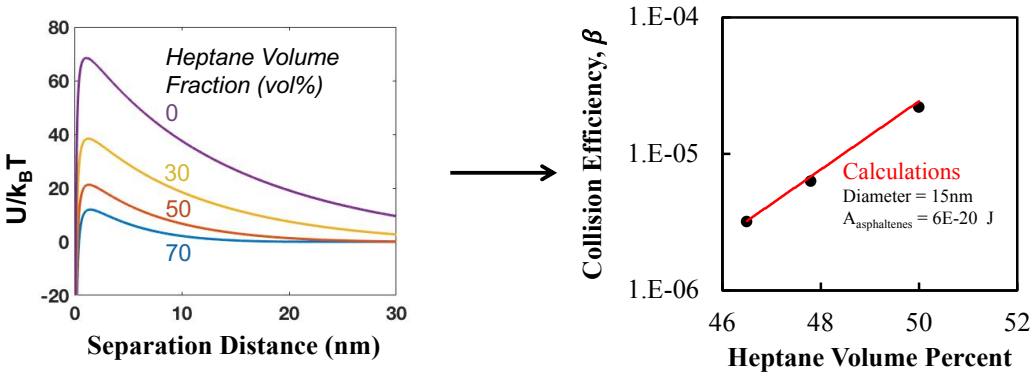

Figure 2.24 – (left) Asphaltene-asphaltene interaction energy as a function of separation distance for different heptane concentrations. (right) Collision efficiency as a function of heptane concentration for K1 crude oil compared with the predicted collision efficiency predicted by the calculations.

The collision efficiency is calculated using Equation 5 and is shown in Figure 2.24 (right). It can be seen that there is an excellent agreement with calculated and experimental values of collision efficiency when considering two particles of 15nm aggregating with a Hamaker constant. The experimental values of collision efficiency in Figure 2.24 (right) are obtained from Figure 2.22.

Note that collision efficiency is a function of the asphaltene particle size. This dependency is related to how attractive forces increases faster with increase of particle diameter than the repulsion forces increase with increase of particle diameter. In the previous section, single collision efficiency was obtained for each heptane concentration (Figure 2.22), where an average collision efficiency for all particles sizes in the aggregation process was obtained.

2.3.5. Unified Aggregation Model with Crude Oils

In the geometric form of the population balance, it was assumed that the collision kernel is a function of the particle sizes undergoing aggregation. This assumption results on the coupling population balance equation for each k-mer. If this restriction is relaxed and the collision kernel is assumed to be independent of particle size, the differential equations become decoupled and Equation 2 can be solved analytically with the following solution [22]:

$$\frac{C_k(t)}{C_1(0)} = \frac{4}{(\alpha t + 2)^2}\left[\frac{\alpha t}{\alpha t + 2}\right]^{k-1} \tag{9}$$

Where $C_1(0)$ is the initial concentration of nanoparticles immediately after destabilization. This concentration is the plateau value of centrifugation curves, e.g., Figures 2.9. α is defined as:

$$a = \frac{8k_B T}{3\mu}\beta C_1(0) \tag{10}$$

A proportionality can be extracted from Equation 9 and 10 where the detection time of asphaltene precipitation as follow [14]

$$\frac{t_{detection}\sqrt{C_1(0)}}{\mu} \propto \frac{1}{\beta} \tag{11}$$

The viscosity and concentration of unstable asphaltenes can be measured experimentally. The collision efficiency is controlled by the strength of interaction forces between aggregating asphaltenes and can be estimated from Equation 5. Assuming that the asphaltene-asphaltene interaction is proportional to the mismatch between the solubility parameter of asphaltenes and solubility parameter of solvents [14], it can be written that

$$\beta \sim e^{(\delta_{asphaltenes}-\delta_{solvents})^2} \quad (12)$$

Combining Equations 11 and 12, a relationship between detection time and changes in solubility parameter can be obtained

$$\ln\left[\frac{t_{detection}\sqrt{C_1(0)}}{\mu}\right] \propto \left(\delta_{asphaltenes} - \delta_{solution}\right)^2 \quad (13)$$

When applying Equation 13 to the detection time curves of different crude oils, shown in Figure 2.6, the detection time curves collapse onto a single line as shown in Figure 2.25.

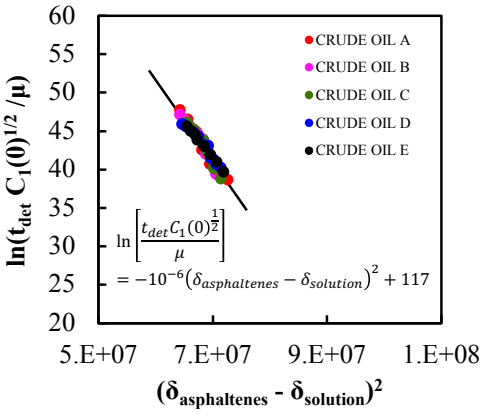

Figure 2.25 – Master curve of the unified aggregation model [14]

A comparison between the solubility parameters obtained from aggregation model and the solubility parameter obtained from the Buckley correlation of refractive index [25] is available in Appendix A.

In section 2.3.6, the aggregation model will be applied to detection time curves of model oil where the solubility parameter of solution is well defined.

2.3.6. Unified Aggregation Model with Model Oils

The aggregation model is applied to the detection time curves for model oils shown in Figure 2.7. In these experiments, the solubility parameter of asphaltene is kept constant and the effect of solubility parameter of solution investigated by changing the solvents. Therefore, based on the aggregation model, the detection time curves for a given asphaltene should collapse when the log $(t_{det}C_1(0)^{1/2}/\mu)$ is plotted as a function of solubility parameter of solution without having to subtract the solubility parameter of asphaltenes. This plot is shown in Figure 2.26.

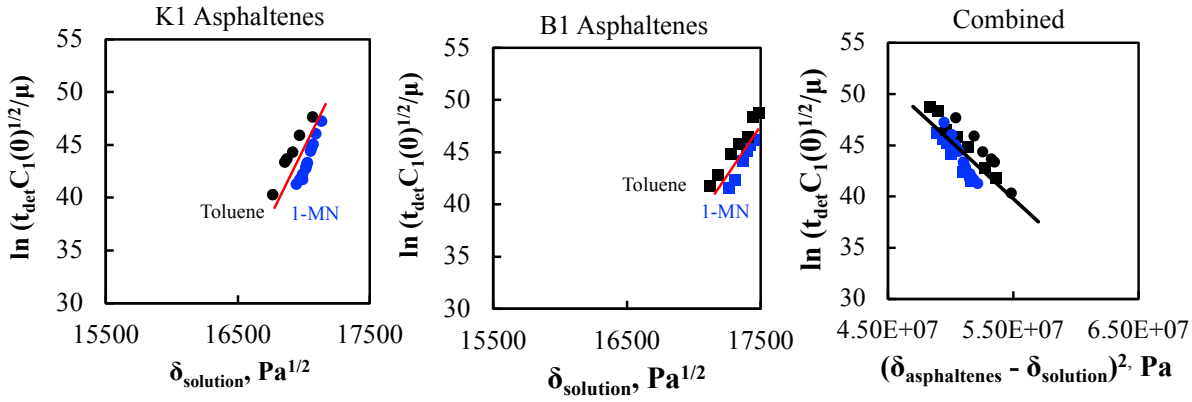

Figure 2.26 – Principles of the unified aggregation model applied to the model oil mixtures [14]

Indeed, the detection time curves for each asphaltene collapse onto a line indicating that the underlying physics of the unified aggregation model is able to explain the aggregation process.

2.4. Effect of Type of Precipitant on Asphaltene Destabilization and Aggregation

The effect of n-alkane on the asphaltene detection time was investigated using n-alkanes of 6, 7, 8, 9, 10, 12, and 15 carbons. The detection time was measured as a function of n-alkane concentration in a model oil of 1 wt% K1 asphaltene dissolved in toluene. Experimental results are presented in Figure 2.28 (a). As the length of the n-alkane chain increases from 6 to 15 carbons, their respective densities, viscosities, and solubility parameters increase. By applying the

asphaltene aggregation model to the experimental data, the change in detection time due to viscosity and solubility parameter of the n-alkane can be factored out and the solubility parameter distribution of the asphaltene can be obtained. In this way, the asphaltene polydispersity can be characterized. Figure 2.28 (right) shows how all the different crude oils and model oils with different precipitants collapse into the master curve. Again, one notes the excellent agreement of the data and model.

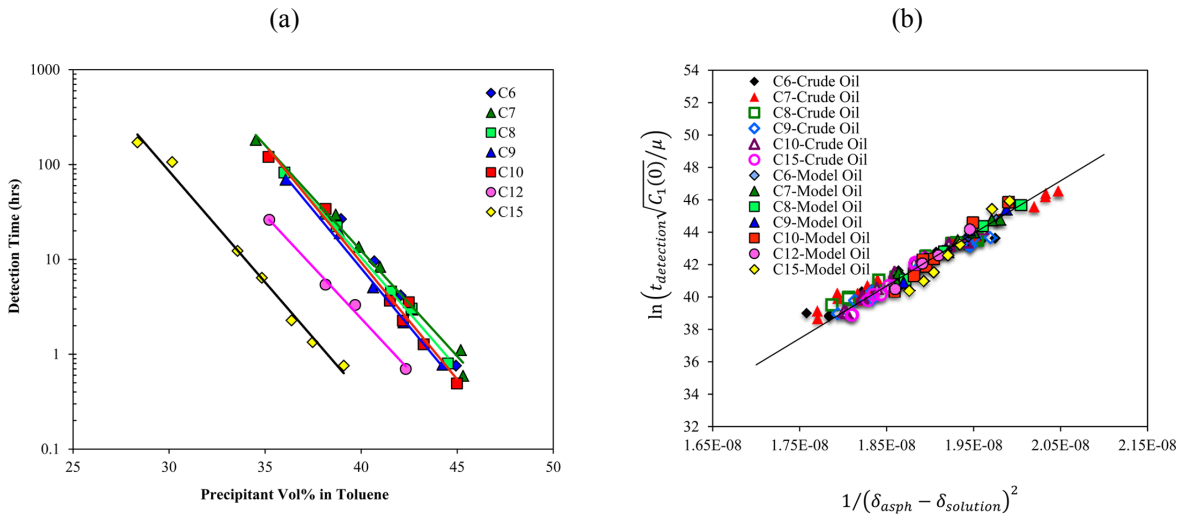

Figure 2.27 – Detection time of asphaltene aggregation as a function of precipitant concentration for K1 model oil crude oil (a), and the aggregation model applied to the experimental data of crude oils and to model oils (b). [26]

The effect of precipitant type on the yield of asphaltene precipitation was studied using the centrifugation technique with GM2 crude oil. The yield of asphaltene precipitated as a function of length of n-alkane for different n-alkane concentrations is presented in Figure 2.28. Here one observes that the effect of the length of n-alkane on the yield of asphaltenes precipitated is more pronounced at high n-alkane concentrations, e.g. 90vol%. Mitchell and Speight [27] have observed similar behavior for the high alkane concentrations, where the amount of precipitated asphaltenes decrease as the length of n-alkane chain increases. This relationship between precipitation yield and precipitant carbon number has been attributed to the polydispersity of asphaltenes [26].

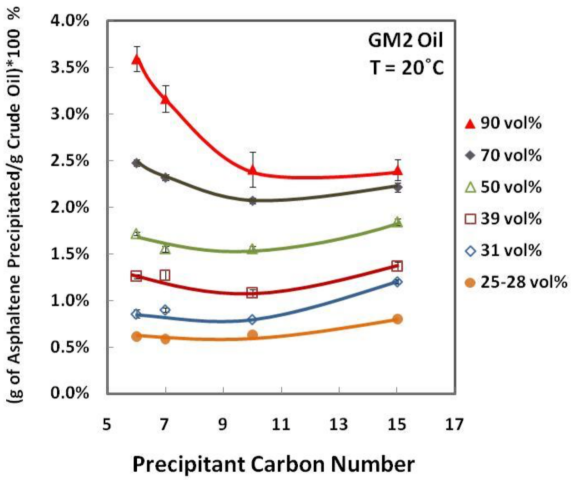

Figure 2.28 – Yield of asphaltene precipitated of GM2 crude oil as a function of length of n-alkane carbon number for different alkane concentrations.[28]

2.5. Effect of Asphaltene Concentration on Asphaltene Destabilization and Aggregation

The effect of asphaltene concentration on the detection time of asphaltene aggregation was investigated. Experimental results show that as the asphaltene concentration increases from 0.1 to 1 wt% for a fixed heptane concentration, the detection time decreases. However, as the asphaltene concentration increases from 1 to 8 wt% the detection time increases for a fixed heptane concentration. For example, we see at 44 vol% heptane, the detection times increase from 2 hours to 6 hours to 25 hours as the asphaltene concentration increases from 1 wt% to 3 wt% to 5 wt%. Consequently, as the concentration of asphaltenes in model oil increases from 0.1 wt% to 8 wt%, a minimum detection time is observed at around 1wt% K1 asphaltenes in toluene. The decrease in detection time for asphaltene concentrations below 1wt% can be explained by the fact that the collision frequency between asphaltenes increases as asphaltene concentration increases.

The detection time curves for asphaltene concentrations greater than 1 wt% are shown in Figure 2.29 (a). As the asphaltene concentration in the mixture increases, the participation of the soluble asphaltenes in solution becomes more significant. In this way, by taking into account the

presence of soluble asphaltenes in the solution's solubility parameter, the unified asphaltene aggregation model can explain the results obtained, as it can be seen by the collapsing of results onto a single line shown in Figure 2.29 (b).

(a) (b)

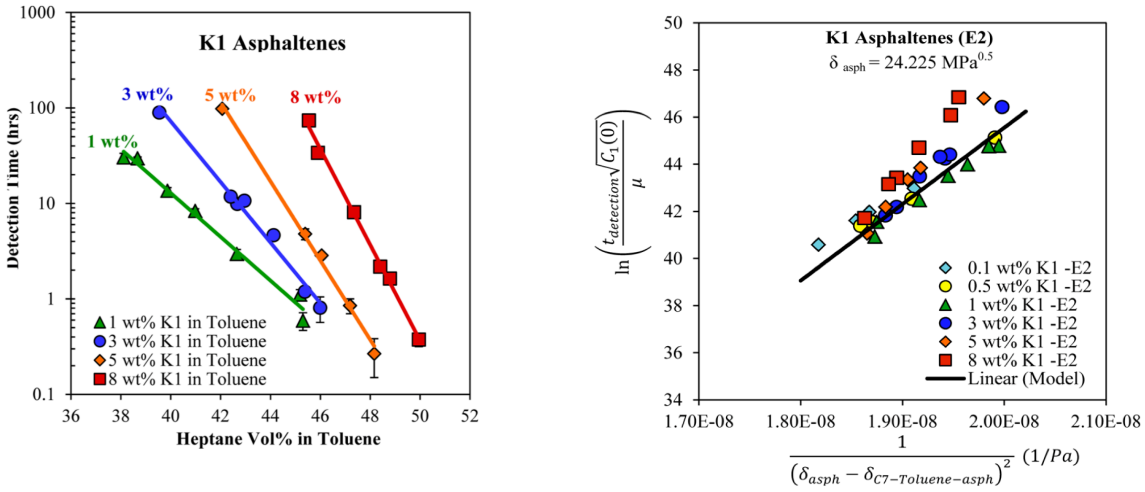

Figure 2.29 – The effect of asphaltene concentration on the asphaltene detection time as a function of heptane concentration in model oil. [29]

$$\delta_{solution} = \phi_{heptane}\,\delta_{heptane} + \phi_{toluene}\,\delta_{toluene} + \phi_{soluble\ asphaltenes}\,\delta_{asphaltenes} \qquad (16)$$

2.6. Summary

Asphaltenes are polyaromatic crude oil compounds that undergo an aggregation process once they are destabilized by precipitants such as n-alkanes. The amount of asphaltenes and the rate by which asphaltenes grow in solution depend on the crude oil and on the concentration of n-alkanes in the oil-alkane mixture. Bulk flocculation and deposition experiments have demonstrated that there is no such thing as an "onset concentration", i.e., a concentration of alkane in oil-alkane mixture below which asphaltenes are inherently stable. The kinetics of asphaltene aggregation, assessed by means of detection time measurements, can be explained by unified aggregation model. The unified aggregation model is derived from the population balance with the Smoluchoswski

collision kernel, an Arrhenius type of relation between the collision efficiency and the difference of solubility parameters of the solution and the asphaltenes. The unified aggregation model successfully predicts the aggregation of asphaltenes in dozens of combinations of different crude oil, model oils, precipitants, and asphaltenes.

2.8. References

[1] "Baker Hughes." [Online]. Available: http://www.bakerhughes.com/products-and-services/production/upstream-chemicals/flow-assurance-services/asphaltene-paraffin-control-ppds. [Accessed: 08-Jan-2016].

[2] O. C. Mullins, H. Sabbah, J. Eyssautier, A. E. Pomerantz, L. Barré, A. B. Andrews, Y. Ruiz-Morales, F. Mostowfi, R. McFarlane, L. Goual, R. Lepkowicz, T. Cooper, J. Orbulescu, R. M. Leblanc, J. Edwards, and R. N. Zare, "Advances in Asphaltene Science and the Yen–Mullins Model," *Energy Fuels*, vol. 26, no. 7, pp. 3986–4003, Jul. 2012.

[3] K. H. Altgelt and M. M. Boduszynski, *Composition and Analysis of Heavy Petroleum Fractions*, 1st Editio. CRC Press, 1993.

[4] M. P. Hoepfner, C. V. B. Fávero, N. Haji-Akbari, and H. S. Fogler, "The fractal aggregation of asphaltenes.," *Langmuir*, vol. 29, no. 28, pp. 8799–808, 2013.

[5] O. C. Mullins, "The Modified Yen Model †," *Energy Fuels*, vol. 24, no. 4, pp. 2179–2207, 2010.

[6] S. Wang, J. Liu, L. Zhang, J. Masliyah, and Z. Xu, "Interaction forces between asphaltene surfaces in organic solvents.," *Langmuir*, vol. 26, no. 1, pp. 183–90, Jan. 2010.

[7] S. Wang, J. Liu, L. Zhang, Z. Xu, and J. Masliyah, "Colloidal Interactions between Asphaltene Surfaces in Toluene," *Energy Fuels*, vol. 23, no. 2, pp. 862–869, Feb. 2009.

[8] P. Wattana, D. J. Wojciechowski, G. Bolaños, and H. S. Fogler, "Study of Asphaltene Precipitation Using Refractive Index Measurement," *Pet. Sci. Technol.*, vol. 21, no. 3–4, pp. 591–613, Jan. 2003.

[9] K. Kraiwattanawong, H. S. Fogler, S. G. Gharfeh, P. Singh, W. H. Thomason, and S. Chavadej, "Thermodynamic Solubility Models to Predict Asphaltene Instability in Live Crude Oils †," *Energy Fuels*, vol. 21, no. 3, pp. 1248–1255, May 2007.

[10] I. A. Wiehe, *Process Chemistry of Petroleum Macromolecules*. CRC Press, 2008.

[11] J. Creek, J. Wang, and J. Buckley, "Verification of Asphaltene-Instability-Trend (ASIST) Predictions for Low-Molecular-Weight Alkanes," *SPE Prod. Oper.*, vol. 24, no. 2, pp. 5–8, 2009.

[12] T. Maqbool, A. Balgoa, and H. Fogler, "Revisiting asphaltene precipitation from crude oils: A case of neglected kinetic effects," *Energy Fuels*, no. 9, pp. 3681–3686, 2009.

[13] C. Vilas Bôas Fávero, T. Maqbool, M. Hoepfner, N. Haji-Akbari, and H. S. Fogler, "Revisiting the flocculation kinetics of destabilized asphaltenes," *Adv. Colloid Interface Sci.*, vol. 244, pp. 267–280, 2017.

[14] N. Haji-Akbari, P. Masirisuk, M. P. Hoepfner, and H. S. Fogler, "A Unified Model for Aggregation of Asphaltenes," *Energy Fuels*, vol. 27, no. 5, pp. 2497–2505, May 2013.

[15] J. Beck, W. Svrcek, and H. Yarranton, "Hysteresis in asphaltene precipitation and redissolution," *Energy Fuels*, vol. 19, no. 3, pp. 944–947, 2005.

[16] M. P. Hoepfner, "Investigations into Asphaltene Deposition, Stability, and Structure, PhD thesis," University of Michigan, 2013.

[17] M. P. Hoepfner, V. Limsakoune, V. Chienmeechao, T. Maqbool, and H. S. Fogler, "A

Fundamental Study of Asphaltene Deposition," *Energy Fuels*, no. 27, pp. 725–735, 2013.

[18] W. Chaisoontornyotin, N. Haji-Akbari, H. S. Fogler, and M. P. Hoepfner, "A Combined Asphaltene Aggregation and Deposition Investigation," *Energy Fuels*, p. acs.energyfuels.5b02427, 2016.

[19] M. P. Hoepfner, V. Limsakoune, V. Chuenmeechao, T. Maqbool, and H. S. Fogler, "A Fundamental Study of Asphaltene Deposition," *Energy Fuels*, vol. 27, no. 2, pp. 725–735, Feb. 2013.

[20] T. Maqbool, S. Raha, M. P. Hoepfner, and H. S. Fogler, "Modeling the Aggregation of Asphaltene Nanoaggregates in Crude Oil−Precipitant Systems," *Energy Fuels*, vol. 25, pp. 1585–1596, 2011.

[21] S. K. Friedlander, *Smoke, dust, and haze: Fundamnetals of aerosol dynamics*. 2000.

[22] P. L. Krapivsky, S. Redner, and E. Ben-Naim, *A kinetic view of statistical physics*. 2011.

[23] I. D. Morrison and S. Ross, *Colloidal dispersions : suspensions, emulsions, and foams*. Wiley-Interscience, 2002.

[24] J. N. Israelachvili, *Intermolecular and surface forces*. Academic Press, 2011.

[25] J. S. Buckley, G. J. Hirasaki, Y. Liu, S. Von Drasek, J.-X. Wang, and B. S. Gill, "Asphaltene Precipitation and Solvent Properties of Crude Oils," *Pet. Sci. Technol.*, vol. 16, no. 3–4, pp. 251–285, 1998.

[26] N. Haji-Akbari, P. Teeraphapkul, A. T. Balgoa, and H. S. Fogler, "Effect of *n* -Alkane Precipitants on Aggregation Kinetics of Asphaltenes," *Energy Fuels*, vol. 29, no. 4, pp. 2190–2196, 2015.

[27] D. L. Mitchell and J. G. Speight, “The solubility of asphaltenes in hydrocarbon solvents,” *Fuel*, vol. 52, no. 2, pp. 149–152, Apr. 1973.

[28] P. Srikiratiwong, “Effects of n-alkane precipitants and temperature on the kinetics of asphaltene precipitation, MS Thesis,” Chulalongkorn University, 2010.

[29] N. Haji-Akbari, P. Teeraphapkul, and H. S. Fogler, “Effect of Asphaltene Concentration on the Aggregation and Precipitation Tendency of Asphaltenes,” *Energy Fuels*, vol. 28, no. 2, pp. 909–919, Feb. 2014.

CHAPTER III

Polydispersity, Fractionation, and Characterization of Asphaltenes

3.1. Introduction

Asphaltenes are the molecules in crude oil that can be dissolved in aromatic solvents, such as toluene, and that will precipitate in presence of n-alkanes, such as heptane. There is an immense number of different molecules in crude oil that are classified as asphaltenes [1]. Molecules classified as asphaltenes share three features: (1) They have both aliphatic and aromatic carbons in their molecular structure, (2) they have sulfur, nitrogen, and oxygen as heteroatoms, and (3) they can have a number of heteroatoms metals such as have nickel, vanadium, and iron in their structure. The ratio between aliphatic and aromatic carbons (i.e., the aromaticity) will vary for each molecule, and so will the number of the heteroatoms and organometallics. Theoretically, one could measure the aromaticity of every single molecule of asphaltenes from a given crude oil, and then compute the aromaticity distribution of asphaltenes, i.e., plot of abundancy (e.g., %) as a function of aromaticity. The shape of this distribution would constitute the so-called asphaltenes polydispersity, in this case polydispersity of the aromaticity. The same type of distribution and polydispersity can theoretically be obtained for the other asphaltene molecular properties.

When an n-alkane is added to crude oil, a fraction of the asphaltenes will destabilize. As the concentration of n-alkane in oil increases, the fraction of asphaltenes that become unstable increases. The difference in the amount of asphaltenes that are unstable in two different n-alkane concentrations, say 40 and 80 vol% of heptane, is attributed to the asphaltene polydispersity. Within the solubility class of asphaltenes, some of the molecules will be destabilized at a 40 vol%

of heptane, but other molecules will require 80 vol% of heptane to destabilize. Therefore, one would expect a difference between the asphaltene molecules that are destabilized at 40 vol% of heptane and the ones that require 80 vol% of heptane to destabilize. This difference is a manifestation of asphaltene polydispersity.

For a fixed concentration of n-alkane in oil, the amount of unstable asphaltenes that grow to sizes that can be removed by centrifugation increases with time. A hypothesis for the early and late removal of asphaltenes is shown in Figure 3.1 (a). The mass of asphaltenes that aggregated and were removed by centrifugation as a function of time for a mixture of 46.5 vol% heptane in crude oil K1 is shown in Figure 3.1 (b).

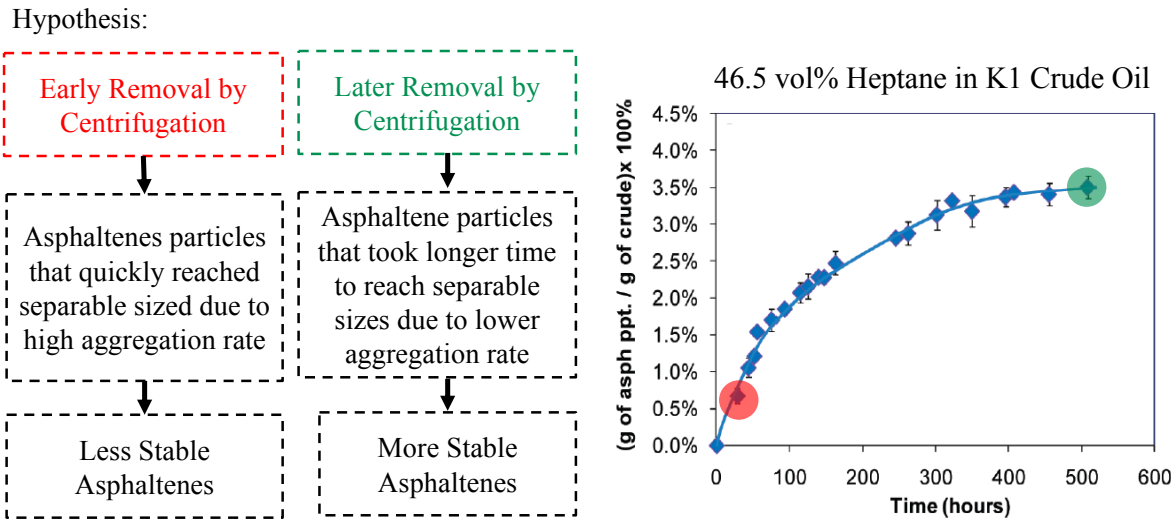

(a) (b)

Figure 3.1 – (a) Mass of asphaltene removed by centrifugation as a function of time [2] and (b) hypothesis that relates removal of asphaltenes from oil-heptane mixture at different times having different stability.

Experimental results in Figure 3.1 show that some asphaltenes grow to sizes that can be centrifuged out of the mixture 20 hours after heptane addition to crude oil K1, while some

asphaltenes required over 500 hours of oil-heptane contact time to grow to sizes that can be removed by centrifugation. It is supposed that the asphaltenes removed at 20 hours grew faster and are less stable than the ones removed after 500 hours. Therefore, the difference in the mass of asphaltenes removed at early versus later times can also be attributed to the polydispersity of asphaltenes.

In this investigation, the destabilization and aggregation kinetics of fractions of asphaltenes were investigated. Two types of fractionations were conducted in this investigation. In the first type of fractionation, asphaltene fractions were obtained at a fixed heptane concentration in oil-heptane mixtures but at different aging times. This fractionation is the time-based fractionation. In the second type of fractionation, fractions were obtained at a fixed time for different heptane concentrations in the oil-heptane mixture. This fractionation is the solubility-based fractionation. The kinetics of destabilization and aggregation of these fractions was studied by measuring the detection time curve and the centrifugation-precipitation curve of the model oil of these fractions. The detection time curve is the time required for asphaltene particles to reach the detectable size of 0.5 um, using optical microscopy, in an oil-heptane mixture as a function of the heptane concentration. The centrifugation-precipitation curve is amount of precipitated asphaltenes from an oil-heptane mixture as a function of the heptane concentration. *The relative stability of these fractions will be ranked according to their detection time curve. The fractions that require a higher heptane concentration to yield a detection time of 1 hour, for instance, are said to be more stable than a asphaltene that require a lower heptane concentration for same detection time.*

It is believed that the aromaticity, quantity of heteroatoms, and quantity of metals in molecules dictates the stability of asphaltenes. However, the relationship between each of these

three parameters and the asphaltene stability is not yet established. Attempting to establish this relationship by studying whole asphaltenes is challenging given that their stability would depend simultaneously on aromaticity, quantity of heteroatom, and quantity of metals in molecules, which are all present in whole asphaltenes. However, it is expected that the portions of asphaltenes obtained with the fractionation methods, i.e., solubility- and time-based fractionations, will have different stabilities and possibly different composition. For instance, suppose that aromaticity is a leading parameter determining the stability of asphaltenes and suppose increase in aromaticity result in decrease of asphaltene stability. In this case, a fractionation method that generate asphaltene fractions with different stability would consequently generate fractions with different aromaticity than the original asphaltenes. It is also expected that the asphaltene fractions will have a smaller polydispersity in aromaticity than the unfractionated asphaltenes. With the aim of relating asphaltene stability to asphaltene composition, the asphaltene fractions were characterized using elemental analysis (i.e., carbon, hydrogen, and nitrogen content). In addition to elemental analysis, the solubility parameter as measured by the aggregation model [3] and the radius of gyration in toluene [4] were also obtained.

3.2. Experimental Methods

3.2.1. Fractionation of asphaltenes

Asphaltenes were extracted from our crude oils A, B, and C using n-heptane as precipitant at a ratio of 40 volumes of heptane for 1 volume of crude oil. After extraction, asphaltenes were washed with n-heptane, and dried in oven at 70^{o}C. The asphaltenes extracted from crude oil A, B, and C are called asphaltenes A, B, and C, respectively.

A schematic of the fractionation procedure is presented in Figure 3.2.

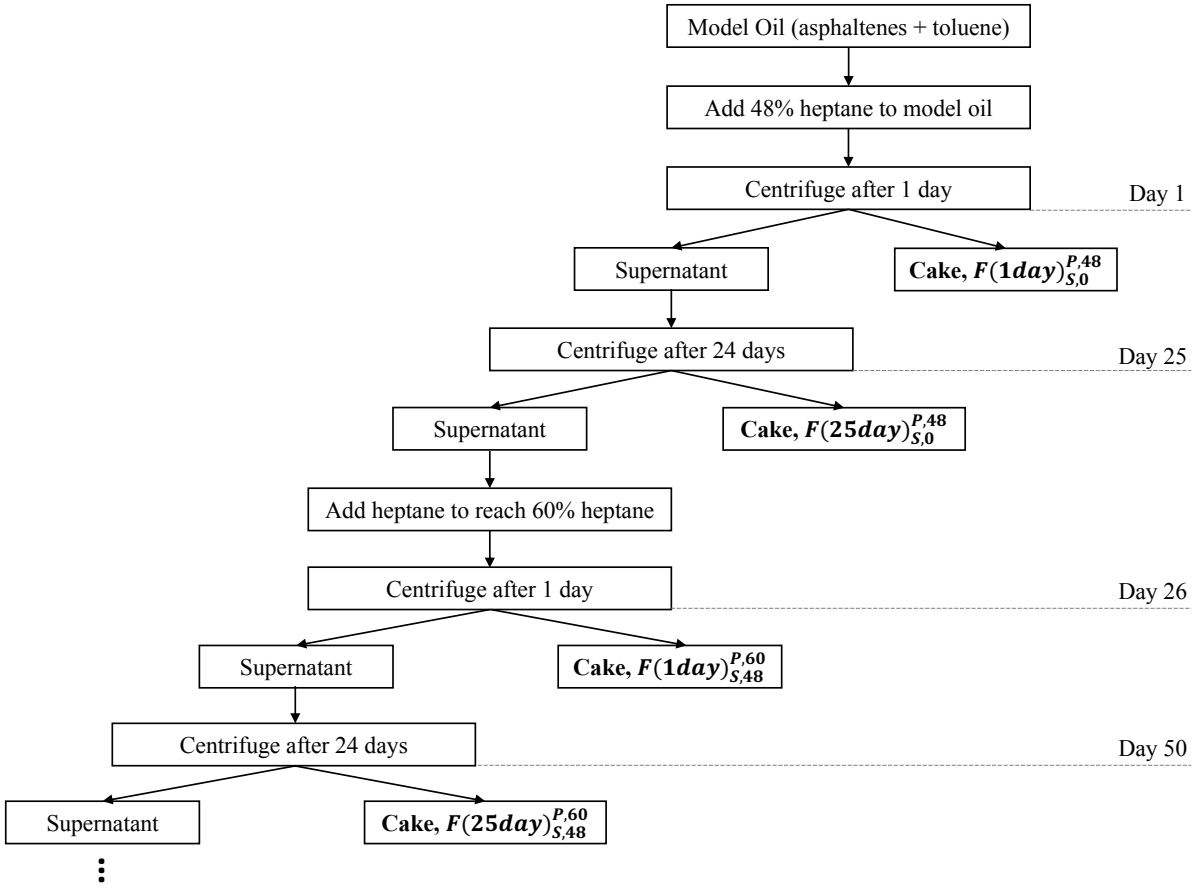

Figure 3.2 - Schematic of the solubility-based and time-based fractionation process used in this investigation

The fractionation procedure, solid asphaltenes were added to toluene to obtain a model oil containing 8 wt% of asphaltenes. The model oil is kept under agitation until all asphaltenes are dissolved and no particles can be detected under optical microscopy. Heptane is then added to the model oil to obtain an oil-heptane mixture of 48 vol% of heptane. One day (twenty four hours) after the heptane addition, the oil-heptane mixture is centrifuged to obtain a supernatant and a centrifugation cake, which constitute the first asphaltene fraction. This fraction of asphaltenes was

soluble in pure model oil, i.e., 0 vol% heptane, but precipitated 1 day after addition of 48 vol% of heptane to model oil. The nomenclature adopted for this fraction is $F(1day)_{S,0}^{P,48}$.

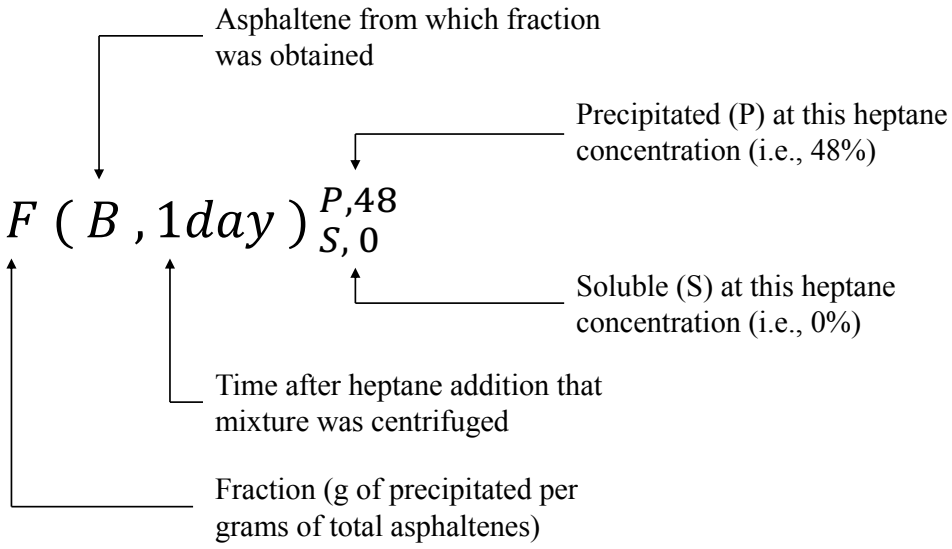

Figure 3.3 – Notation used to name asphaltene fractions

The supernatant of the centrifugation after 1 day was then aged for 24 days and centrifuged again. The cake obtained in this second centrifugation will be called $F(25day)_{S,0}^{P,48}$. Next, more heptane will be added to the supernatant of the second centrifugation to obtain a mixture containing 60 vol% of heptane. One day after the second addition of heptane, the mixture is centrifuged to obtain a new cake, $F(1day)_{S,48}^{P,60}$. This supernatant is aged for 24 days and centrifuged to obtain one more cake, $F(25day)_{S,48}^{P,60}$. Two more steps of fractionation were performed but are not shown in the schematics from Figure 3.2. The notation used to name the asphaltene fractions is explained in Figure 3.3.

The list of all fractions obtained for Asphaltenes B and C are shown in Table 3.1.

Table 3.1 - Solubility-based and time-based fractionation of asphaltenes B and C

Heptane Concentration	Aging Time Before Centrifugation	Fractions of Asphaltenes B	Fractions of Asphaltenes C	Days since first heptane addition
48	1 day	$F(B, 1day)_{S,0}^{P,48}$	$F(C, 1day)_{S,0}^{P,48}$	1
	25 days	$F(B, 25day)_{S,0}^{P,48}$	$F(C, 25day)_{S,0}^{P,48}$	25
60	1 day	$F(B, 1day)_{S,48}^{P,60}$	$F(C, 1day)_{S,48}^{P,60}$	26
	25 days	$F(B, 25day)_{S,48}^{P,60}$	$F(C, 25day)_{S,48}^{P,60}$	50
70	1 day	$F(B, 1day)_{S,60}^{P,70}$	$F(C, 1day)_{S,60}^{P,70}$	51
	25 days	$F(B, 25day)_{S,60}^{P,70}$	-	75
96	1 day	$F(B, 1day)_{S,70}^{P,96}$	$F(C, 1day)_{S,70}^{P,96}$	76

3.2.2. Detection Time Experiments

The detection time curve of asphaltene destabilization was obtained for asphaltene B and C and for each fraction of asphaltenes B and C. The asphaltene of interested was first dissolved in toluene to obtain a model oil with asphaltene content of 1 wt%. Second, heptane was added to model oil to obtain an oil-heptane mixture of the desired heptane volume fraction. The oil-heptane mixture is then continually inspected under optical microscopy for presence of particles as the mixture ages. The time required for particles to be detected under the microscope is the detection time of destabilization for that given heptane volume fraction. This procedure was repeated for different volume fractions of heptane in oil-heptane and the detection times recorded in order to obtain a plot of the detection time as a function of the volume percent of heptane. The experimental result in this plot is also referred to as detection time curve. Note that optical microscopy can detect

particles of 0.5um and larger. Therefore, the detection time of destabilization is defined as the time required for asphaltenes to reach sizes of 0.5 after addition of n-alkane to oil.

3.2.3. Centrifugation-precipitation curve of asphaltenes

The centrifugation-precipitation curve of asphaltenes was obtained for unfractionated and fractionated asphaltenes. The asphaltene of interested was first dissolved in toluene to obtain a model oil with asphaltene content of 1 wt%. Second, heptane was added to model oil to obtain an oil-heptane mixture of the desired heptane volume fraction. One hour after the addition of heptane to oil, the oil-heptane mixture was centrifuged in a 1.5 mL centrifuge tube for 10 minutes at 16,000 g-force. After centrifugation, a cake of asphaltenes was obtained and supernatant was decanted. The centrifugation cake was dried, and mass of cake was measured. This procedure was repeated for different volume fractions of heptane in oil-heptane and the masses of dried centrifugation are recorded. A plot of mass of cake as a function of the volume percent of heptane in the oil-heptane mixture is obtained as result. The experimental result in this plot is also referred to as centrifugation-precipitation curve.

3.2.4. Radius of gyration of asphaltenes in toluene

Bruker Nanostar SAXS Equipment was used to perform scattering measurements of asphaltenes dissolved in deuterated toluene. The concentration of asphaltenes in the asphaltene-toluene mixture if 1 wt%. The X-ray generator was set at 40 kV and 35 mA with 0.5 second per frame and 900 second per sample. Guinier approximation was then used to get an average shape-independent size, radius of gyration, for asphaltenes.

3.2.5. Hydrogen, carbon, and nitrogen content of asphaltenes

The content of carbon, hydrogen, and nitrogen of the asphaltenes were determined by standard combustion method using a Carlo Erba model 1108 analyzer.

3.3. Experimental Results

The quantity in each fraction of asphaltenes in terms of percentage of total asphaltenes is shown in Table 3.2.

Table 3.2 – Percentage of unfractionated asphaltenes that constitutes each fraction (g fraction/g unfractionated)%

	Fractions of Asphaltenes B	**Fractions of Asphaltenes C**
$F(1day)_{S,0}^{P,48}$	0	22.3
$F(25day)_{S,0}^{P,48}$	0	10.9
$F(1day)_{S,48}^{P,60}$	28.8	32.1
$F(25day)_{S,48}^{P,60}$	10.1	3.87
$F(1day)_{S,60}^{P,70}$	28.2	8.53
$F(25day)_{S,60}^{P,70}$	6.90	- -
$F(1day)_{S,70}^{P,96}$	26.0	22.3
Unfractionated	100	100

When fractionating asphaltenes B, the centrifugation of the oil-heptane mixture containing 48 vol% of heptane at 1 and 25 days generated no cakes. For this reason, the quantity of $F(\mathrm{B}, 1day)_{S,0}^{P,48}$ and $F(\mathrm{B}, 25day)_{S,0}^{P,48}$ are indicated as 0 in Table 3.2.

When fractionating asphaltenes C, no centrifugation was performed for oil-heptane mixture containing 70 vol% of heptane after 25 days, i.e., $F(25day)^{P,70}_{S,60}$. For this reason, a hyphen is placed in Table 3.2.

3.3.1. Time-based fractionation of asphaltenes

Hypothesis: *For a fixed heptane concentration, asphaltenes precipitated earlier in time are less stable than asphaltenes precipitated later in time.*

In the time-based fractionation, asphaltene fractions are obtained at a fixed heptane volume fraction in oil-heptane mixtures but at different aging times. The experimental results for time-based fractionation are shown in Figure 3.4.

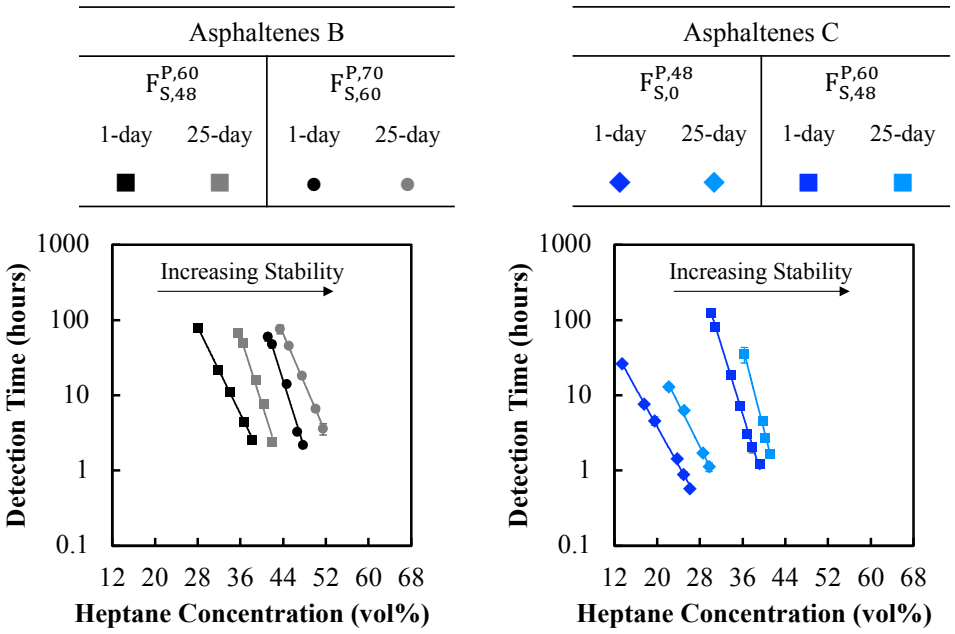

(a) (b)

Figure 3.4 – Detection time curves of asphaltenes obtained with time-based fractionation for (a) Asphaltenes B (b) and Asphaltenes C

The detection time curves presented in Figure 3.4 show that the time-based fractionation generates asphaltene fractions that have different detection time curves. The relative stability of these fractions can be ranked based on their detection time curves, for example, the fractions that requires a higher heptane concentration to yield a detection time of 10 hours, e.g., $F(\mathrm{B})_{\mathrm{S},48}^{\mathrm{P},60}$ after 25 days, is said to be more stable than a asphaltene that require a lower heptane concentration for same detection time, e.g., $F(\mathrm{B})_{\mathrm{S},48}^{\mathrm{P},60}$ after 1 day. This definition of relative stability is applied to detection time curves that have approximately same slope, which is the case here.

These results validate the hypothesis presented in Figure 3.1 that states that the asphaltene fraction obtained 1 day after heptane addition undergos a faster aggregation process than the fraction obtained after 25 days. The difference in the rate of aggregation translates to difference in the detection time curve, shown in Figure 3.4, and finally a difference in stability.

3.3.2. Solubility-based fractionation of asphaltenes

Hypothesis: *Asphaltenes precipitated at a lower heptane concentration are less stable than asphaltenes precipitated at a higher heptane concentration*

In the solubility-based fractionation, fractions are obtained at different heptane concentrations in oil-heptane mixture. The detection time curves for asphaltene fractions obtained by the solubility-based fractionation are presented in Figure 3.5. The detection time of the unfractionated asphaltenes are shown in red for reference.

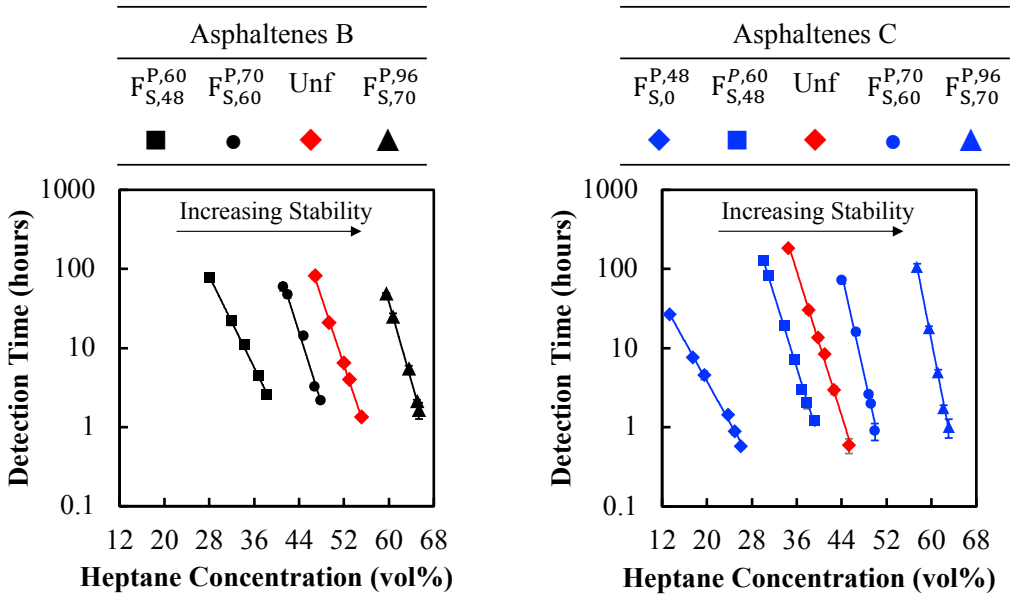

Figure 3.5 – Detection time curve of asphaltenes fractions obtained by solubility-based fractionation. (a) Asphaltenes B, and (b) Asphaltenes C.

It can be seen from Figure 3.5 that the solubility-based fractionation generated asphaltene fractions that have different detection time curves. This result validates the hypothesis that the asphaltenes precipitated at a lower heptane concentration are less stable than asphaltenes precipitated at a higher heptane concentration.

Experimental results from Figures 3.4 and 3.5 have shown that the asphaltenes B and C are comprised of fractions of asphaltenes of different stabilities. The stability of the unfractionated asphaltenes, as measured by the detection time curve, falls in between the detection time curve of its fractions. This trend will be discussed in Section 4.2 where detection time curve of recombined asphaltene fractions is presented.

3.3.3. Radius of gyration of asphaltenes and fractions of asphaltenes

The radius of gyration of the unfractionated and fractionated asphaltenes when suspended in toluene were using measured using small angle X-ray scattering Radius of gyration was obtained via Guinier fitting at small scattering angles. Experimental results are shown in Figure 3.6.

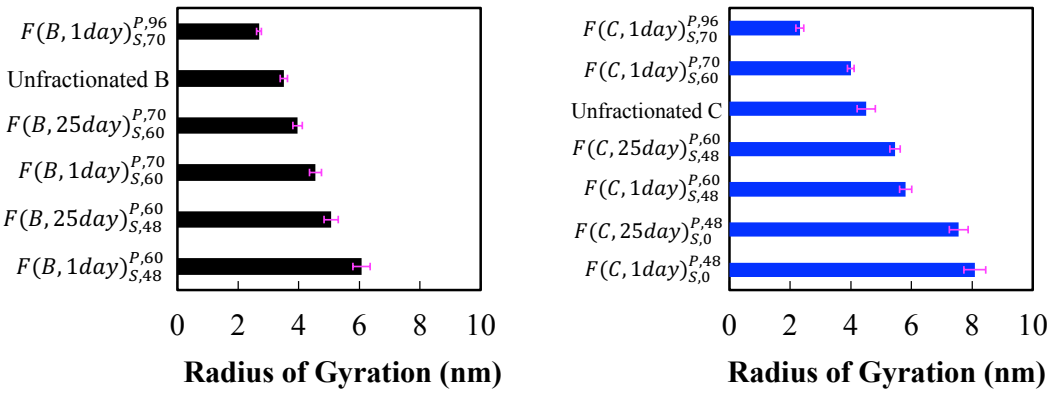

(a) (b)

Figure 3.6 – Radius of gyration of asphaltenes, whole and fractionated, when suspended in toluene as measured by small angle X-ray scattering. (a) Asphaltene B and (b) Asphaltene C

Experimental results presented in Figure 3.6 show that the fractions of asphaltenes have different radius of gyrations when suspended in toluene. The fraction $F(\mathrm{B}, 1day)^{\mathrm{P,60}}_{\mathrm{S,48}}$, which is the least stable fraction of asphaltene B with detection time curve on the most left in Figure 3.6 (a), has the largest radius of gyration among all asphaltene B fractions. On the other hand, the fraction $F(\mathrm{B}, 1day)^{\mathrm{P,96}}_{\mathrm{S,70}}$, which is the most stable fraction with the detection time curve to the most right in Figure 3.6 (b), has the smallest radius of gyration of all fraction of asphaltene B. Similar trends are observed for asphaltene C. These results indicate that there is a relationship between the asphaltene radius of gyration and their stability and this relationship will be discussed in section 4.3.

3.3.4. Solubility of asphaltenes, fractions of asphaltenes, and blend of asphaltene fractions in toluene

Hypothesis: *Asphaltenes with higher stability can dissolve asphaltenes of lower stability in toluene*

Three fractions of asphaltenes A were obtained: $F(A)_{S,0}^{P,42}$, $F(A)_{S,42}^{P,75}$ and $F(A)_{S,75}^{P,95}$ and used for further investigation. In regard to the amount of asphaltene precipitated, the mass fraction of $F(A)_{S,0}^{P,42}$ corresponded to about 20 wt% of the total asphaltenes in the model oil, fraction $F(A)_{S,42}^{P,75}$ corresponded to 79 wt%, and fraction $F(A)_{S,75}^{P,95}$ corresponded to 1 wt% of asphaltenes A. Three model oils were prepared with these fractions. The first model oil consisted of 1 wt% $F(A)_{S,0}^{P,42}$ in toluene, the second model oil contained 1 wt% $F(A)_{S,42}^{P,75}$ in toluene, and the third model oil contained 1wt% of $F(A)_{S,75}^{P,95}$ in toluene. It was observed that the model oil of fraction $F(A)_{S,0}^{P,42}$ did not dissolve entirely based on an optical microscopy analysis. This result is intriguing, given that for the model oil containing 1 wt% of unfractionated asphaltenes A, all asphaltenes were dissolved. It was then hypothesized that in order to dissolve $F(A)_{S,0}^{P,42}$ in toluene, the other fractions of asphaltenes A need to be present in the model oil. This change in the solubility of asphaltenes is likely due to a change in size of asphaltene clusters formed in the model oil. To test this hypothesis, an experiment was performed where five model oils, each containing 1 wt% of $F(A)_{S,0}^{P,42}$ in toluene, were prepared. Next, different amounts of $F(A)_{S,75}^{P,95}$ were added to these model oils. The concentrations of $F(A)_{S,75}^{P,95}$ in the model oils ranged from 0 to 1 wt%. The amount of dissolved asphaltenes in each model oil was then measured by centrifuging the model oil for 10 minutes at 16,000 g-force in a 1,5 mL centrifuge tube. The supernatant of centrifugation if decanted, and

centrifugation cake is dried. It is expected that the mass of undissolved asphaltenes decreases as fraction $F(A)_{S,75}^{P,95}$ is added to the model oil. The experimental results of mass of undissolved asphaltenes as a function of mass fraction of $F(A)_{S,75}^{P,95}$ are shown in Figure 3.7.

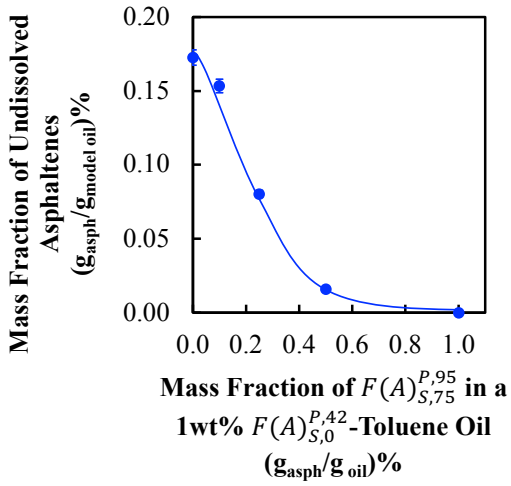

Figure 3.7 – Mass fraction of undissolved asphaltenes as a function of fraction of $F(A)_{75,S}^{95,P}$ added to a 1 wt% $F(A)_{0,S}^{42,P}$ model oil.

It was observed that for the model oil containing no $F(A)_{S,75}^{P,95}$, 17 wt% of asphaltenes could not be dissolved in toluene. However, as the mass fraction of $F(A)_{S,75}^{P,95}$ increased, more asphaltenes were dissolved up to the point where no asphaltenes could be centrifuged out anymore to form a cake. One possible explanation to the reduction in centrifugation cake size is that the asphaltene particles became smaller in diameter and, consequently, can no longer be centrifuged out of the oil at constant centrifugation conditions. In order to test this hypothesis, the size of asphaltenes in the model oil would have to be measured using a technique such as small angle scattering.

The results from Figure 3.7 also indicate the importance of asphaltene-asphaltene interactions in the solubility of asphaltenes in model oil. Two important implications are

conjectured based on the importance of this interaction. First, asphaltenes with a higher stability will help dissolve the asphaltenes of lower stability. And second, when two asphaltene fractions are combined in a model oil, the size of the combined asphaltenes is different than the size that would be obtained by superimposing the sizes of the separate fractions in model oil.

3.3.5. Centrifugation-precipitation curves of asphaltenes, asphaltene fractions, and blend of asphaltene fractions

Hypothesis: *Asphaltene fractions obtained by solubility-based fractionation have different centrifugation-precipitation curves*

The centrifugation-precipitation curves of unfractionated and fractionated asphaltenes A were obtained and compared. To construct the centrifugation-precipitation curve, 1 wt% of each of the fractions was dissolved in toluene to form a model oil. Heptane was added to the model oil, and the oil-heptane mixture was centrifuged to form and separate the precipitated asphaltene cake. The mass of cake was obtained for different concentrations of heptane in oil-heptane mixture. The experimental results are shown in Figure 3.8.

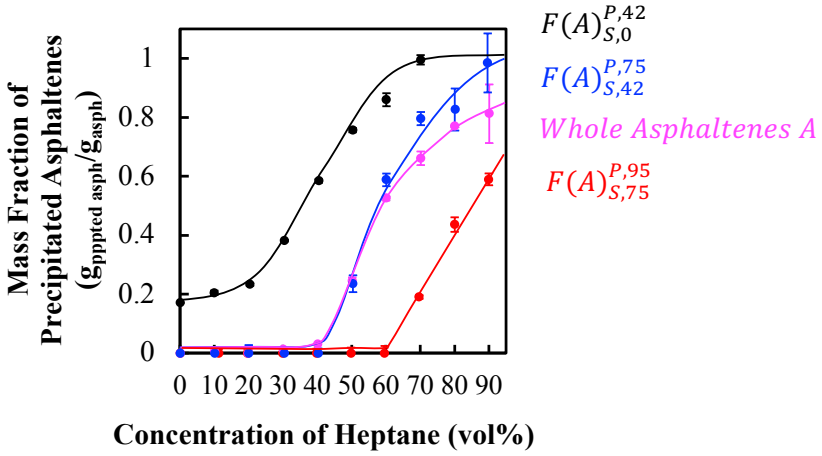

Figure 3.8 – Fraction of precipitated asphaltenes in model oil as a function of heptane concentration for the whole and fractionated asphaltenes.

The results in Figure 3.8 show that the solubility-based fraction generates fractions that have vastly different centrifugation-precipitation curves. While 20 wt% of $F(A)_{S,0}^{P,42}$ is precipitated by 10 vol% of heptane, it takes about 70 vol% of heptane to precipitate the same quantity as the fraction $F(A)_{S,75}^{P,95}$. Additionally, the centrifugation-precipitation curve of the unfractionated asphaltenes A falls in between the centrifugation-precipitation curves of the fractions $F(A)_{S,0}^{P,42}$ and $F(A)_{S,75}^{P,95}$.

Hypothesis: *The centrifugation-precipitation curves of the combined fractions is not equal to the superposition of the centrifugation-precipitation curves of individual fraction.*

Once again it is observed that the behavior of asphaltenes in solutions greatly depend on the asphaltene-asphaltene interactions. In order to verify the importance of the asphaltene-asphaltene interactions, the centrifugation-precipitation curve of combined fractions were obtained and compared. To make this comparison, a model oil containing 1 wt% of the $F(A)_{S,0}^{P,42}$ fraction

and 1wt% of the $F(A)_{S,75}^{P,95}$ fraction was prepared, and the centrifugation-precipitation curve obtained. The experimental result is presented in Figure 3.9.

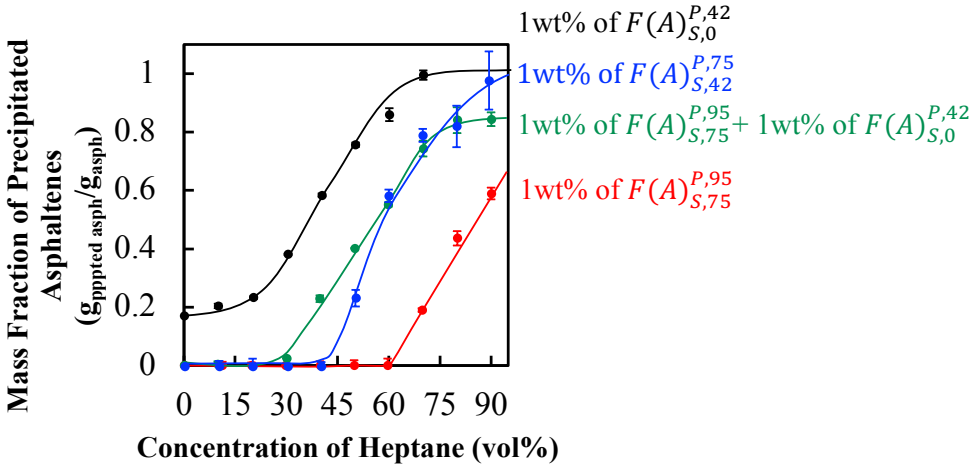

Figure 3.9 - Fraction of precipitated asphaltenes in model oil as a function of heptane concentration a blend of two fractions of asphaltenes.

It can be seen from Figure 3.9 that the solubility curve of the model oil containing the combined fractions yields intermediate values to the separate fractions. Note that the solubility curve of the oil with combined fractions could not be predicted by simple addition of the solubility of the separate fractions. This result once again shows the importance the asphaltene-asphaltene interactions in toluene. In addition, these findings agree with the population balance modeling of asphaltene aggregation where collision efficiency, and therefore stability, of asphaltenes is a function of the heptane concentrations in oil-heptane mixture.

3.4. Discussion

3.4.1. Asphaltene Stability

As previously defined, the relative stability of these fractions was ranked according to their detection time curve. The fractions that require a higher heptane concentration to yield a detection time of 1 hour, for instance, are said to be more stable than an asphaltene that require a lower heptane concentration for same detection time.

Hypothesis: *Asphaltene fractions from different asphaltenes obtained at the same fractionation condition have same stability.*

Solubility-based and time-based fractionations were used to fractionate asphaltenes B and C. The heptane concentrations used for the solubility-based fractionation and the aging times before centrifugation used in the time-based fractionation were chosen such that they are *virtually identical* for fractionation of asphaltenes B and asphaltene C. Therefore, the asphaltene fractions were obtained from different asphaltenes but at the same heptane concentration and aging times of fractionation procedure. The detection time curve of these fractions obtained at the same heptane concentration and aging times are shown in Figure 3.10.

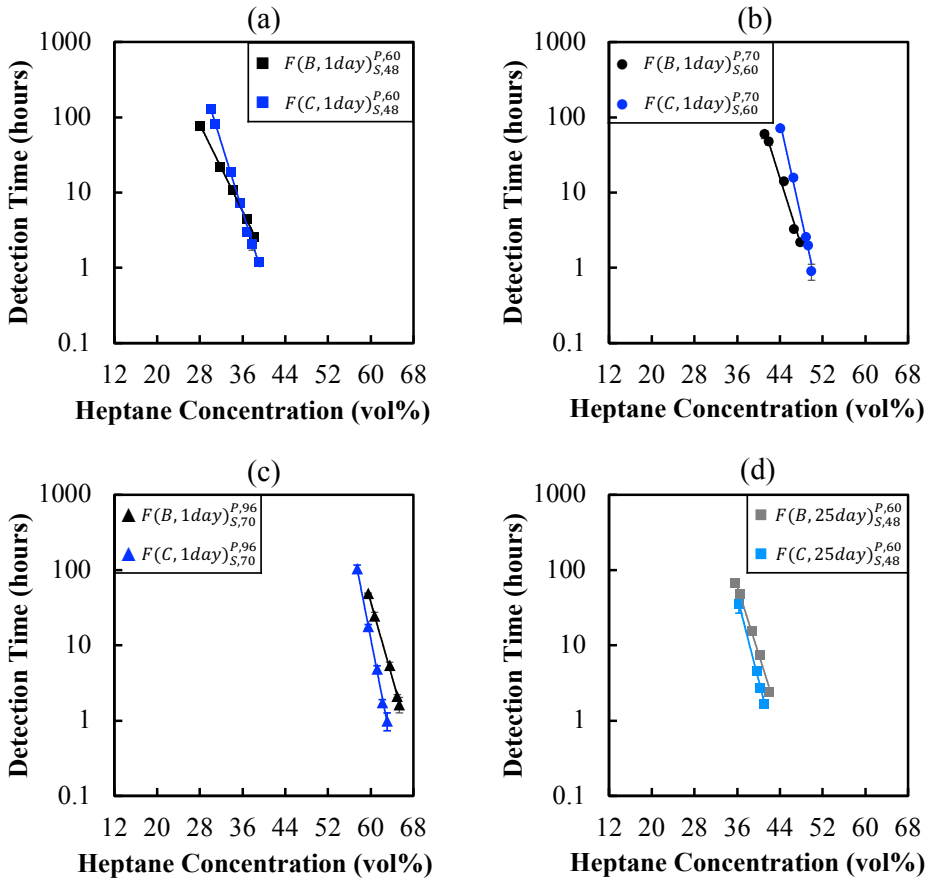

Figure 3.10 - Detection time of asphaltene precipitation for asphaltene fractions obtained at same conditions but from different asphaltenes. Figures (a), (b), (c) correspond to 1 day of aging and Figure (d) correspond to 25 days of aging.

These experimental results (Figure 3.10) show that asphaltene fractions obtained at the same fractionation conditions (e.g., in the case of Figure 3.10 (a) fractions were obtained in 1 day of aging, soluble in 48 vol% of heptane and precipitated at 60 vol% of heptane) but from different asphaltenes have virtually the same detection time curves and, consequently, the same asphaltene stability. This result is striking. It is interesting to note that these fractions with same stability have the same radii of gyration when suspended in toluene, as can be seen in Figure 3.6. They also have the same solubility parameter as measured by the unified aggregation model. However, these fractions do not have the same solubility parameter as measured by the Buckley refractive index

correlation. One question that rises at this point is whether asphaltenes with identical detection time curves would have identical compositions as well. To answer this question, the hydrogen to carbon ratio and nitrogen content of asphaltenes were measured and the experimental results are presented in Figure 3.11.

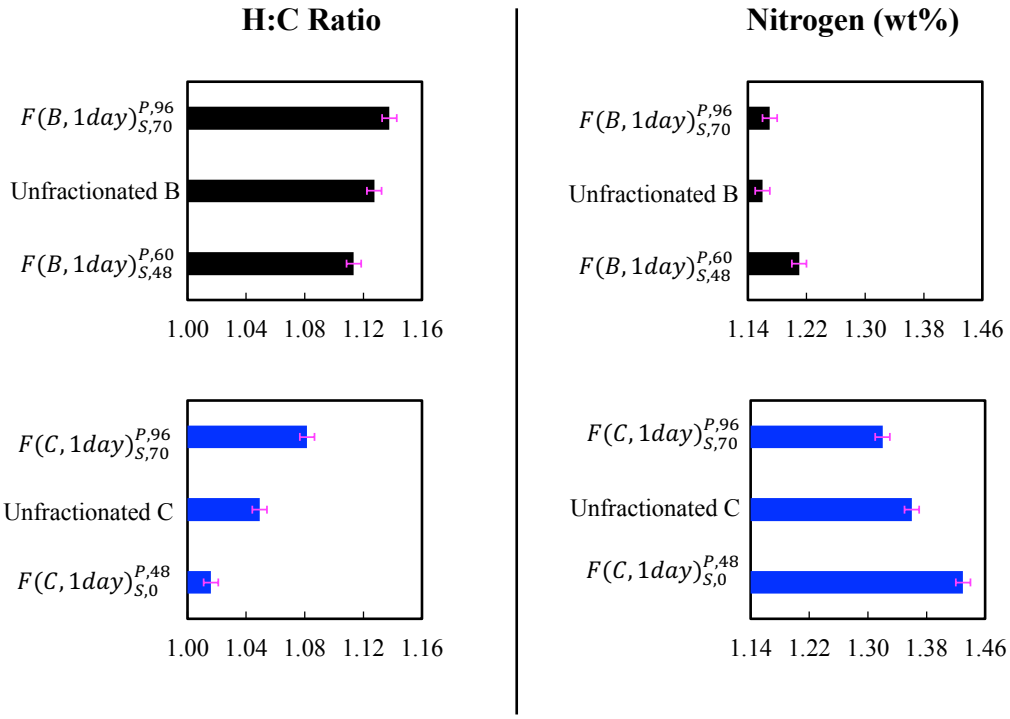

Figure 3.11 – Hydrogen to carbon ratio and nitrogen content of unfractionated and fractionated asphaltenes

One observes that asphaltene fractions with identical stability, i.e., $F(B, 1day)^{P,96}_{S,70}$ and $F(C, 1day)^{P,96}_{S,70}$, have vastly different H:C ratios and nitrogen content. It would be important to identify the molecular properties that fractions $F(B, 1day)^{P,96}_{S,70}$ and $F(C, 1day)^{P,96}_{S,70}$ have in common and that causes these fractions to have identical detection time curves. Further

investigation of this molecular feature can perhaps reveal the mechanism of asphaltene destabilization by n-alkanes.

3.4.2. Detection time curves of combined asphaltene fractions

The solubility parameters of asphaltene fractions $F(B, 1day)_{S,48}^{P,60}$, $F(B, 25day)_{S,60}^{P,70}$, and $F(B, 1day)_{S,70}^{P,96}$ were obtained using the unified aggregation curve, yielded the values of 24.4, 24.0, and 23.6 $MPa^{1/2}$, respectively. The fractions $F(B, 1day)_{S,48}^{P,60}$ and $F(B, 1day)_{S,70}^{P,96}$ were mixed in equal quantities and the solubility parameter of the combined asphaltenes, δ_c, can be calculated as follows

$$\delta_c = \sum \phi_i \delta_i = 0.5 \times 24.4 + 0.5 \times 23.6 = 24.0\ MPa^{\frac{1}{2}} \quad (1)$$

Where δ_c is the solubility parameter of the combined asphaltenes, ϕ_i is the volume fraction of asphaltene fraction *i* in the combined asphaltenes, and δ_i is the solubility parameter of asphaltene fraction *i*. The solubility parameter of asphaltenes can also be calculated using Equation 2.

$$\delta_c^2 = \sum \phi_i \delta_i^2 \quad (2)$$

Given the small differences in the solubility parameter of the asphaltene fractions, calculating the solubility parameter of combined fraction using Equation 2 was expected to lead to comparable results.

The detection time curves for each of the asphaltene fractions and the combined fractions are shown in Figure 3.12.

Concentration of Asphaltenes (wt%)				
■	●	●	▲	
1	0	0.5	0	$F(B, 1day)_{S,48}^{P,60}$
0	1	0	0	$F(B, 25day)_{S,60}^{P,70}$
0	0	0.5	1	$F(B, 1day)_{S,70}^{P,96}$
24.4	24.0	24.0	23.6	$\delta_{asph}(MPa^{\frac{1}{2}})$

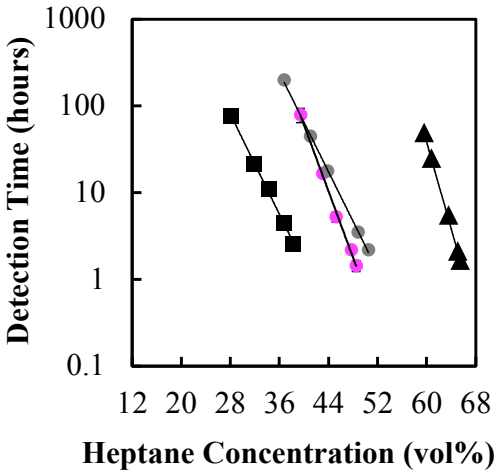

Figure 3.12 – Detection time curve of combined fractions of asphaltenes B

There are two important observations to be made based on the experimental results presented in Figure 3.12. The first observation is related to the detection time of the blend of asphaltene fractions. If the fractions of asphaltenes did not interact when blended, then the detection time curve of the blend would be that of the least stable asphaltenes, i.e., $F(B, 1day)_{S,48}^{P,60}$. However, it can be seen that the blend of fractions yields a detection time curve that falls in between the detection time curves of the individual fractions. Therefore, it can be concluded that the two asphaltenes will interact and behave like an asphaltene with solubility parameter

intermediate to those of the individual fractions. The solubility parameter of the asphaltene blend was calculated using Equation 1 and found to be 24.0 $MPa^{1/2}$. The second observation is regarding the relationship between detection time curve and solubility parameter of asphaltenes. It can be seen that the detection time curves of the blend of fractions (pink dots) and the fraction $F(B, 25day)_{S,60}^{P,70}$ (gray dots) are virtually identical. In addition, the solubility parameter of $F(B, 25day)_{S,60}^{P,70}$ is 24.0 $MPa^{1/2}$, i.e., the same as the solubility parameter of the blend of asphaltene fractions. This result once again indicates the important of asphaltene-asphaltene interactions in the asphaltene stability in solution.

3.4.3. Radius of gyration of asphaltenes suspended in toluene

Experimental results show that fractionating asphaltenes using solubility-based fraction and time-based fractionation generates asphaltene fractions that have different radii of gyration when suspended in toluene. It was also observed that the increase of asphaltene stability resulted in a decrease in radius of gyration. The stability of asphaltenes was evaluated in terms of solubility parameter using the aggregation model. The plot of radius of gyration as a function of solubility parameter of asphaltenes is shown in Figure 3.13 (a). Figure 3.13 (b) shows the plot of radius of gyration as a function of the solubility parameter difference $\left(\delta_{asphaltenes} - \delta_{toluene}\right)^2$.

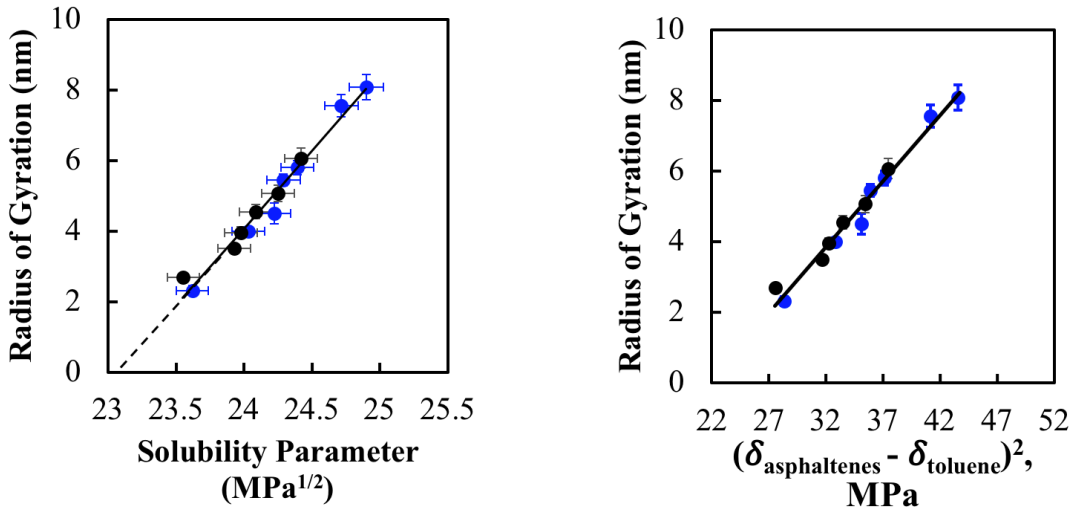

(a) (b)

Figure 3.13 – (a) Radius of gyration of asphaltenes fractions as a function of their solubility parameter and (b) radius of gyration of asphaltenes as a function of the solubility parameter difference $(\delta_{asphaltenes} - \delta_{toluene})^2$.

As it can be seen in Figure 3.13 (a), there exists a linear relationship between radii of gyration of asphaltenes and their solubility parameter. This linear relationship has identical slope and intercept for asphaltenes and fractions of asphaltenes B and C, indicating that regardless of asphaltene origin or fractionation condition, asphaltenes will have the same radius of gyration suspended in toluene *if* they have the same solubility parameter. Therefore, it can be said that the association level of asphaltenes in toluene, in terms of radius of gyration, increases as the attractive forces between asphaltene molecules increases. The attractive forces here are measured in terms of cohesive energy per unit of molecular volume. The extrapolation of the trend obtained in Figure 3.13 (a) indicates that asphaltenes with solubility parameter of 23 $MPa^{1/2}$ would not associate in toluene.

3.5. Conclusions

Time-based and solubility-based fractionations were performed on three asphaltenes of different origins. It was observed that both time-based and solubility-based fractionation generate asphaltene fractions that have different stabilities. Time-based fractionation shows that asphaltenes that precipitated earlier in time on the centrifugation curve are less stable than the asphaltenes that precipitate at a later time.

Measurements of radii of gyration and solubility parameters of asphaltenes revealed a linear relationship between these two quantities. Regardless of asphaltene origin or fractionation condition, as long as they have the same solubility parameter they will have same radius of gyration when suspended in toluene. This result indicates that the grater the cohesive energy per molecular volume, the greater the association of asphaltenes are as measured by the radius of gyration. The correlation obtained can also be used to validate molecular simulations of asphaltene association.

It was also found that asphaltene fractions obtained at the same fractionation condition (e.g., 1 day of aging, soluble at 48 vol% heptane and precipitated at 60 vol% heptane) but from different type of asphaltenes have identical detection time curve and, consequently, same stability. These fractions of identical detection time curve also have same radius of gyration when suspended in toluene and same solubility parameter as measured by the aggregation model. However, they have different composition in terms of carbon, hydrogen, and nitrogen content and also different solubility parameters as measured by the Buckley refractive index correlation.

The findings of this investigation show that asphaltene-asphaltene interaction must be taken in account when computing asphaltene parameters in solution, such as solubility parameter and particle sizes.

3.6. References

[1] K. H. Altgelt and M. M. Boduszynski, *Composition and Analysis of Heavy Petroleum Fractions*, 1st Editio. CRC Press, 1993.

[2] T. Maqbool, A. Balgoa, and H. Fogler, "Revisiting asphaltene precipitation from crude oils: A case of neglected kinetic effects," *Energy Fuels*, no. 9, pp. 3681–3686, 2009.

[3] N. Haji-Akbari, P. Masirisuk, M. P. Hoepfner, and H. S. Fogler, "A Unified Model for Aggregation of Asphaltenes," *Energy Fuels*, vol. 27, no. 5, pp. 2497–2505, May 2013.

[4] M. P. Hoepfner, C. V. B. Fávero, N. Haji-Akbari, and H. S. Fogler, "The fractal aggregation of asphaltenes.," *Langmuir*, vol. 29, no. 28, pp. 8799–808, 2013.

[5] N. Haji-Akbari, P. Teeraphapkul, and H. S. Fogler, "Effect of Asphaltene Concentration on the Aggregation and Precipitation Tendency of Asphaltenes," *Energy Fuels*, vol. 28, no. 2, pp. 909–919, Feb. 2014.

CHAPTER IV

Dissolution of Solid Asphaltenes in Solvents

4.1. Introduction

Asphaltenes are a class of molecules in crude oil that are soluble in aromatics, such as toluene, and insoluble in n-alkanes, such as heptane. During oil production, asphaltenes can deposit on the pores of reservoir and on the wall of wellbore, pipeline, and production equipment [1]. The deposition of asphaltenes can hinder oil production and might require remediation. One common remediation method is the removal of asphaltene deposits using solvents. In this method, an asphaltene solvent, such as xylene, is put in contact with the asphaltene deposit causing the asphaltenes to dissolve. The contact time required for asphaltene deposits to dissolve will depend on the origin of asphaltenes [2] and on the solvent used [3]. In terms of field operation, the contact time that will be used in the remediation is a critical parameter. During remediation, oil production is stopped. Therefore, it is of financial interest to select a contact time of remediation that is long enough to dissolve the deposits while minimizing production down time [4].

The dissolution of asphaltenes has been previously investigated, where it was shown that asphaltenes can be dissolved in mixture of amphiphilic molecules and n-alkanes [3]. The dissolution rate of asphaltenes depended on the n-alkane used and on the amphiphilic molecule used. The dissolution of asphaltene deposits in xylene has also investigated using packed-bed microreactors [4].

In this study, the rate of dissolution of asphaltenes extracted from crude oil is investigated. It is hypothesized that concentration of dissolved asphaltenes on the interface asphaltene-solvent will to depend on the solubility parameter of the asphaltenes and on the solubility parameter of the

solvent. As the difference in solubility parameters increase, asphaltene become insoluble in the solvent, the concentration on the interface decreases and so does the dissolution rate. A schematic of the system is shown in Figure 4.1 [3].

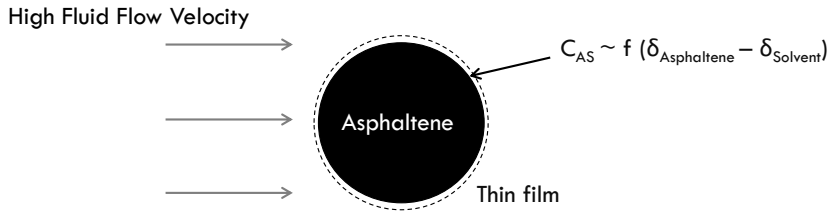

Figure 4.1 – Schematic of asphaltene dissolution of a single particle in a solvent.

The goals of this work are twofold: to develop a method to measure the intrinsic rate of solid asphaltene dissolution in solvents, and determine, if any, relationship between asphaltene dissolution rate and their solubility parameter.

4.2. Experimental Methodology

Asphaltenes are extracted from crude oils A, B, C and D at a 40 to 1 ratio of heptane to oil. Asphaltenes extracted from crude oil A, B, C and D will be referred to as asphaltenes A, B, C and D, respectively. Note that these crude oils and asphaltenes are not the same as the ones in the other Chapters of this dissertation. After extraction, asphaltenes are then dried in oven at 70^{o}C and then sieved to obtain particle sizes in the between 38 to 75um. The sieved particles are then placed on a membrane of polytetrafluoroethylene (PTFE) with pore size of 0.45um in a Milli-Q filter holder that serves as dissolution unit as shown in Figure 4.2 (b). Asphaltenes are added to the dissolution unit with the help of a sieve to assure the particles are homogenously distributed on the top of the membrane. The mass of asphaltenes added to the dissolution unit for an experiment is measured. The solvent is then injected in the dissolution unit at a constant flow rate, and the effluent is collected in small aliquots. The concentration of asphaltenes in each aliquot of the effluent is

measured using a UV-Vis spectrophotometer and a calibration curve obtained at wavelength of 500nm. The schematics of the asphaltene dissolution experiments is shown in Figure 4.2. Similar apparatus has been used in previous study [3].

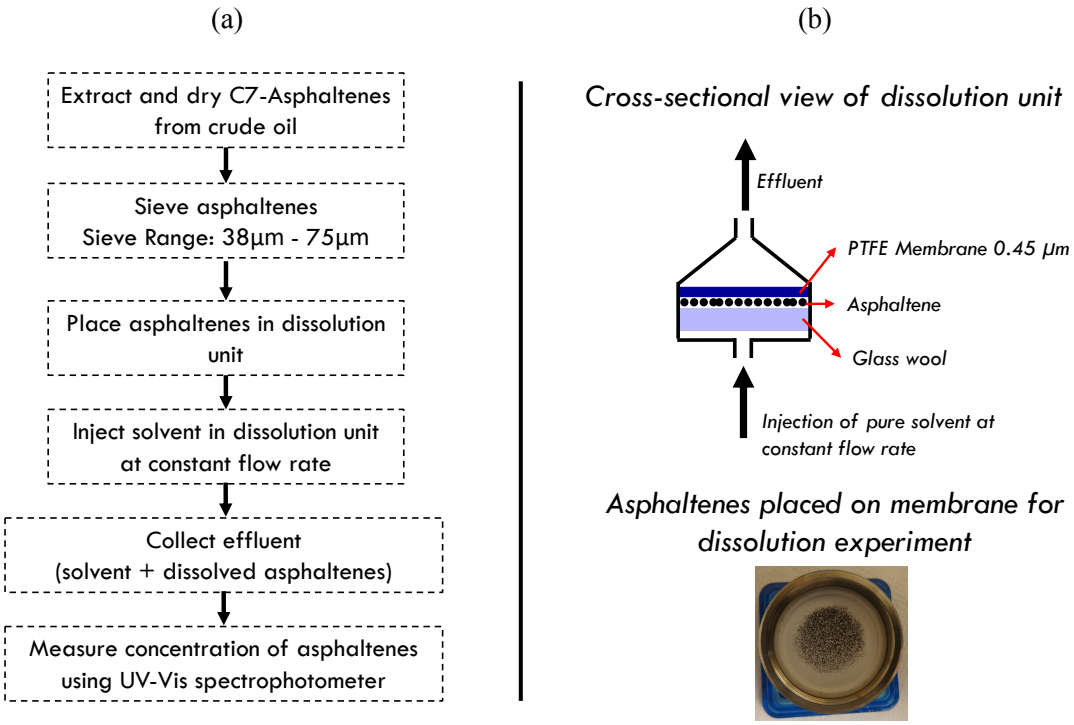

Figure 4.2 – Schematics of the asphaltene dissolution experiment. (a) Experimental procedure, (b) dissolution unit.

Figure 4.3 shows the typical curve of the asphaltene concentration in effluent as a function of volume passed through the dissolution unit. Figure 4.3 (top) shows the vials containing the aliquots of the effluent as the asphaltenes dissolved.

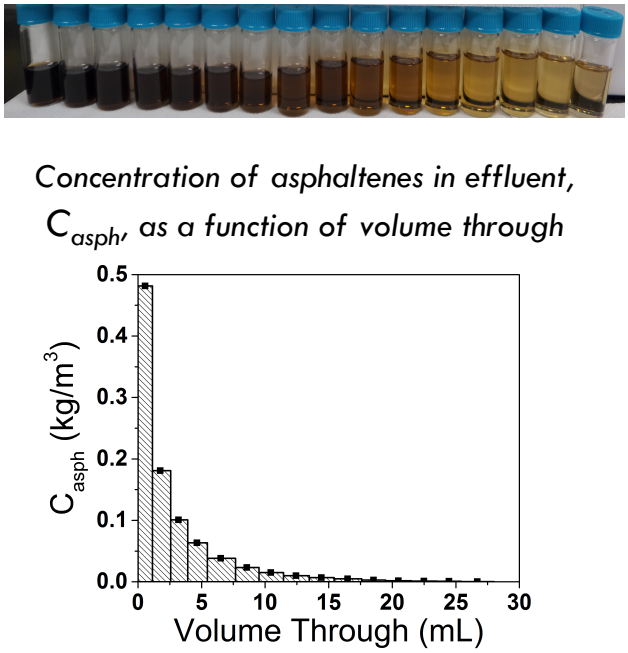

Figure 4.3 – Typical curve of concentration of asphaltenes as a function of volume through

The experimental results presented in Figure 4.3 show that the concentration of asphaltenes in the effluent decreases as solvent is flown through the dissolution unit. The highest concentration of asphaltenes in the effluent is for the first aliquot obtained. This decay in concentrations occur because the amount of asphaltenes available to dissolve in the dissolution unit decreases.

In order to test the reproducibility of the experimental measurements of asphaltene concentration versus volume through, 1.5 mg of asphaltenes D with particle sizes between 38 and 75um are placed in the dissolution unit and the concentration profile of effluent is measured at the flow rate of 60mL/min and 100mL/min. Toluene is used as solvent. The experimental results are shown in Figure 4.4.

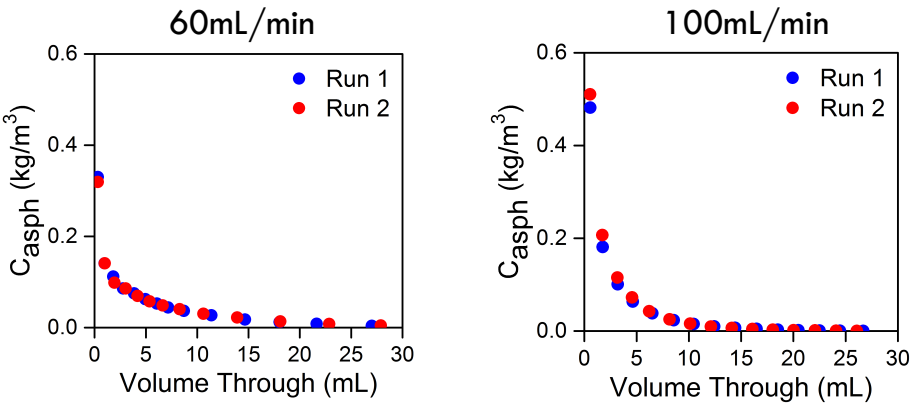

Figure 4.4 – Reproducibility of asphaltene dissolution experiment

Experimental results presented in Figure 4.4 show that the concentration profile of asphaltene dissolution are reproducible within 5% of variance.

A mass balance on the asphaltenes is performed for validation of the dissolution technique. From a mass balance, it is known that the mass of asphaltenes loaded initially in the unit must be equal to the mass of asphaltenes dissolved added to the mass of asphaltenes that remains undissolved on the membrane. For this test, 1.5 mg of asphaltenes D with particle sizes between 38 and 75um are placed in the dissolution unit. Toluene is used as solvent. A plot of the mass of dissolved and undissolved asphaltenes for each experiment are shown in Figure 4.5.

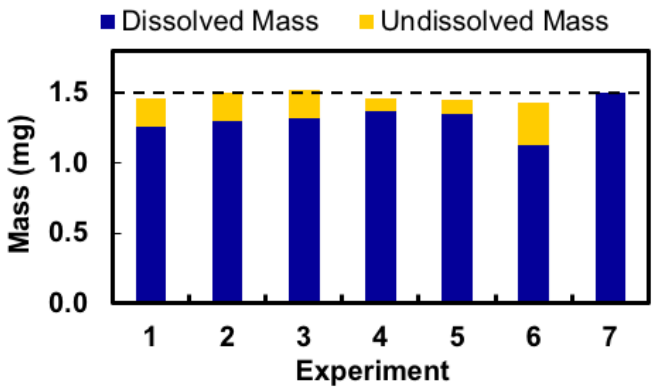

Figure 4.5 – Mass balance of dissolved and undissolved asphaltenes in asphaltene dissolution experiment

Experimental results summarized in Figure 4.5. show that the mass balance of asphaltene is consistent within 2%.

4.3. Experimental Results and Discussion

4.3.1. Effect of solvent fluid flow velocity on asphaltene dissolution rate

The effect of the fluid flow velocity on the asphaltene dissolution rate was investigated. The cross-sectional area of the dissolution unit is kept contact and fluid flow velocity can be calculate by dividing the volumetric flow rate this cross-sectional area. For these experiments, 1.5 mg of asphaltenes D of particle sizes between 38 and 75um are placed in the dissolution unit and the concentration profile of effluent is measured at the flow rate of 0.1, 10, 25, 50, and 100 mL/min. Toluene is used as solvent. An overall balance on the mass asphaltenes, m, in the dissolution unit is performed:

[In] – [Out] + [Generation] = [Accumulation]

$$0 - Q\ C_{asph} + 0 = \frac{dm}{dt} \qquad (1)$$

Where Q is the effluent volumetric flow rate and C_{asph} is the concetration of asphaltenes in effluent. The experimental results are shown in Figure 4.6.

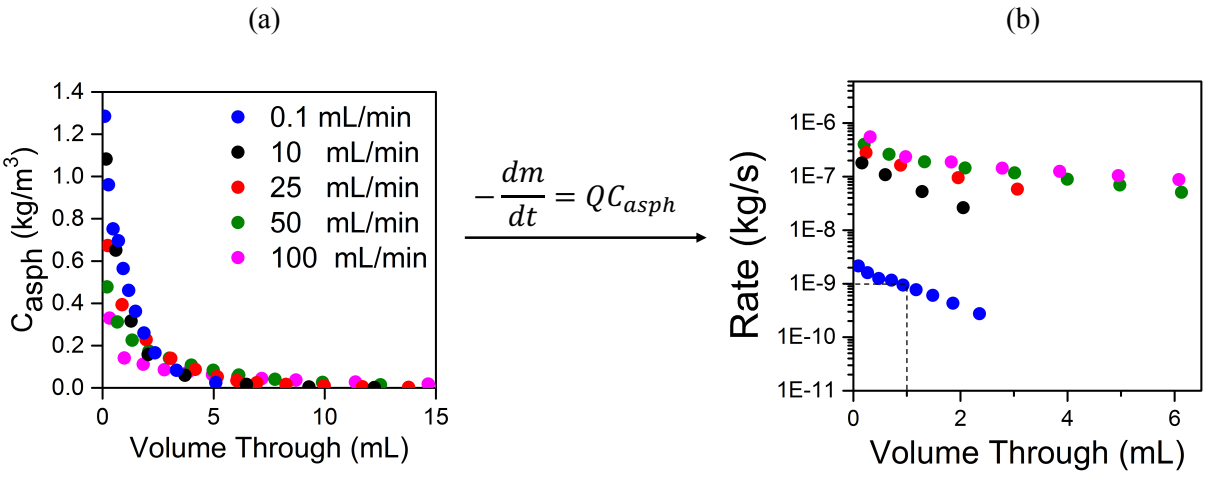

Figure 4.6 – Asphaltene dissolution at different flow rates

Figure 4.6 (a) shows the concentration profile of asphaltenes in the effluent as a function of volume through. The rate of dissolution can be obtained by multiplying the concentration by the volumetric flow rate. The rate of dissolution as a function of volume through is shown in Figure 4.6 (b). It can be seen that for a flow rate of 0.1mL/min, the dissolution rate at the point 1 mL has passed through the unit is 10^{-9} kg/s.

The rate of dissolution is expected to depend on the total surface area of asphaltene particles in the dissolution unit at a certain instant:

$$r_a = -k\mathrm{A}_{\mathrm{asph}}\, m_{asph} \tag{2}$$

Where r_a is the dissolution rate of asphaltenes with units of kg/s, k is the specific dissolution rate with units of (kg/s)/m^2, A_{asph} is the specific surface area of asphaltenes in m^2/kg, and m_{asph} is the mass of asphaltenes in the dissolution unit. A mass balance performed on the asphaltenes in the dissolution unit yields

$$Q\frac{d}{dV}m_{asph} = r_a \tag{3}$$

Where Q is the flow rate of solvent and V is the volume of solvent passed through. Substituting the rate equation, Equation 2, in the mass balance, Equation 3, and as a first approximation assuming that k (units of kg/s/m^2) and A_{asph} remains approximately constant as asphaltenes dissolve and reduce in size, the expression for mass of asphaltenes at any time in the dissolution unit can be obtained. This expression is presented as Equation 3.

$$m_{asph} = m_0 e^{-kA_{asph}\frac{V}{Q}} \tag{4}$$

Where m_0 is the initial mass of asphaltenes loaded in the dissolution unit. From the overall mass balance, Equation 1, the rate of dissolution was obtained directly from the concentration effluent profile, as shown in Figure 4.6. For this reason, an expression that relates dissolution rate to volume of solvent through is obtained by substituting Equation 4 into Equation 1, i.e.,

$$r_a = -kA_{asph} m_0 \mathrm{e}^{-kA_{asph}\frac{V}{Q}} \tag{5}$$

Taking the log of Equation 4 leads to

$$log\, r_a = log\left(-k\, A_{asph} m_0\right) - \, k\, A_{asph} \frac{1}{Q} V \tag{6}$$

The dissolution rate constant, k, is redefied in terms of mass by letting

$$k' = kA_{asph} \tag{7}$$

Where k` is the specific dissolution rate and has units of (kg/s)/kg or simply 1/s. Equation 5 then be re-written as

$$log\, r_a = log(-k'\, m_0) - \, k' \frac{1}{Q} V \tag{8}$$

From Equation 8, the specific rate of dissolution can be extracted from both the slope and from the intercept of the plot of (log r_a) as a function of volume passed through (V).

The initial dissolution rate, i.e., r_a when $V \rightarrow 0$, was obtained from Figure 4.6 (a) for the different flow rates, and the plot of initial rate as a function of flow rate is presented in Figure 4.7.

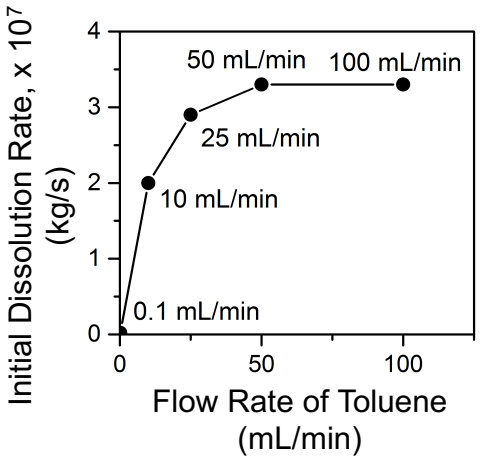

Figure 4.7 – Asphaltene dissolution rate as a function of flow rate

The experimental results from Figure 4.7 show that the dissolution rate first increases then reaches a plateau for flow rates higher than 50mL/min. The initial increase of dissolution rate with increase of flow rate is likely due to the decrease of the mass transfer boundary layer around the asphaltene particle dissolving. For flow rates greater than 50mL/min, mass transfer boundary layer is thin enough such that the rate of dissolution is limited by the rate at which asphaltene dissolve, and not by the rate at which asphaltenes diffuse away from particle. However, the scaling relation between rate and flow rate in Figure 4.7 follows a scaling of 1, i.e., $r_a \sim Q^1$. According to the Frössling correlation, the rate of dissolution of in a mass-transfer limited process is expected to scale with the power of ½, i.e. $r_a \sim Q^{1/2}$. This discrepancy in the scaling relation suggests that the dissolution rate measured is not governed by the diffusion of asphaltenes away from the particle. Studies of dissolution of polymer solid particles in solvents shows that there are other mechanisms that can dominate the rate of solid dissolution solvents[5]–[7]. One possible mechanism that where

particle will swell in contact with solvent and break as it dissolves. This dissolution mechanism disagrees with the one where asphaltene particles dissolves layer by layer.

The effect of fluid flow velocity on the dissolution of asphaltenes in chloroform was also investigated. In these experiments, 1.5 mg of asphaltenes C are loaded to the dissolution unit. The asphaltene particle sizes are kept between 38 and 75um. The experimental results are presented in Figure 4.8.

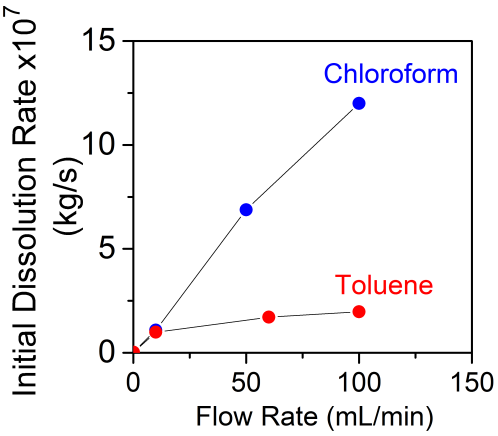

Figure 4.8 – Asphaltene dissolution rate as a function of flow rate for different solvents

It can be seen from Figure 4.8 that, while the dissolution rate of asphaltenes increases then reaches a plateau when toluene is used as a solvent. However, the dissolution rate in chloroform keeps increasing and no plateau is observed within the flow rate range of this investigation. The scaling relation between rate and flow rate follows a power of 1, i.e., $r_a \sim Q^1$, chloroform and for the toluene before plateau is reached.

4.3.2. Effect of asphaltene origin on the dissolution rate

The effect of the asphaltene origin on the asphaltene dissolution rate is assessed in this section. The specific rate of dissolution of asphaltenes A, B, C and D are measured. The solubility

parameter of asphaltenes A, B, C, and D is 24.25, 23.01, 23.01, and 23.81 $MPa^{1/2}$. These values of solubility parameter were obtained using the Buckley correlation of refractive index [8]. The specific rate of dissolution was obtained by measuring the initial rate of dissolution for the initial masses of 0.5, 1.0, 1.5 and 2.0 mg of asphaltenes loaded in the dissolution unit. The slope of initial rate versus initial mass provides the specific dissolution rate in terms of mass, i.e., k` defined in Equation 6. Experimental results for asphaltenes D with particle sizes 38 and 75um, using toluene as solvent at a flow rate 60mL/min are presented in Figure 4.9.

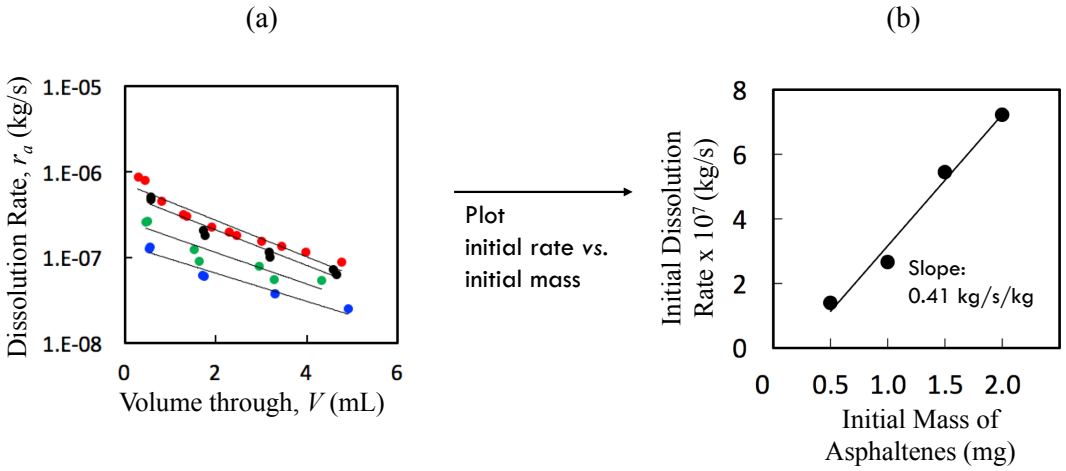

Figure 4.9 – Measurement of specific rate of dissolution, k`. Initial mass of asphaltenes of 0.5 (blue), 1.0 (green), 1.5 (black) and 2.0mg (red).

Figure 4.8 (a) presents the plot of initial dissolution rate as a function of mass of asphaltenes loaded in the dissolution unit. A linear relationship between rate and mass is observed. The slope of the line provides the specific dissolution rate, k`.

In the process of layer by layer dissolution of solid spheres, the dissolution rate is expected to scale with mass with the power of 2/3, i.e., $r \sim m^{2/3}$ (see Appendix D for derivation of equation that leads to this scaling), which is not the case in the results presented in Figure 4.9. The scaling of 2/3 is obtained from the relationship of spheres diameter with their area and their mass. For

perfect spheres, area and mass scales with the sphere diameter with power or 2 and 3, respectively, i.e., area ~ d^2 and mass ~ d^3, respectively. However, asphaltenes are porous non-spherical particles. The scaling relation for porous material is area ~ $d^{>2}$ and mass ~ $d^{<3}$. For the hypothetical case of a porous material where area ~ $d^{2.5}$ and mass ~ $d^{2.5}$, the dissolution rate would scale with power of one, i.e., rate ~ m^1. In fact, this scaling has been observed before in previous studies[3].

The intrinsic rate of dissolution is also measured for asphaltenes A, B and C. The experimental results are presented in Figure 4.10.

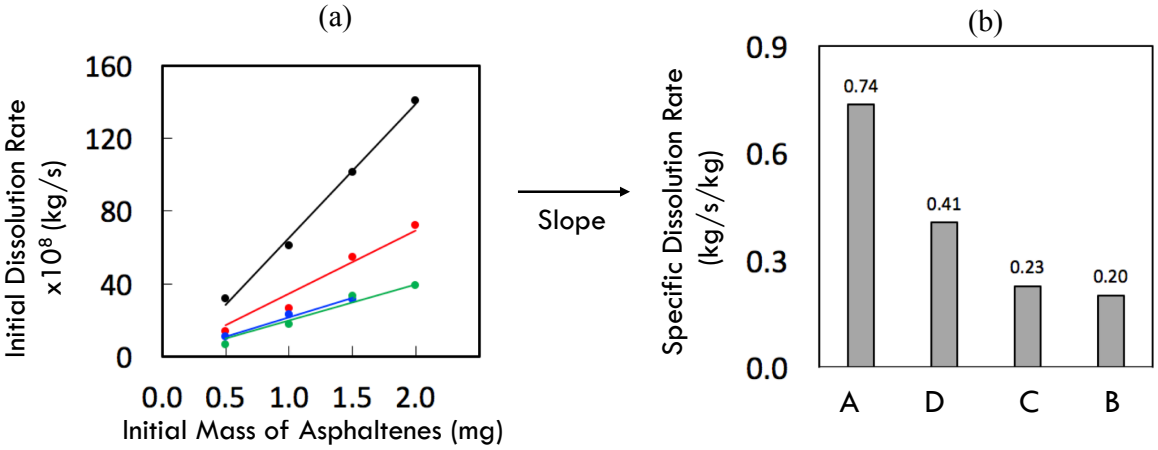

Asphaltene	• A, •B, • C, • D
Asphaltene Particle Size	38µm < d < 75µm
Solvent	Toluene
Flow Rate	60mL/min

Figure 4.10 – Specific dissolution rate for asphaltenes A, B, C and D.

Experimental results presented in Figure 4.10 show that the asphaltene dissolution rate of asphaltenes in toluene vary from 0.74 to 0.20 (kg/s)/kg. For a proper comparison of specific dissolution rates, the dissolution rate k` from Figure 4.10 should be divided by the specific surface area of each asphaltenes to obtain the rate k in terms of surface area, i.e., kg/s/m^2. However, the

specific surface areas of asphaltene particles were not measured in this investigation. Further investigation is necessary to reveal the asphaltene property that controls their dissolution rate.

4.4. Summary

An experimental methodology was developed to measure rates of asphaltene dissolution in solvents. The increase of fluid flow velocity around asphaltene particle lead to a first increase then plateau of the dissolution rate. This dependency of rate and fluid flow velocity is typical of systems where rates are diffusion-limited at low fluid flow velocities and reaction-limited at high fluid flow velocities. However, the scaling relation between rate and fluid flow velocity in the region of velocities is different than the scaling predicted by the Frössling correlation. This difference suggests that the dissolution process at low flow fluid flow velocities is not governed entirely by the diffusion of dissolved asphaltenes away from asphaltene particle.

The specific dissolution rate of asphaltenes, k`, from different crude oils was obtained at high fluid flow velocities, where the dissolution rate is independent of the flow velocity. Asphaltene from different origins were found to have different dissolution rates in toluene, ranging from 0.20 to 0.74 (kg/s)/kg. However, this difference in dissolution rate can be due to differences in the asphaltene specific surface area. The specific surface area of asphaltenes was not measured to verify this hypothesis. In the case where the differences in the measured dissolution rates, k`, are due differences in asphaltene surface area, the four asphaltenes would have the same dissolution rate in terms of area, i.e., kg/s/m^2. This result would be intriguing as the 4 asphaltenes are from different crude oils and have different solubility parameters. Experimental results also show that the solvent plays a role in the dissolution process, and the rate of dissolution of asphaltenes in chloroform is higher than in toluene.

4.5. References

[1] J. Creek, J. Wang, and J. Buckley, "Verification of Asphaltene-Instability-Trend (ASIST) Predictions for Low-Molecular-Weight Alkanes," *SPE Prod. Oper.*, vol. 24, no. 2, pp. 5–8, 2009.

[2] V. Nalwaya, V. Tantayakom, P. Piumsomboon, and S. Fogler, "Studies on Asphaltenes through Analysis of Polar Fractions," *Ind. Eng. Chem. Res.*, vol. 38, no. 3, pp. 964–972, 1999.

[3] P. Permsukarome, C. Chang, and H. S. Fogler, "Kinetic Study of Asphaltene Dissolution in Amphiphile/Alkane Solutions," *Ind. Eng. Chem. Res.*, vol. 36, no. 9, pp. 3960–3967, Sep. 1997.

[4] A. Yen, "Packed-bed Microreactors for Understanding of the Dissolution Kinetics and Mechanisms of Asphaltenes in Xylenes," in *16th International Conference on Petroleum. Phase Behavior and Fouling*, 2015.

[5] K. Ueberreiter and F. Asmussen, "Velocity of dissolution of polymers. Part I," *J. Polym. Sci.*, vol. 57, no. 165, pp. 187–198, Mar. 1962.

[6] B. a. Miller-Chou and J. L. Koenig, "A review of polymer dissolution," *Prog. Polym. Sci.*, vol. 28, no. 8, pp. 1223–1270, Aug. 2003.

[7] I. Devotta, V. D. Ambeskar, A. B. Mandhare, and R. a. Mashelkar, "The life time of a dissolving polymeric particle," *Chem. Eng. Sci.*, vol. 49, no. 5, pp. 645–654, Jan. 1994.

[8] J. S. Buckley, G. J. Hirasaki, Y. Liu, S. Von Drasek, J.-X. Wang, and B. S. Gill, "Asphaltene Precipitation and Solvent Properties of Crude Oils," *Pet. Sci. Technol.*, vol. 16, no. 3–4, pp. 251–285, 1998.

CHAPTER V

A Mechanistic Investigation of Asphaltene Deposition

Published at *Energy Fuels*, 2016, vol. 30, pp 8915–8921

5.1. Introduction

5.1.1. Destabilization and aggregation of asphaltenes in crude oil

Asphaltenes are the most polar molecules in crude oil that form nanometer-sized clusters of nanoaggregates[1]–[5]. Upon the addition of n-alkane to crude oil, a fraction of asphaltenes become unstable and undergo an aggregation process, resulting in a net growth of asphaltene nanoparticles[1], [6]–[9]. The fraction of asphaltenes that become unstable and the rate by which unstable asphaltenes grow is a function of crude oil origin[6], [8], concentration of n-alkane in oil-alkane mixture[1], [6], [8], the type of n-alkane[10], and temperature[11]. As the concentration of n-alkane in oil-alkane mixtures increase, the fraction of asphaltenes that become unstable and the aggregation rate increases. The total content of asphaltenes in a crude oil (usually given in mass of asphaltenes per mass of crude oil) is determined using the standard ASME method with a concentration of 97.6 vol% of n-alkane in oil (equivalent to 40:1 volumes of n-alkane:oil)[12]. At n-alkane concentrations below 97.6 vol%, the fraction of asphaltenes that remain in suspended solution and do not undergo aggregation process are called stable asphaltenes[1]. Hoepfner et al[1] observed that fractal dimension of unstable asphaltenes differs from that of stable asphaltenes.

Although much is known about the destabilization and aggregation of asphaltenes in the bulk of oil-alkane mixture, the mechanisms by which asphaltenes deposit have not been fully elucidated. A short review of the current understanding in asphaltene deposition is presented in the next section.

5.1.2. Previous investigations on asphaltene deposition

The current literature on asphaltene destabilization and deposition can be separated into two categories. In one category the asphaltene are are destabilized by change in pressure and/or temperature of crude oil in order to induce deposition[13]. In the second category precipitants (e.g. n-alkanes) are added to crude oil to induce asphaltene destabilization and thus precipitation[14]–[17]. Relationships between asphaltene destabilization induced by pressure and/or temperature and solvent-addition have been proposed by Creek et al[18] and by Kraiwattanawong et al[19]. In the investigation presented here, asphaltene precipitation and deposition will be induced by addition of an n-alkane, heptane, to crude oil.

Asphaltene deposition has been studied in different geometries such as tubes, the Couette apparatus, porous media, and micro-models. Hoepfner et al[14] and Chaisoontornyotin et al[20] have investigated the deposition of asphaltenes in capillary tubes with different crude oils and n-alkanes. They have observed that asphaltene deposits are formed even at n-alkane concentrations below the point of instantaneous asphaltene aggregation detection. Nabzar et al[21] investigated the formation of asphaltene deposits in porous media and capillary tubes. The scaling relations between rate of deposit formation and flow rate were found to be independent of crude oil origin and were attributed to the diffusion of depositing asphaltenes, at low flow rates, and to a dynamic equilibrium between hydrodynamic and adhesion forces on a depositing asphaltene at high flow rates. Hashmi et al[15] also studied asphaltene deposition in capillary tubes and observed similar behavior to Nabzar et al at high flow rates. Bennett[22] and Eskin et al[23] introduced the asphaltene particle size as an important variable in the asphaltene deposition process, where an interplay between shear and adhesion forces on depositing asphaltenes will determine whether the asphaltene will adhere to the surface.

In this research, a packed bed apparatus is introduced to investigate asphaltene deposition. The effect of unstable asphaltene concentration and fluid flow rate on the specific rate of asphaltene deposition are investigated. Experimental results are explained using a diffusion-limited deposition model, and the diffusivity of depositing asphaltenes is obtained. The asphaltene deposit profile along the packed bed length is measured for Oil B and compared to the profile predicted by the deposition model, showing an excellent agreement. This investigation sheds light on the process of asphaltene deposition by identifying a generic feature, i.e., comparable diffusivity values of nanometer-sized asphaltene, observed in asphaltene deposition from several crude oils from different parts of the world.

5.2. Experimental Methods

5.2.1. Asphaltene deposition

The asphaltene deposition apparatus consists of a glass column (10mm of inner diameter) packed with stainless steel beads (3 and 4mm in diameter, grade 100, SS 316). The column is packed such that there are 4 beads of 4 mm forming square horizontal lattices with a 3 mm bead placed in between lattices. The bed contains 148 beads of 4mm-diameter, 36 beads of 3mm-diameter, with a total bed height of 13.2cm (unless stated otherwise). The upward flow of oil-alkane mixture is promoted by a peristaltic pump. Heptane is used as n-alkane is all experiments in this investigation.

The oil-heptane mixture, referred here as “reservoir mixture”, is prepared by adding heptane to crude oil at the flow rate of 3mL/min while the mixture is kept well stirred. After the desired concentration of heptane in oil-heptane is reached, heptane addition is stopped and the reservoir mixture is placed in the deposition apparatus, shown in Figure 5.1. The reservoir mixture is then fed to packed bed at the desired flow rate. To prevent any aging effects, i.e., increase in

asphaltene particle size due to aggregation, the reservoir mixture is replaced with a fresh mixture at a pre-determined frequency, referred to as reservoir replacement.

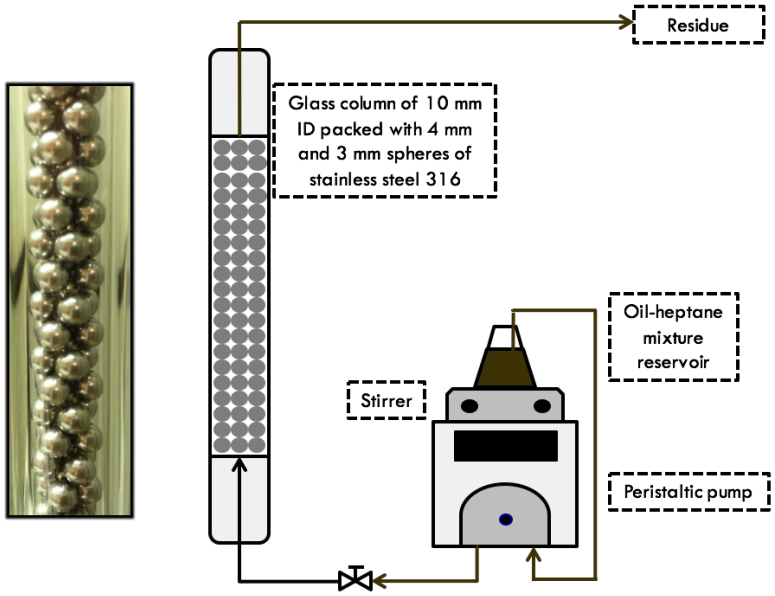

Figure 5.1 – Asphaltene deposition apparatus

The size of asphaltenes particles plays an important role on the dominating deposition mechanism. For example, micron-size particles tend not to deposit on pipe wall during fluid flow[14], [23]. However, the micron-size particle can settle down by gravity and cause deposition. Therefore, in this scenario, the dominating deposition mechanism would be gravitational settlement. On the other hand, this investigation is concerned with the deposition mechanism of asphaltene particles during fluid flow and that are not susceptible to the effect of gravitational forces. For this reason, the heptane concentration in the oil-heptane mixture and the frequency of reservoir replacement are chosen such that the size of unstable asphaltene particles that flow through the packed bed is kept below 500nm. The 500nm size is the minimum limit for optical microscopy detection, and it is chosen for a practical reason.

After running the oil-heptane mixture through the packed bed for a specified amount of time, i.e., the run-time, the packed bed is drained at a flow rate of 0.05g/min. Chloroform is then injected through bed and the mixture of chloroform and retained material is collected in vial and placed in oven at 75^{o}C. After chloroform is evaporated, the mass of retained material is measured. The mass of retained material is composed of the mass of deposit, if any, and the mass of liquid trapped. For an experiment with a run-time of 1 minute, the mass of deposit is insignificant and the mass of retained material is equal to mass of liquid trapped. Therefore, the mass of liquid trapped for a given crude oil at a given heptane concentration is obtained by measuring the mass of retained material of a 1-minute run-time deposition experiment. The mass of deposit is then obtained by subtracting the mass of liquid trapped from the mass of retained material.

5.2.2. Content of unstable asphaltenes

The concentration of unstable asphaltenes for a given oil-heptane mixture was determined using the centrifugation method described by Maqbool et al[6]. Heptane is added to crude oil at 3mL/min while oil-heptane mixture is kept well stirred. When the desired heptane concentration is reached, heptane addition is stopped. The oil-heptane mixture is then placed in sealed vial and kept stirred as it ages. An aliquot of 1.5mL of the mixture is taken over time and centrifuged for 10min at 24,000x g-force. Upon centrifugation the asphaltenes that have grown larger than the centrifugation cut-off size will form a cake on the bottom of centrifuge tube. The supernatant is then removed from the centrifuge tube and the cake is washed with heptane, dried, and its mass is recorded. The concentration of asphaltenes separated out by centrifugation is then calculated. When the concentration of asphaltenes that can be separated by centrifugation no longer varies as oil-heptane mixture ages, the concentration of unstable asphaltenes at the given heptane concentration for a given crude oil is obtained and recorded (given in kg of unstable asphaltenes

per m^3 of oil-heptane mixture). Note that short time span experiments to determine the unstable asphaltenes content can lead to very large errors.

5.2.3. Measurement of asphaltene detection time

At sufficiently low oil-heptane mixture, the time it takes for unstable asphaltenes to reach 0.5 μm can be measured by time-resolved optical microscopy[6], [8]. In this method, heptane is added to crude oil at 3mL/min and oil-heptane is kept well stirred. Heptane addition is stopped when desired heptane concentration is reached. The oil-heptane mixture is then placed in sealed vial and kept stirred as it ages. Aliquots of oil-heptane mixture are taken over time, placed on microscopy slide, and observed under an optical microscope. The time it takes for solids to be detected after heptane addition is called detection time. The detection time of asphaltene aggregation decreases as heptane concentration increases in a given crude oil. The heptane concentration at which asphaltene aggregation is detected within approximately 5 minutes is referred to as the heptane concentration of instantaneous detection.

5.3. Modeling Asphaltene Deposition in Packed Beds.

In this section, a model for the deposition of asphaltene nanoparticles in packed bed is derived. The deposition process is modeled as a reaction ($A \rightarrow D$), where A is the unstable asphaltene in the bulk of the fluid and D the deposit on surface. The concentration of unstable asphaltenes at the deposition surface is assumed to be zero, and their diffusion through a mass-transfer boundary layer will control the deposition rate[24], [25]. The rate of asphaltene deposition in a diffusion-limited process is not a function of the surface properties where deposit is building upon, as long as the surface allows asphaltene to deposit. The interfacial phenomenal of deposition is modeled mathematically as a homogeneous first-order reaction with the appropriate choice of

mass-transfer coefficient, k_c. In this way, a mass balance of asphaltene flowing and depositing in the packed bed is [26]:

$$UA_c \frac{dC_A}{dz} + k_c a_c A_c C_A = 0 \quad (1)$$

Where C_A is the concentration of unstable asphaltenes, z the distance along the bed, U is the superficial velocity, A_c, the cross sectional area of the bed and a_c area per volume of bed. Integrating Equation (1) with the initial condition $C_A = C_{A_0}$ at $z = 0$ gives

$$C_A = C_{A_0} e^{-\frac{k_c}{U} a_c z} \quad (2)$$

The average rate of asphaltene deposition in packed bed of length L is given by the rate of disappearance of A which is the difference between the inlet and outlet mass flow rates. Thus:

$$Rate_{dep} = [F_A|_{z=0} - F_A|_{z=L}] \quad (3)$$

Substituting for the mass flow rate, F_A, in terms of concentration a superficial velocity

$$Rate_{dep} = \left[UA_c C_{A_0} - UA_c C_A|_{z=L}\right] \quad (4)$$

Combining Equation (2) and (4) we get

$$Rate_{dep} = C_{A_0} UA_c \left(1 - e^{-\frac{k_c}{U} a_c L}\right) \quad (5)$$

By expanding the exponential function in Equation (5) in a series, we obtain:

$$Rate_{dep} = C_{A_0} UA_c \left(1 - \left[1 - \frac{k_c}{U} a_c L + \frac{1}{2}\left(\frac{k_c}{U} a_c L\right)^2 + O(3)\right]\right) \quad (6)$$

For a short packed bed, when $\left(\frac{k_c}{U} a_c L\right)^2 \sim 0$, we retain only the first and second term of the expansion, and the deposition rate becomes

$$Rate_{dep} = \ k_c \, A_c \, a_c \, L \, C_{A_0} \tag{7}$$

The only unknown parameter is the mass transfer coefficient k_c. Empirical correlations of k_c were obtained by Wakao et al[27] and Thones and Kramer[28] for packed beds:

$$Sh = 2 + Re^{\frac{1}{2}} Sc^{\frac{1}{3}} \tag{8}$$

Where $Sh = \frac{\phi}{(1-\phi)} \frac{k_c d_b}{D}$, $Re = \frac{\rho U d_b}{\mu \, (1-\phi)}$, and $Sc = \frac{\mu}{\rho \, D}$.

From Equation (8), we see when $Re^{\frac{1}{2}} Sc^{\frac{1}{3}} \gg 2$, $k_c$can be written as:

$$k_c = Sh \frac{D}{d_b} \frac{1-\phi}{\phi} = \frac{D}{d_b} \frac{1-\phi}{\phi} \left(\frac{\rho U d_b}{\mu \, (1-\phi)} \right)^{\frac{1}{2}} \left(\frac{\mu}{\rho \, D} \right)^{\frac{1}{3}} \tag{9}$$

Using $a_c = \frac{6(1-\phi)}{d_b}$, and substituting Equation (9) into Equation (7):

$$Rate_{dep} = \ C_{A_0} A_c \, \frac{D}{d_b} \frac{1-\phi}{\phi} \left(\frac{\rho U d_b}{\mu \, (1-\phi)} \right)^{\frac{1}{2}} \left(\frac{\mu}{\rho \, D} \right)^{\frac{1}{3}} \frac{6(1-\phi)}{d_b} \, L \tag{10}$$

By collecting the variables together and by letting $U = \frac{q}{\rho A_c}$, where q is the mass flow rate, the rate of deposition (g/s) can be written as:

$$Rate_{dep} = \ 6 \, A_c^{\frac{1}{2}} d_b^{-\frac{3}{2}} \frac{(1-\phi)^{\frac{3}{2}}}{\phi} \, \rho^{-\frac{1}{3}} \mu^{-\frac{1}{6}} D^{\frac{2}{3}} q^{\frac{1}{2}} \, L \, C_{A_0} \tag{11}$$

Consequently, the mass of deposit at a given run-time is given by:

$$m_{dep} = \ 6 \, A_c^{\frac{1}{2}} d_b^{-\frac{3}{2}} \frac{(1-\phi)^{\frac{3}{2}}}{\phi} \, \rho^{-\frac{1}{3}} \mu^{-\frac{1}{6}} D^{\frac{2}{3}} q^{\frac{1}{2}} \, L \, C_{A_0} t \tag{12}$$

5.4. Experimental Results

5.4.1. Effect of unstable asphaltene concentration in oil-heptane mixture on asphaltene deposition rate

The concentration of heptane in the oil-heptane mixture dictates the amount of asphaltenes that will become unstable and how fast the unstable asphaltenes will aggregate for a given crude oil. The bulk detection time is a function of heptane concentration (which is a measure of instability) is shown in Table 1.

Table 5.1 – Detection time of asphaltene aggregation for Crude Oil C

Heptane Concentration wt%	**Detection Time (hours)**
28.0	13 ± 0.2
29.5	7 ± 0.2
31.0	4 ± 0.2
33.0	2 ± 0.2

In this section, the asphaltene deposition rate is measured as a function of the unstable asphaltene concentration. To determine this relationship in a two-step process. First we need to determine the deposition rate as a function of heptane concentration (see Figure 5.2). Next, we determine the concentration of unstable asphaltenes as a function of heptane concentration (See Figure 5.3). In order to obtain oil-heptane mixtures with different concentrations of unstable asphaltenes, the concentration of heptane in Oil C will be varied.

To determine the rates, we first measure the mass of deposit for a run-time of 8 hours for each heptane concentration, keeping the flow rate of oil-heptane mixture constant at 0.6 g/min and

replacing the reservoir every 2 hours. The specific rate of deposition shown in Figure 5.2 is obtained by dividing the mass of deposit by the run-time and by the total wetted area of the packed bed.

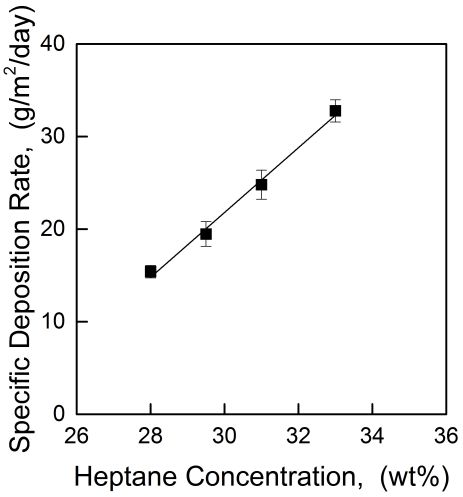

Figure 5.2 – Asphaltene deposition rate as a function of heptane concentration in Oil C.

The concentration of unstable asphaltenes for each heptane concentration is measured using the centrifugation technique and is shown in Figure 5.3.

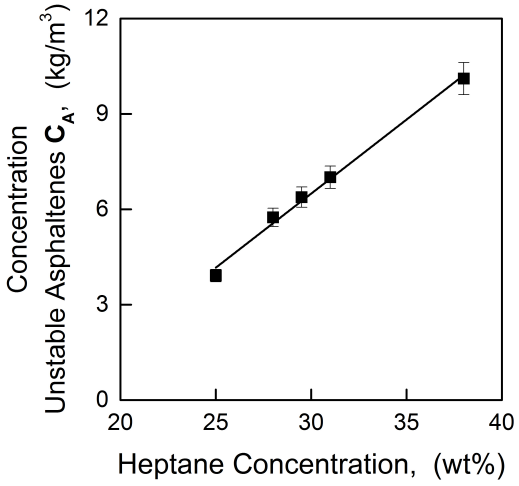

Figure 5.3 – Concentration of unstable asphaltenes as a function of heptane concentration in Oil C.

Note in Figures 5.2 and .3 that as the concentration of heptane increases in oil-heptane mixture, both the asphaltene deposition rate and the concentration of unstable asphaltene increase.

From Equation (13) we see that the rate of deposition should vary linearly with the concentration of unstable asphaltenes.

$$Rate_{dep} \sim C_{A_0} \tag{13}$$

Using Figures 5.2 and 5.3 we determine the asphaltene deposition rate as a function of concentration of unstable asphaltenes as shown in Figure 5.4.

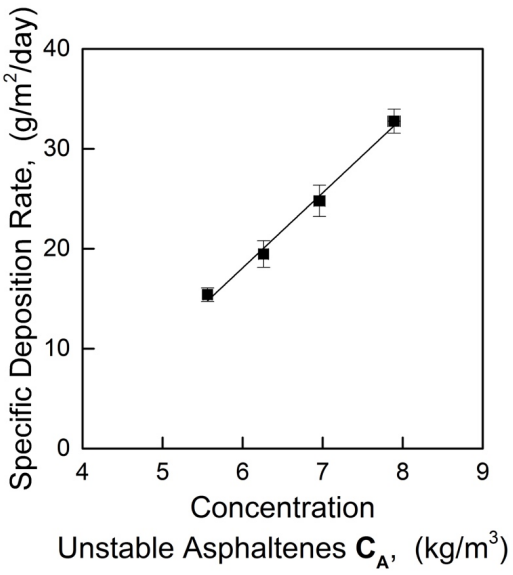

Figure 5.4 – Asphaltene deposition rate as a function of concentration of unstable asphaltenes in heptane-oil mixtures

As it can be seen from Figure 5.4, a linear relation between deposition rate and concentration of unstable asphaltenes is indeed observed. Form the slope of plot in Figure 5.4, the diffusivity of depositing asphaltenes for Oil C was found to be 4.3 x 10^{-12} m^2/s.

Now that we have shown that the asphaltene deposition rate increases linearly with the concentration of unstable asphaltenes as predicted by Equation (11), we will study the effect of flow rate on asphaltene deposition rate.

5.4.2. Effect of flow rate on deposition rate

Because Oil C had been consumed by previous experiments, Oils A, B, D and E were also used to determine the effect of flow rate on deposition. A mixture of 67% heptane in crude Oil E was passed through the packed bed for a specified run-time and flow rate. The bulk detection time of asphaltene aggregation for this heptane concentration and crude oil is 12 hours. The reservoir was replaced every 12 hours to guarantee that packed bed was fed with unstable asphaltenes smaller than 500nm at all times. The mass of deposit as a function of run-time for different flow rates, (g/min), is shown in Figure 5.5.

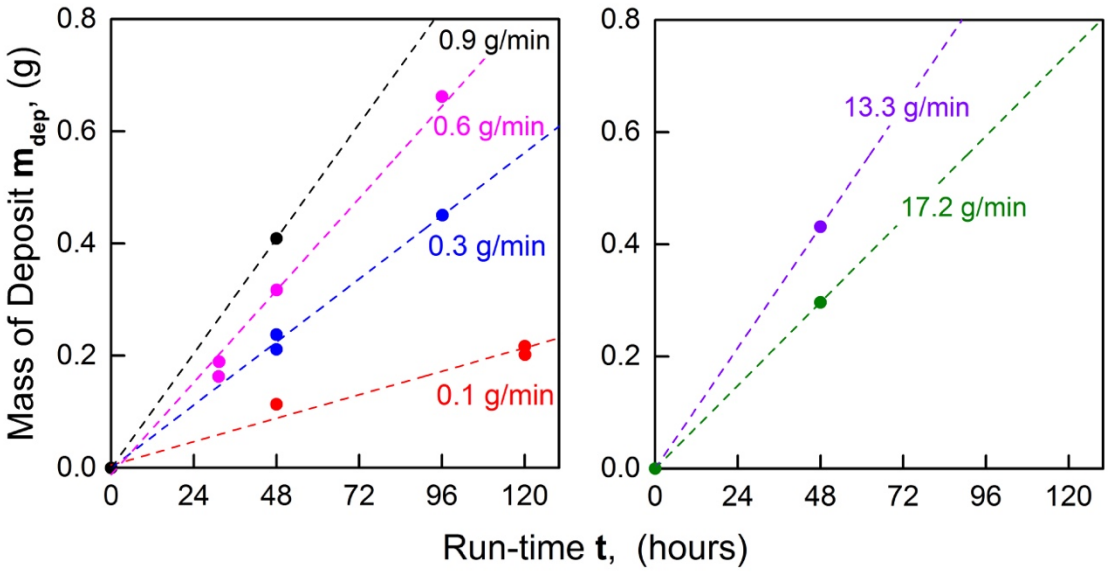

Figure 5.5 – Mass of deposit as a function of run-time at different flow rates for 67% heptane in Oil E.

The deposited materials were characterized for asphaltene content that showed that the deposits of the 96 hours and 120 hours of run-time are composed of approximately 50 wt% of asphaltenes, indicating that material retained in packed bed is indeed an asphaltene deposit. Images of the deposited material in the packed bed are shown in Appendix F.

As predicted from Equation (12) one observes that the mass of deposit increases linearly as run-time increases for a given flow rate. The slopes of the lines in Figure 5.5 give the asphaltene deposition rates, which are shown as a function of fluid flow velocity in Figure 5.6.

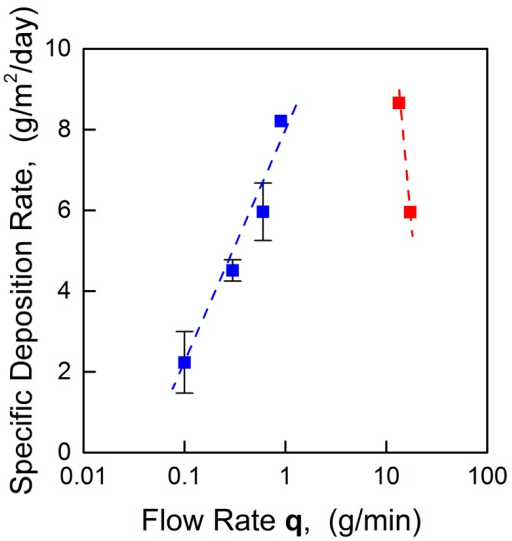

Figure 5.6 – Asphaltene deposition rate as a function of fluid flow rate for 67% heptane in Oil E.

Figure 5.6 shows the specific rate of deposition as a function of flow rate. As the fluid flow velocity increases, the deposition rate first increases (shown in blue, where the Reynolds number is ≤ 1) then decreases (shown in red, where $Re > 1$). The increase in deposition rate occurs due to a decrease of mass-transfer boundary layer thickness as flow rate increases. The decrease in deposition rate, on the other hand, cannot be explained solely by mass transfer principles and is associated with sloughing at high shear stresses exerted by the fluid on depositing asphaltenes.

In order to study the asphaltene deposition when diffusion controls the deposition rate, the asphaltene deposition rate of different crude oils was measured as a function of fluid flow rate for Reynolds numbers less than, i.e. $Re < 1$. In all experiments, the heptane concentration and reservoir replacement were chosen such that the asphaltene particles size fed to pecked bed is kept in sizes smaller than 500nm. Experimental results are presented in Figure 5.7.

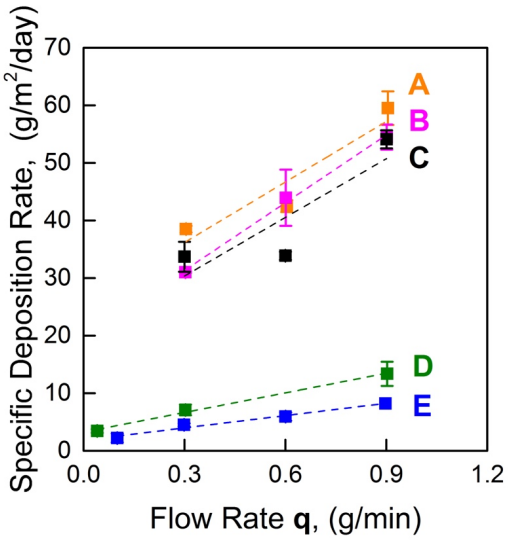

Figure 5.7 – Asphaltene deposition rate as a function of fluid flow rate for different oil-heptane mixtures (A, B, C, D, E) (See Table 2 for experimental conditions).

Legend of Figure 5.7 is presented in Table 5.2.

Table 5.2 – Experimental conditions for results presented in Figure 5.7

Code	Crude Oil	Heptane Concentration (wt%)	Detection Time (hours)	Reservoir Replacement (hours)	Concentration of Unstable Asphaltenes (kg/m^3)
A	Oil A	24.0	2 ± 0.2	2	19.7
B	Oil B	22.5	2 ± 0.2	2	4.5
C	Oil C	33.0	2 ± 0.2	2	9.0
D	Oil D	65.6	12 ± 0.2	12	1.2
E	Oil E	67.0	12 ± 0.2	12	0.90

Note that for all 5 sets of experiments, the asphaltene deposition rate increases as the flow rate increases.

Equation (11) shows that for a diffusion-limited deposition process in packed bed, the deposition rate, $Rate_{dep}$, scales with power of one half with the fluid flow rate q, i.e.,

$$Rate_{dep} \sim q^{\frac{1}{2}} \tag{14}$$

Therefore, when plotting the experimental results of Figure 5.6 in scaled deposition rate J vs. $q^{1/2}$, where

$$J = \frac{Rate_{dep}}{6\, A_c^{\frac{1}{2}} d_b^{-\frac{3}{2}} \frac{(1-\phi)^{\frac{3}{2}}}{\phi}\, \rho^{-\frac{1}{3}} \mu^{-\frac{1}{6}}\, L\, C_{A_0}} \tag{15}$$

One should obtain lines with slopes that contain information on the diffusivity of depositing asphaltenes.

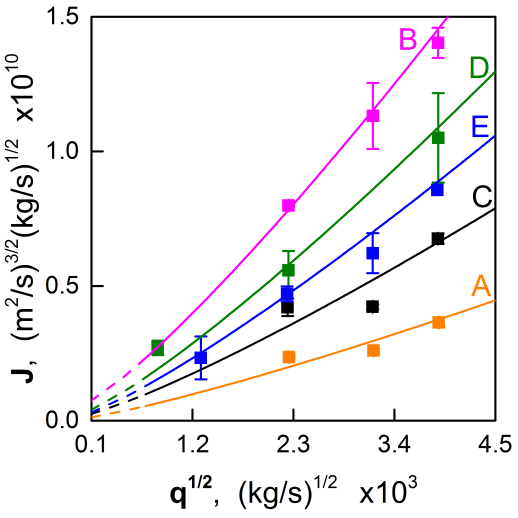

Figure 5. 8 – Scaled deposition rate J as a function of flow rate, q1/2.

By calculating the slope of lines in Figure 5.8, the diffusivity can be obtained. Diffusivity values are presented in Table 3.

Table 5.3 – Diffusivity values of depositing asphaltenes extracted from plot in Figure 5.8

Code	Crude Oil	Heptane Concentration (wt%)	Diffusivity (m^2/s) x10^{12}	Relative Error (%)
A	Oil A	24.0	7.1	0.025
B	Oil B	22.5	4.1	1.2
C	Oil C	33.0	3.5	1.5
D	Oil D	65.6	1.8	31
E	Oil E	67.0	0.67	16

Our deposition model given by Equation (11) suggests that a plot of $\left(\frac{J}{D^{\frac{2}{3}}}\right) vs. \left(q^{\frac{1}{2}}\right)$ should result in a collapse of all experimental data onto a single line.

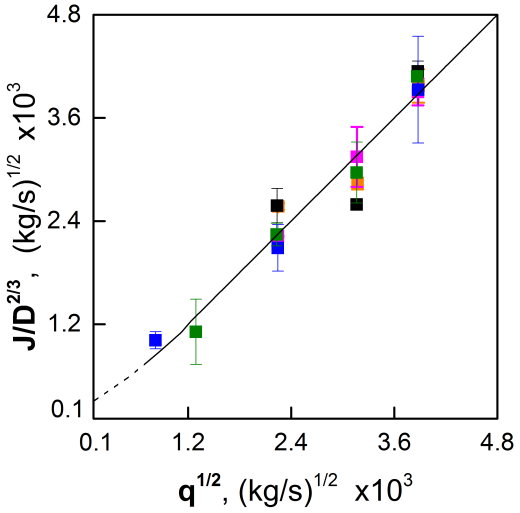

Figure 5.9 – Scaling analysis of asphaltene deposition rate

As it can be seen in Figure 5.9 all experimental results collapse onto a single line, indicating that the diffusion-limited model captures the underlying physics of the asphaltene deposition process at the investigated conditions.

In the next section the asphaltene deposit profile along the packed bed length will be measured and compared with the one predicted by Equation (12).

5.4.3. Asphaltene deposit profile along the packed bed

The diffusivity of depositing asphaltenes was obtained in the previous section from asphaltene deposition rate measurements as a function of fluid flow rate in a short packed bed. The diffusivity of depositing asphaltenes can also be obtained from the the asphaltene deposit profile (i.e., m_{dep} *vs.* L) for a given flow rate. There are, therefore, at least two different methods to obtain the diffusivity of depositing asphaltenes using the packed bed apparatus. The diffusivity obtained in short packed beds from an analysis of the deposition rate as a function of the square root of the mass flow rate should be the same as that obtained in long packed beds from an analysis of the mass of the deposit as a function of distance.

In this section, the asphaltene deposit profile will be obtained experimentally for the mixture of 22.5 wt% heptane in Oil B at different flow rates and run-times. The deposit profile is measured by running a deposition experiment at a given flow rate and run-time with six packed beds, each identical to the one used in previous section, connected in series. The mass of deposit is then measured for each packed bed at the end of the experiment, and the total mass of deposit, m_{dep}, as a function of packed bed length, L, is presented in Figure 5.10.

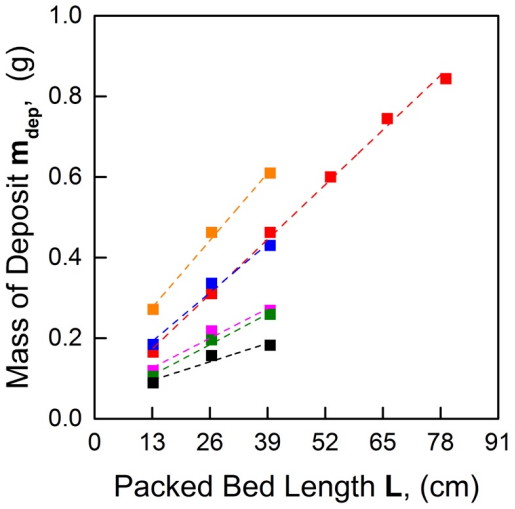

	Flow Rate (g/min)	Run-Time (hours)
■	0.6	12
■	0.9	6
■	0.3	12
■	0.9	4
■	0.6	6
■	0.3	6

Figure 5.10 – Mass of deposit as a function of packed bed length at different run-times and flow rate for 22.5 wt% heptane in Oil B.

As it can be seen in Figure 5.10, the total mass deposited increases virtually linearly along the packed bed. Additionally, for a given flow rate, the longer the run-time the greater the mass deposited.

From rearranging Equation (12), it can be written:

$$\frac{m_{dep}}{q^{\frac{1}{2}}\, t} = 6\, A_c^{\frac{1}{2}} d_b^{-\frac{3}{2}} \frac{(1-\phi)^{\frac{3}{2}}}{\phi}\, \rho^{-\frac{1}{3}}\, \mu^{-\frac{1}{6}}\, D^{\frac{2}{3}}\, C_{A_0}\, L \qquad (16)$$

Equation (16) shows that by plotting $\left(\frac{m_{dep}}{t\, q^{\frac{1}{2}}}\right)$ as a function of length of packed bed L the experimental data collapse onto a single line, given that the packed bed and mixture properties are kept constant. The plot of $\left(\frac{m_{dep}}{t\, q^{\frac{1}{2}}}\right)$ as a function of L presented in Figure 5.11.

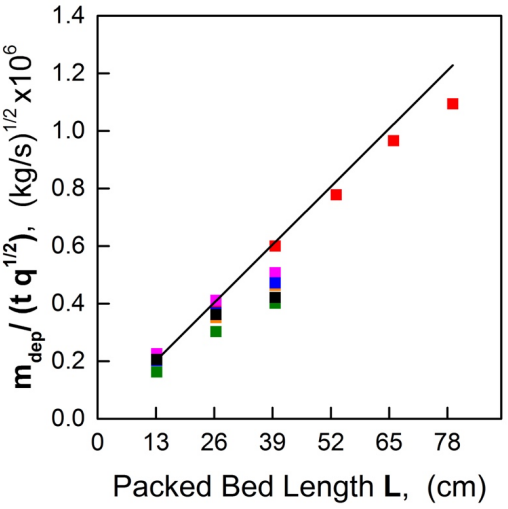

Figure 5.11 – Normalized mass of deposit along the packed bed and prediction according to diffusion-limited deposition model. Deposit profile as predicted by deposition model presented in solid black line. See Figure 5.10 for color legend.

As it can be seen in Figure 5.11, the experimental data collapse onto a single line when normalized by the run-time and flow rate.

In order to check for the self-consistency on the diffusivity value probed by the two different methods (i.e., $Rate_{dep}$ *vs.* $q^{1/2}$ and m_{dep} *vs.* L), the calculated and experimental deposition profile will be compared. This calculated deposition profile is obtained using Equation (16) with the diffusivity value obtained in Section 4.2 (Table 3) for this very same crude oil and heptane concentration (22.5 wt% heptane in Oil B). If the deposition model captures the physics of the process, then the calculated and experimental results should be in agreement. The calculated deposition profile is shown as a black solid line in Figure 5.11. As it can be seen, the calculated values of $\left(\frac{m_{dep}}{t\,q^{\frac{1}{2}}}\right)$ *vs.* L are in excellent agreement with experimental data, verifying the self-consistency of the two different methods used to obtain the diffusivity of depositing asphaltenes.

The self-consistency verified here is very important for two reasons. First, it indicates that the specific rate of deposition (i.e., the deposition rate per unit of area) is correctly measured. The correct measurement of specific rate in the packed bed apparatus gives the packed bed technique an advantage over the use of capillary tubes to study asphaltene deposition. In capillary tubes it has been observed that asphaltene deposits can be concentrated at the entrance region of the tube [14]. This region is of unknown length and thickness, resulting in inaccurate values of specific rate of deposition. Secondly, our deposition model captures the underlying physics of the deposition process in the packed bed apparatus.

5.5. Discussion

The diffusion coefficient of asphaltene in toluene was measured by Durand et al [29] using DOSY-NMR. It was found that the diffusion coefficients range from ~ $3.5x10^{-10}$ m^2/s for the nanoaggregates to ~ $3x10^{-11}m^2/s$ for the macroaggregates, with variance of approximately 10%. In this investigation, heptane was added to crude oil causing the unstable asphaltenes to grow over time. From the Stokes-Einstein equation we know an increase in asphaltene particles will cause the asphaltene diffusion coefficient to decrease at a fixed fluid viscosity. Given that toluene is a solvent for asphaltenes and that it has a low viscosity compared to crude oils, the diffusion coefficients of asphaltene in toluene should provide the upper bound of the highest diffusivities in heptane-oil systems. Indeed, as it can be seen in Table 3, the diffusivity values for all oil-heptane mixtures are indeed lower than the values reported by Durant et al[29].

The diffusivity of particles in an infinite body of stagnant liquid is given by the ratio between the thermal motion and drag forces on the particle. For the case of spherical particles, the Stokes-Einstein equation, Equation 17, predicts that particles of identical size immersed liquids of different viscosities will exhibit different diffusivity value.

$$D = \frac{k_B T}{3\,\pi\,\mu\,d} \tag{17}$$

The shape of the particles, proximity to walls and to other particles, etc., are expected to cause the actual diffusivity to deviate from that one predicted by the Stokes-Einstein equation. In order to gain an understanding of the physical meaning of the diffusivity values obtained in this study (Table 3), the equivalent asphaltene particle diameters are calculated using the Stokes-Einstein equation and values are shown in Table 4.

Table 5.4 – Asphaltene particle diameter calculated using the Stokes-Einstein equation

Crude Oil	**Heptane Concentration (wt%)**	**Asphaltene Particle Diameter (nm)**
Oil B	22.5	13 ± 1
Oil C	33.0, 31.0, 29.5, 28.0	27 ± 1
Oil C	33.0	58 ± 1
Oil D	65.6	58 ± 18
Oil E	67.0	74 ± 1
Oil A	24.0	106 ± 17

The estimated diameter of asphaltene particle contributing to deposit formation is in agreement with experiments, when the unstable asphaltenes passed through the packed bed have particle sizes below 500nm at all times. Additionally, the particle diameter obtained for the Oil C at different heptane concentrations, i.e., 27nm, is lower than the value obtained for the deposition experiment at 33% heptane, i.e., 58nm. This difference in particle size is in agreement with the trends observed by Maqbool et al[7] who found that the average asphaltene particle size increases as the heptane concentration increases for a fixed aging time of a specified oil-heptane mixture.

Indeed, in this investigation, an aging time of 2 hours and heptane concentration of 33 wt% provided a greater particle size than the average size at lower heptane concentrations, i.e., 33, 31, 29.5, and 28 wt%. Note that the values of asphaltene diffusivity and particle diameters shown in Table 3 and 4 are only estimates that depend on a number of factors such as measurement of asphaltene content of deposits, concentration of unstable asphaltenes, and correlation for mass transfer coefficient used to calculate the diffusivity.

Additional information on the effect of 1) asphaltene particle size, 2) diameter of beads in packed bed, and 3) material of beads in packed bed on the asphaltene deposit formation are presented in Appendix G.

5.6. Conclusions

A new apparatus to study asphaltene deposition is introduced. The apparatus consists of a packed bed of stainless steel beads over which a mixture of oil and precipitant is flown and the asphaltene deposit monitored. The asphaltene deposition rate was measured as a function of fluid flow rate for crude oils from different origins and at different heptane concentrations in oil-heptane mixtures. The asphaltene deposit profile along the packed bed was also investigated. Experimental results show three important findings. (1) It was observed that the asphaltene deposition rate increases linearly with the concentration of unstable asphaltenes. (2) The deposition rate of unstable asphaltenes scaled with the square root of the fluid flow velocity in viscous flow regime, indicating that the asphaltene deposition process can be explained by a diffusion-limited deposition of nanoparticles. And (3), the asphaltene deposition profile along the packed bed matches theoretical behavior predicted by the diffusion-limited correlations for mass-transfer deposition.

5.7. Nomenclature

U	$\frac{m}{s}$	Superficial Velocity
A_c	$m^2{}_{cross\ sectional}$	Cross-sectional area of empty column
C_{A_0}	$\frac{g}{m^3}$	Concentration of A at packed bed inlet
z	m	Axial coordinate
k_c	$\frac{m}{s}$	Mass-transfer coefficient
a_c	$\frac{m^2{}_{wetted\ surface}}{m^3{}_{col}}$	Total area of beads per volume of empty column
$Rate_{dep}$	$\frac{g}{s}$	Asphaltene deposition rate
L	m	Length of packed bed
D	$\frac{m^2}{s}$	Diffusion coefficient of depositing asphaltenes
ρ	$\frac{kg}{m^3}$	Density of fluid
μ	$Pa.s$	Viscosity of fluid
d_b	m	Diameter of beads
ϕ	$-$	Porosity of packed bed (void fraction)
m_{dep}	g	Mass of deposit

q	$\frac{kg}{s}$	Mass flow rate
d	m	Asphaltene particle diameter
k_B	$J\,K^{-1}$	Boltzmann constant
T	K	Temperature

5.8. Bibliography

[1] M. P. Hoepfner, C. V. B. Fávero, N. Haji-Akbari, and H. S. Fogler, "The fractal aggregation of asphaltenes.," *Langmuir*, vol. 29, no. 28, pp. 8799–808, 2013.

[2] O. C. Mullins, H. Sabbah, A. E. Pomerantz, L. Barre, A. B. Andrews, Y. Ruiz-Morales, F. Mostowfi, R. McFarlane, L. Goual, R. Lepkowicz, T. Cooper, J. Orbulescu, R. M. Leblanc, J. Edwards, R. N. Zare, J. Eyssautier, and L. Barré, "Advances in Asphaltene Science and the Yen − Mullins Model," *Energy Fuels*, vol. 26, p. 3986−4003, 2012.

[3] J. Eyssautier, P. Levitz, D. Espinat, J. Jestin, J. Gummel, I. Grillo, and L. Barré, "Insight into asphaltene nanoaggregate structure inferred by small angle neutron and X-ray scattering.," *J. Phys. Chem. B*, vol. 115, no. 21, pp. 6827–37, Jun. 2011.

[4] G. P. Dechaine and M. R. Gray, "Membrane diffusion measurements do not detect exchange between asphaltene aggregates and solution phase," *Energy Fuels*, vol. 25, no. 2, pp. 509–523, 2011.

[5] S. R. Bagheri, A. Bazyleva, M. R. Gray, W. C. McCaffrey, and J. M. Shaw, "Observation of liquid crystals in heavy petroleum fractions," *Energy Fuels*, vol. 24, no. 8, pp. 4327–4332, 2010.

[6] T. Maqbool, A. Balgoa, and H. Fogler, "Revisiting asphaltene precipitation from crude oils: A case of neglected kinetic effects," *Energy Fuels*, no. 9, pp. 3681–3686, 2009.

[7] T. Maqbool, S. Raha, M. P. Hoepfner, and H. S. Fogler, "Modeling the Aggregation of Asphaltene Nanoaggregates in Crude Oil−Precipitant Systems," *Energy Fuels*, vol. 25, pp. 1585–1596, 2011.

[8] N. Haji-Akbari, P. Masirisuk, M. P. Hoepfner, and H. S. Fogler, "A Unified Model for Aggregation of Asphaltenes," *Energy Fuels*, vol. 27, no. 5, pp. 2497–2505, May 2013.

[9] C. Vilas Bôas Fávero, T. Maqbool, M. Hoepfner, N. Haji-Akbari, and H. S. Fogler, "Revisiting the flocculation kinetics of destabilized asphaltenes," *Adv. Colloid Interface Sci.*, 2016.

[10] N. Haji-Akbari, P. Teeraphapkul, A. T. Balgoa, and H. S. Fogler, "Effect of *n* -Alkane Precipitants on Aggregation Kinetics of Asphaltenes," *Energy Fuels*, vol. 29, no. 4, pp. 2190–2196, 2015.

[11] T. Maqbool, P. Srikiratiwong, and H. S. Fogler, "Effect of Temperature on the Precipitation Kinetics of Asphaltenes," *Energy Fuels*, vol. 25, no. 2, pp. 694–700, Feb. 2011.

[12] "ASTM D6560-12." .

[13] K. Akbarzadeh, H. Zhongxin, and G. Broze, "Flow-Through Tests Advance Researchers' Understanding of Asphaltene Deposition," *World oil*, no. February 2010, pp. 105–107, 2010.

[14] M. P. Hoepfner, V. Limsakoune, V. Chienmeechao, T. Maqbool, and H. S. Fogler, "A Fundamental Study of Asphaltene Deposition," *Energy Fuels*, no. 27, pp. 725–735, 2013.

[15] S. M. Hashmi, M. Loewenberg, and A. Firoozabadi, "Colloidal asphaltene deposition in laminar pipe flow: Flow rate and parametric effects," *Phys. Fluids*, vol. 27, no. 8, p. 83302,

2015.

[16] J. Wang, J. S. Buckley, and J. L. Creek, “Asphaltene Deposition on Metallic Surfaces,” *J. Dispers. Sci. Technol.*, vol. 25, no. 3, pp. 287–298, 2004.

[17] H. Alboudwarej, W. Svrcek, A. Kantzas, and H. W. Yarranton, “A Pipe-Loop Apparatus to Investigate Asphaltene Deposition,” *Pet. Sci. Technol.*, vol. 22, no. 7 & 8, pp. 799–820, 2004.

[18] J. Creek, J. Wang, and J. Buckley, “Verification of Asphaltene-Instability-Trend (ASIST) Predictions for Low-Molecular-Weight Alkanes,” *SPE Prod. Oper.*, vol. 24, no. 2, pp. 5–8, 2009.

[19] K. Kraiwattanawong, H. S. Fogler, S. G. Gharfeh, P. Singh, W. H. Thomason, and S. Chavadej, “Thermodynamic Solubility Models to Predict Asphaltene Instability in Live Crude Oils †,” *Energy Fuels*, vol. 21, no. 3, pp. 1248–1255, May 2007.

[20] W. Chaisoontornyotin, N. Haji-Akbari, H. S. Fogler, and M. P. Hoepfner, “A Combined Asphaltene Aggregation and Deposition Investigation,” *Energy Fuels*, p. acs.energyfuels.5b02427, 2016.

[21] L. Nabzar and M. Aguiléra, “The Colloidal Approach . A Promising Route for Asphaltene Deposition Modelling,” *Oil Gas Sci. Technol.*, vol. 63, no. 1, pp. 21–35, 2008.

[22] C. A. Bennett, “A Theory Describing Asphaltene Adhesion Fouling Inside Heat Exchanger Tubes,” *Heat Transf. Eng.*, vol. 33, no. 15, pp. 1246–1250, Dec. 2012.

[23] D. Eskin, J. Ratulowski, K. Akbarzadeh, and S. Andersen, “Modeling of asphaltene deposition in a production tubing,” *AIChE J.*, vol. 58, no. 9, pp. 2936–2948, 2012.

[24] T. G. M. van de Ven, “Colloidal Hydrodynamics.” Academic Predd Limited, p. 582, 1989.

[25] D. C. Prieve and E. Ruckenstein, “Effect of London forces upon the rate of deposition of Brownian particles,” *AIChE J.*, vol. 20, no. 6, pp. 1178–1187, 1974.

[26] H. S. Fogler, *Elements of chemical reaction engineering*. 2016.

[27] N. Wakao and T. Funazkri, “Effect of fluid dispersion coefficients on particle-to-fluid mass transfer coefficients in packed beds,” *Chem. Eng. Sci.*, vol. 33, pp. 1375–1384, 1978.

[28] D. Thoenes and H. Kramers, “Mass transfer from spheres in various regular packings to a flowing fluid,” *Chem. Eng. Sci.*, vol. 8, no. 3–4, pp. 271–283, Jun. 1958.

[29] E. Durand, M. Clemancey, J.-M. Lancelin, J. Verstraete, D. Espinat, and A.-A. Quoineaud, “Effect of Chemical Composition on Asphaltenes Aggregation,” *Energy Fuels*, vol. 24, no. 2, pp. 1051–1062, Feb. 2010.

CHAPTER VI

Asphaltene Destabilization, Aggregation, and Deposition in the Presence of Amphiphilic Molecules

6.1. Introduction

Asphaltenes are a class of molecules in crude oil that are soluble in aromatics, such as toluene, and insoluble in n-alkanes, such as heptane. During oil production, asphaltenes can deposit on the pores of reservoir and on the wall of wellbore, pipeline, and production equipment [1]. Amphiphilic molecules are known for to affect the behavior of asphaltenes in oil by avoiding and remediating asphaltene deposition [2]–[8]. The effect of these type of compounds, such as dodecylbenzene sulfonic acid and dodecylphenol, on the kinetics of asphaltene destabilization and aggregation has never been reported in the literature. In this investigation, the effect of the length of the alkyl chain, functional group, and number of repeating units on the asphaltene detection time, the centrifugation curve and the deposition rate in packed bed is investigated.

6.2. Experimental Methods

6.2.1. Addition of amphiphilic compounds to crude oil

The effect of amphiphilic compounds on the asphaltene destabilization and aggregation kinetics was investigated. In this investigation, amphiphilic compounds were added to the crude oil, and the oil-amphiphile mixture that is referred to as treated oil. In order to prepare an oil-amphiphile mixture, the volume of oil required for the desired experiments was separated into a glass bottle such that the head space of the bottle was less than the volume of oil in it. A Drummond microdispenser was used to add the necessary volume of amphiphile to oil. The crude oil treated

with amphiphile was shaken for 12 hours at 200 rpm using an orbital shaker at room temperature (22 ^{o}C). After 12 hours of agitation, the treated oil was used in detection time experiments, centrifugation experiments, and deposition experiments.

6.2.2. Detection time experiments

The detection time of asphaltene precipitation [9] was measured for crude oil and crude oils treated with the amphiphile compounds. In these experiments, heptane was added to oil at a controlled flow rate while the oil was continuously stirred. When the desired volume fraction of heptane in the oil-heptane mixture was reached, usually within 3 minutes, the flask was sealed, and mixture was kept stirred. Aliquots were then withdrawn as time elapsed and examined under the microscope for presence of detectable particles. Sampling was continued until particles were detected in micrographs. The detection time was defined as the time required for asphaltene particles to reach a size of 0.5 μm where they could be observed under the microscope. This procedure was repeated for different volume fractions of heptane in oil-heptane and the detection times recorded for different oils. A plot of the detection time as a function of the volume percent of heptane in the oil-heptane mixture was obtained as result. The experimental results in this plot is also referred to as detection time curve. The detection time curve was determined for a number of amphiphiles, namely dodecylbenzene sulfonic acid (DBSA), docecylbenzene (DB) and dodecylphenol (DP).

6.2.3. Centrifugation experiments

For the centrifugation experiments [9], heptane was added to oil while keeping the oil well mixed. When the desired volume fraction of heptane in the oil-heptane mixture was reached, the flask was sealed, and mixture continuously stirred. At specific times, aliquots are withdrawn and placed in 1.5 mL microcentrifuge tubes. The tubes were then centrifuged for 10 minutes at 16,000

g-force. The centrifugation separates asphaltenes that were aggregating to form a centrifugation cake and a supernatant. The centrifugation cake is typically comprised of 50 wt% asphaltenes and 50 wt% maltenes. The supernatant is decanted, the cake was washed with heptane and dried in oven at 70 ^{o}C. The washing of cake with heptane removes the maltenes from cake. The mass of dried cake was measured and the plot of mass of cake as a function of aging time of oil-heptane mixture is called the centrifugation curve.

6.2.4. Asphaltene deposition experiments in packed bed apparatus

Treated oil was placed into a 100 mL round bottle flask containing a stir bar such that the total mass of oil-heptane mixture would be 55 grams. Heptane was added to the oil while keeping the oil well mixed. The oil-heptane mixture was then injected in the packed bed for the deposition experiment, while the flow rate was controlled with a peristaltic pump. The flow rate was checked periodically to ensure it remained constant. After 8 hours, flow through the packed bed was stopped, the direction of the pump flow was reversed, and flow rate set to approximately 1 g/hour. After draining the packed bed, the deposited material was collected by injecting chloroform through the packed bed and collecting the effluent. The vial containing the effluent was then put in an evaporator for 7 days in order to evaporate the solvent and obtain a dry cake. The mass of collected material deposit was then measured. The details of this methodology can be found elsewhere [10].

6.3. Experimental Results

6.3.1. Effect of functional group of amphiphilic molecules

6.3.1A Detection time experiments

The detection time curve for pure oil H and oil H treated with 10,000 ppm of each dodecylbenzene sulfonic acid (DBSA), dodecylbenzene (DB), and dodecylphenol (DB) were obtained experimentally. The experimental results are shown in Figure 6.1.

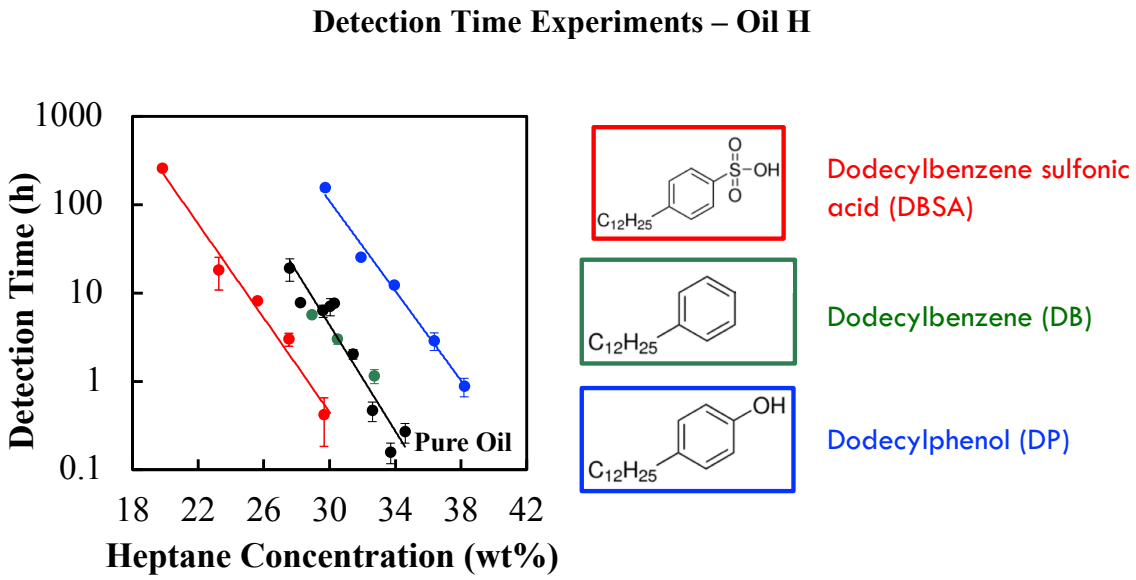

Figure 6.1 – Detection time curve for oil H and oil H treated with 10,000 ppm of dodecylbenzenesulfonic acid (DBSA), dodecylbenzene (DB), and dodecylphenol (DP).

The detection time curves in Figure 6.1 show that dodecylphenol (DP) is able to delay the detection time of asphaltene precipitation, while dodecylbenzene sulfonic acid (DBSA) accelerates the time of detection. On the other hand, treating oil with DB results in no measureable changes of detection time. If detection time of precipitation is a result of the interactions between asphaltenes, then two conclusions can be made from the results in Figure 6.1. First, a functional

group is required in an amphiphile molecule for the asphaltene-asphaltene interaction to be altered. And second, the functional group itself will affect the asphaltene-asphaltene interaction.

For the case where the amphiphilic molecule leads to a delay in detection time of asphaltene precipitation, i.e., when oil is treated with dodecylphenol, it is hypothesized that the hydroxyl group anchors on the heteroatoms on asphaltenes[2], leaving the alkyl chain behind that will increase the repulsion forces between asphaltenes. ***(Project 1)*** This hypothesis can be tested by running experiments with amphiphilic molecules with hydroxyl and function group and alkyl chains with less than 12 carbons. As the alkyl chain length decreases, the effect of this molecules on the asphaltene-asphaltene repulsion forces is expected to decrease.

On the other hand, treated oil H with DBSA would result in either an effective increase of attraction forces between asphaltenes or in an effective decrease of repulsion forces. ***(Project 2)*** Further investigation is required to understand how the interaction of DBSA and asphaltenes can result such changes in asphaltene interaction forces. Investigating the effect of DBSA concentration on the asphaltene detection time might help reveling the nature of asphaltene-DBSA interaction [2], [11], [12].

6.3.1B Centrifugation Experiments

Centrifugation experiments were performed with oil H and Oil H treated with 10,000 ppm of dodecylbenzene sulfonic acid (DBSA), dodecylbenzene (DB), and dodecylphenol (DB). The experimental results are presented in Figure 6.2.

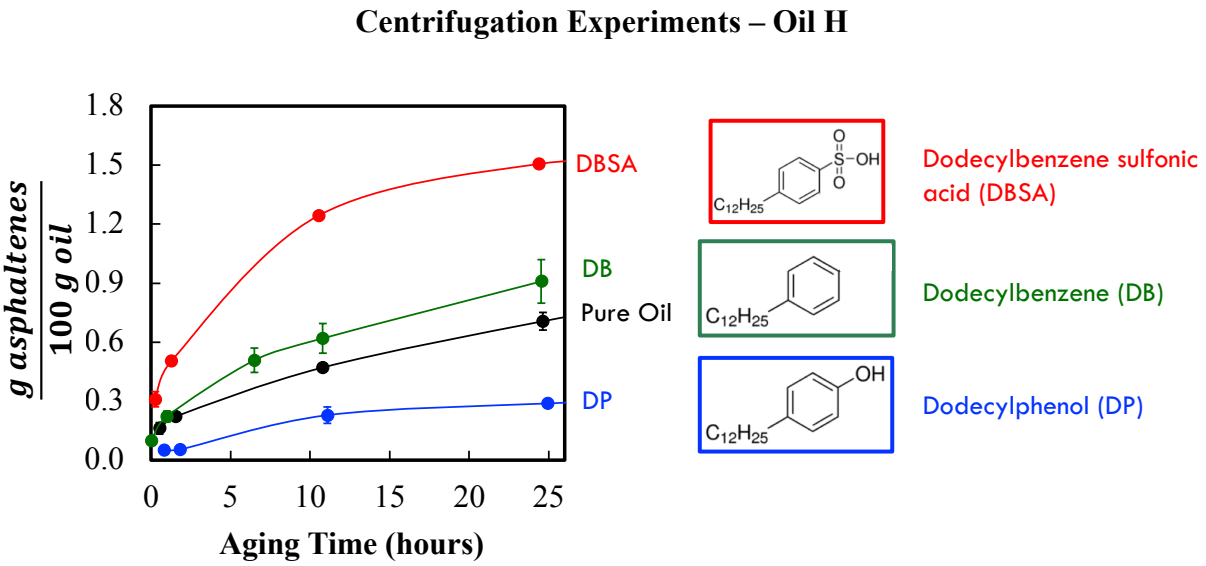

Figure 6.2 – Centrifugation curves for oil H and oil H treated with 10,000 ppm of dodecylbenzenesulfonic acid (DBSA), dodecylbenzene (DB), and dodecylphenol (DP). Experiments were performed at a heptane concentration of 30wt%.

Experimental results from Figure 6.2 indicate that the amount of asphaltenes that can be precipitated from oil-heptane mixture is affected by the presence of the amphiphilic molecules. Adding DBSA to oil H resulted in an increase of the amount of asphaltenes precipitated while DP results in a decrease in the amount precipitated when compared the base where were no amphiphiles were added. The addition of DB to oil H results in a slight increase in the amount of asphaltenes precipitated. ***(Project 3)*** It is recommended that experiments with pure oil and DB be re-run to assure that difference observed in results from Figure 6.2 are within experimental error.

It is hypothesized that the hydroxyl group anchors on the heteroatoms on asphaltenes[2], leaving the alkyl chain behind resulting in an increase in the repulsion forces between asphaltenes. ***(see Project 1)*** This hypothesis can be tested by running experiments with amphiphilic molecules with hydroxyl and function group and alkyl chains with less than 12 carbons. As the alkyl chain length decreases, the effect of the DP molecule on the asphaltene-asphaltene repulsion forces is expected to decrease.

6.3.1C Deposition Experiments

Asphaltene deposition experiments were performed with oil H treated with DBSA and DP at different concentrations as well as with untreated oil H. The experimental results are presented Figure 6.3.

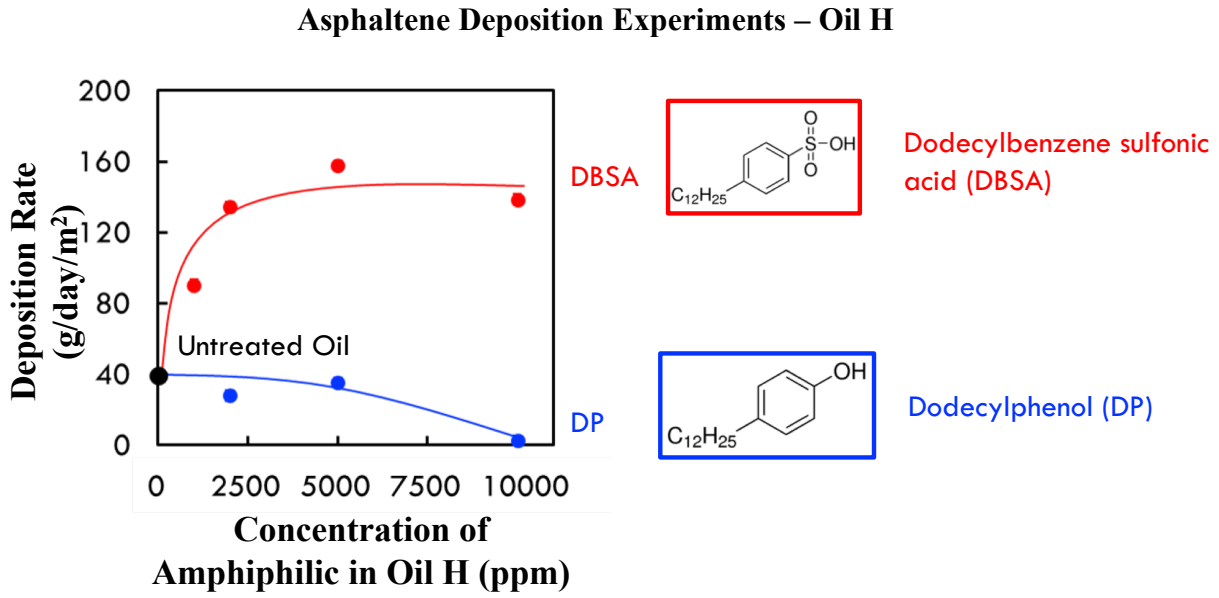

Figure 6.3 – Asphaltene deposition rate as function of concentration of DBSA and DP in Oil J. Experiments were performed at a heptane concentration of 30wt% and flow rate of 1.2 g/min.

It can be seen from Figure 6.3 that treating oil with DBSA results in a significant increase in the asphaltene deposition rate while treatment with DP caused deposition rate to decrease to zero at a concentration of 10,000 ppm. For the experiments where oil was treated with DP, no particles were detected under microscopy in the oil-heptane mixture fed to the packed bed. On the other hand, the experiments with DBSA particles were detected. In order to gain an insight on the effect of the amphiphilic molecules on asphaltene deposition, ***(Project 4)*** it would be important measure deposition rate in presence of amphiphiles where asphaltene particles are kept below 500nm. The experimental results should then be presented in a plot of deposition rate as a function

of concentration of unstable asphaltenes. Note that the amphiphiles not only affected the deposition rate but also affected the quantity of unstable asphaltenes in the oil-heptane mixture (See Figure 6.2). The diffusion-limited deposition model [10] can then be applied to obtain the diffusivity of the depositing asphaltenes. The model is valid for deposition of asphaltene particles smaller than 500 nm in an oil-heptane mixture under Stokes flow. The diffusivities of asphaltenes for the oil treated with amphiphiles should then be compared with the diffusivity of asphaltenes from the base case, i.e., untreated oil. If the diffusivity of asphaltenes that were treated with amphiphiles is several orders of magnitude lower than the diffusivity of base case, then this difference would serve as evidence that the deposition process in presence of amphiphile is reaction-limited. A deposition efficiency term could then be added to the diffusion-limited model and the deposition efficiency can then be obtained for the case of oil treated with amphiphiles.

6.3.2. Effect of amphiphilic molecules alkyl chain length

The effect of alkyl chain length was investigated for the amphiphilic molecules with a hydroxyl as the functional group. The centrifugation experiment results for dodecylphenol and nonylphenol are presented in Figure 6.4.

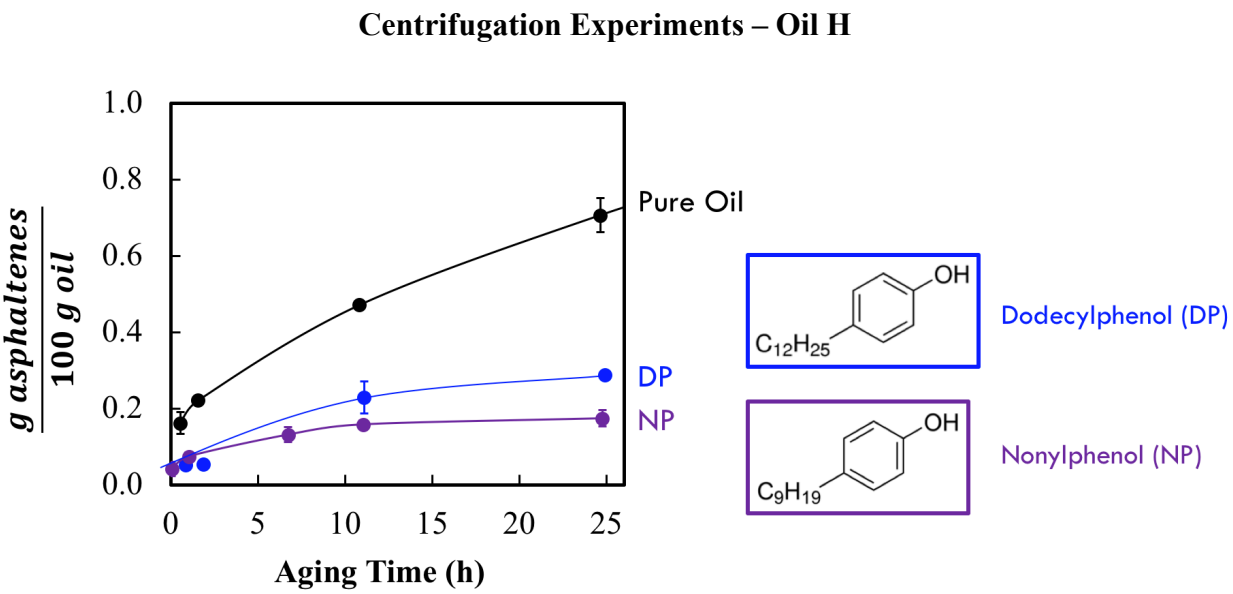

Figure 6.4 – Centrifugation curve for oil H untreated and treated with 10,000 ppm of DP and NP. Experiments performed with 30wt% heptane in oil-heptane mixture.

The experimental results in Figure 6.4 show that treating oil with NP or DP will result in a decrease of the amount of asphaltenes that can be precipitated from the oil-heptane mixture destabilized with 30wt% heptane. In addition, the results show that fewer asphaltenes are precipitated when oil was treated with NP when compared with oil treated with DP. This result indicates that the amphiphilic molecule with 9 carbons in the alkyl chain length was able to increase the repulsion forces between asphaltenes more than the amphiphilic molecule with 12 carbons. While this observation seems to go against the hypothesis that the alkyl chain of the amphiphilic molecule adds to the polymer brush of asphaltenes, it is important to note that the molar concentration of NP and DP in the treated oil are different. In these experiments, the concentration in ppmv was kept constant. ***(see Project 1)*** It would be important to perform experiments where the molar concentration of amphiphilic molecules in oil is kept constant while the length of alkyl chain is changed.

6.3.3. Effect of number of repeating units in amphiphilic molecules

The effect of the number of repeating units in the amphiphilic molecule on the centrifugation curve was investigated. Nonylphenol, containing 1 repeating unit, and poly-nonylphenol containing from 3 to 4 units, were used in this investigation. The experimental results are presented in Figure 6.5.

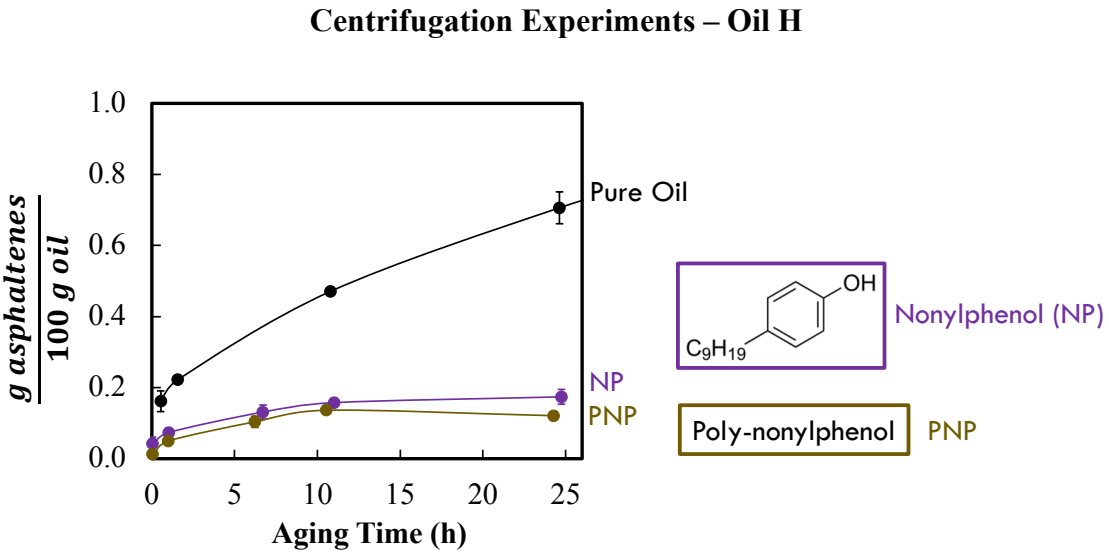

Figure 6.5 – Centrifugation curve for oil H untreated with treated with 10,000 ppm of NP and PNP. The PNP has a molecular weight of approximately 900g/mol. Experiments were performed at 30wt% heptane.

A decrease in the amount of asphaltene precipitated was observed when oil was treated with either NP or PNP. In order to further understand the mechanism of stabilization given by the PNP compared to NP, ***(Project 5)*** it would be important to identify the molecular structure of the polymer. The challenge in conducting this study on polymer of amphiphiles is on obtaining the polymer with known composition. Chemical vendors such as Nalco will not provide both the chemical and the molecular formula. A possible route to conduct these experiments is by sourcing the chemicals Tergitol NP-X from Dow Chemical.

6.3.4. Elemental analysis of precipitated asphaltenes

The carbon, hydrogen, nitrogen, oxygen, and sulfur content were measured for the asphaltenes precipitated 24 hours after heptane addition to untreated oil H, oil H treated with DBSA and also with oil H treated with DP. The results were then compared with the control case, i.e., untreated oil, and shown in Figure 6.6. These asphaltenes are the same as those shown in centrifugation curve in Figure 6.2.

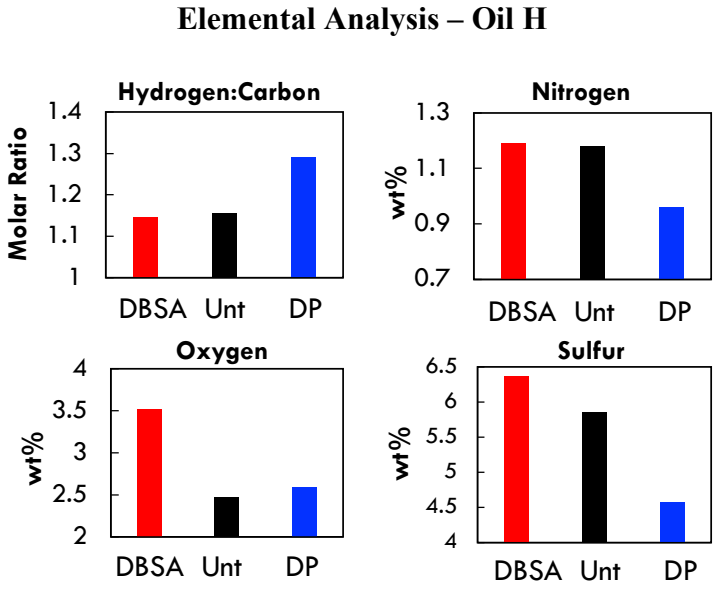

Figure 6.6 – Elemental analysis of asphaltenes that precipitated for untreated oil H, oil H treated with DBSA and oil H treated with DP.

The chemical characterization of the asphaltenes presented in Figure 6.6 suggests that DP is interacting with asphaltene molecules that are rich in sulfur and nitrogen and is preventing these asphaltenes from precipitating. The asphaltenes that do precipitate in presence of DP seem to have a H:C ratio higher than the untreated asphaltenes and about the same oxygen content. In order to interpret the H:C ratio and oxygen content, it is necessary to know the quantity of dodexylphenol in these asphaltenes. ***(Project 6)*** For further investigations, it would be measure the quantity of

amphiphiles that are associated with the asphaltene cakes. Fourier transform infrared spectroscopy has been used previously to such measurements[2], [13].

As shown in Figure 6.6, the sulfur and the oxygen content of the asphaltene precipitated in presence of DBSA is higher in the asphaltenes precipitated in absence of DBSA. This result suggest that DBSA is associated to asphaltenes that were precipitated by heptane.

The results of elemental analysis of precipitated asphaltenes indicates that the effect of the amphiphilic molecules will depend on the chemistry of the asphaltenes. It is therefore expected that different oils will have a different response when they are treated with the same amphiphilic molecules. In section 6.3.5. the effect of DBSA and DP on the centrifugation experiment of a different oil, oil E, was investigated.

6.3.5. Effect of DBSA and DP on a different oil (Oil E)

The effect of DBSA and DP on the centrifugation curve of oil E was investigated. The experimental results are presented in Figure 6.7.

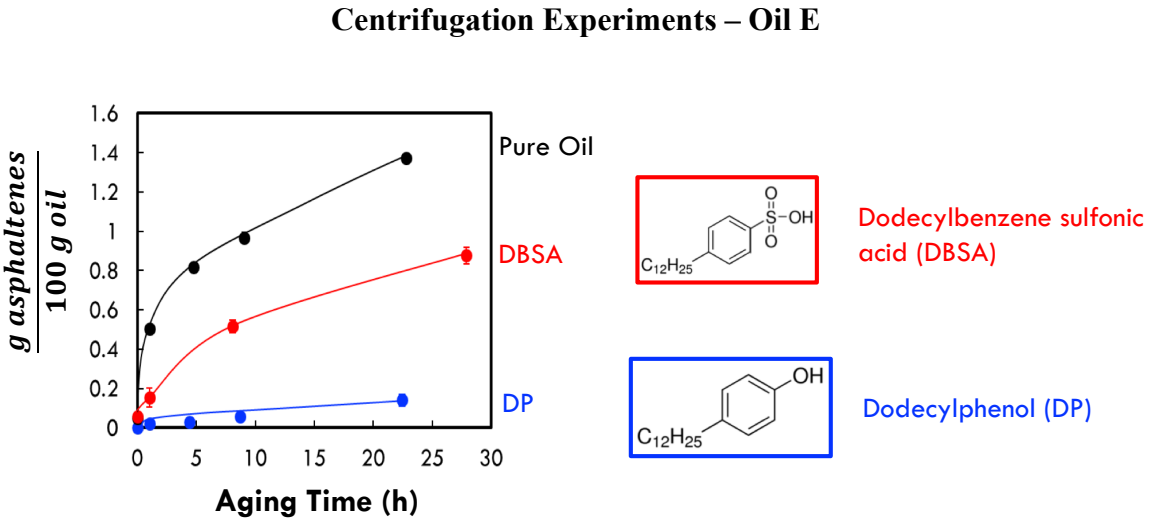

Figure 6.7 – Centrifugation curve for untreated oil E and treated with 10,000 ppm of DBSA and DP. The experiments were performed at a heptane concentration of 52.5wt%.

Experimental results in Figure 6.7 show that treating oil E with DBSA results in a decrease of the mass precipitated. The effect of DBSA on oil E is the opposite to the effect in oil H, where treating oil with DBSA resulted in increase of mass precipitated. This difference in response to DBSA for oils H and E can be the key in revealing mechanism of interaction between DBSA and asphaltenes. ***(Project 7)*** Chemical characterization of the asphaltenes from oil E are required to carry on this study.

6.4. Summary

The addition of amphiphilic molecules to crude oil can affect asphaltene destabilization, aggregation, and deposition. The functional group of the amphiphilic molecule and the type of crude oil will play a major role in how asphaltene destabilization and aggregation is affected. Treating oils H and E with dodecylphenol resulted in a decrease of the amount of asphaltenes precipitated. Elemental analysis of deposit suggests that dodecylbenzene interacts with asphaltenes containing high nitrogen and sulfur content, preventing these asphaltenes from precipitating. Dodecylbenzene sulfonic acid have opposite effects in oil H and oil E; it resulted in an increase of precipitation in oil H while the precipitation in oil E decreases.

6.5. Future Work

6.5.1. Project 1

Hypothesis: The hydroxyl group of the amphiphile anchors on the heteroatoms an asphaltene. The alkyl chain of this amphiphile is then incorporated to the alkyl chains of the asphaltenes, resulting in an increase of the repulsion forces between asphaltenes.

Experiment: Measure the detection time of asphaltene precipitation in the presence of amphiphiles with hydroxyl as function group and alkyl chains containing 3, 6, 9, and 12 carbons.

The concentration of amphiphile in oil, in moles of amphiphile per mass of oil, should be kept constant in this experiment.

Expected results: The detection time of asphaltene precipitation is expected to increase as the length of alkyl chain increases. The increase of detection time would be a result of the increase in repulsion forces between asphaltenes as the length of alkyl chain increases.

6.5.2. Project 2

Hypothesis: The sulfonic acid in an amphiphile increases the attraction forces between asphaltenes, resulting in an acceleration of the aggregation process.

Experiment: Measure the detection time of asphaltene precipitation in presence of two different sulfonic acid amphiphiles: one containing an alkyl chain of 3 carbons and the other containing 12 carbons.

Expected results: The detection time of precipitation is expected to remain constant as alkyl chain increases in the benzene sulfonic acid, indicating that the functional group sulfonic acid has a leading effect on the asphaltene-asphaltene interaction.

6.5.3. Project 3

Hypothesis: The presence of a functional group in the amphiphilic molecule is necessary for the amphiphile to modify the interactions between asphaltenes.

Experiment: Perform detection time experiments in presence of amphiphile molecules with 12 carbons in the alkyl chain and three different functional groups: sulfonic acid, hydroxyl, and no functional group. The concentration of the amphiphile in oil, in moles of amphiphiles per mass of oil, must be kept constant.

Expected results: The amphiphile with a sulfonic acid is expected to decrease the detection time of precipitation. The amphiphile with hydroxyl is expected to increase the detection time. And the amphiphile with no functional group is expected to have no effect on the detection time of precipitation.

6.5.4. Project 4

Hypothesis: The effect of dodecylbenzene sulfonic acid and dodecyl phenol on asphaltene deposition is due primarily to changes in the concentration of unstable asphaltenes caused by the amphiphiles.

Experiment: Measure deposition rate in presence of amphiphiles where asphaltene particles are kept below 500nm. The experimental results should then be presented in a plot of deposition rate as a function of concentration of unstable asphaltenes. The diffusion-limited deposition model [10] can then be applied to the experimental data to obtain the diffusivity of the depositing asphaltenes. The diffusivities of asphaltenes for the oil treated with amphiphiles should then be compared with the diffusivity of asphaltenes from the base case, i.e., untreated oil.

Expected results: The diffusivity of the depositing asphaltenes is expected to remain unaffected as oil is treated with amphiphile.

6.5.5. Project 5

Hypothesis: The polymer form of an amphiphile has a greater impact on the asphaltene precipitation, aggregation, and deposition than the monomer of the amphiphile.

Experiment: Measure the detection time of asphaltene precipitation in presence of amphiphile and amphiphile polymer with increasing molecular weight. In this test, the proportion

between number of monomer and mass of crude oil should be kept constant. A possible route to conduct these experiments is by sourcing the chemicals Tergitol NP-X from Dow Chemical.

Expected result: The detection time of asphaltene precipitation is expected to increase as the molecular weight of polymer increases.

6.5.6. Project 6

Hypothesis: The amphiphile containing sulfonic acid or hydroxyl as functional group anchors irreversibly with the heteroatoms of an asphaltene. The nature of the anchoring mechanism is an acid-base type of reaction.

Experiment: Dissolve solid asphaltenes in toluene to form a model oil and then add amphiphile to the model oil. Precipitate the asphaltenes from model oil using heptane and inspect supernatant for presence of amphiphile. Conduct experiment at increasing concentration of amphiphiles in model oil.

Expected Results: At low amphiphile concentrations in model oil, no amphiphiles are expected to be found in the supernatant. In this case, all amphiphiles would be anchored to the to the precipitated asphaltenes. As the concentration of amphiphiles in model oil increases, the asphaltenes become saturated with amphiphiles and amphiphile will be detected in the supernatant. The precipitated asphaltene can be analyzed with Fourier transform infrared spectroscopy to identify the nature of the amphiphile-asphaltene bold.

6.5.7. Project 7

The effect of dodecylbezene sulfonic acid (DBSA) on asphaltene precipitation, aggregation, and deposition is crude oil dependent. To reveal the interaction between crude oil and DBSA,

crude oil containing asphaltenes of different heteroatom content should be identified and detection time in presence of DBSA should be tested.

6.5. References

[1] J. Creek, J. Wang, and J. Buckley, "Verification of Asphaltene-Instability-Trend (ASIST) Predictions for Low-Molecular-Weight Alkanes," *SPE Prod. Oper.*, vol. 24, no. 2, pp. 5–8, 2009.

[2] C. Chang and H. Fogler, "Stabilization of asphaltenes in aliphatic solvents using alkylbenzene-derived amphiphiles. 1. Effect of the chemical structure of amphiphiles on asphaltene stabilization," *Langmuir*, no. 5, pp. 1749–1757, 1994.

[3] S. M. Hashmi and A. Firoozabadi, "Effective Removal of Asphaltene Deposition in Metal-Capillary Tubes," *SPE J.*, vol. 21, no. 5, pp. 1747–1754, 2016.

[4] A. H. Saeedi Dehaghani and M. H. Badizad, "Inhibiting asphaltene precipitation from Iranian crude oil using various dispersants: Experimental investigation through viscometry and thermodynamic modelling," *Fluid Phase Equilib.*, vol. 442, pp. 104–118, 2017.

[5] R. Skartlien, S. Simon, and J. Sjöblom, "A DPD study of asphaltene aggregation: The role of inhibitor and asphaltene structure in diffusion-limited aggregation," *J. Dispers. Sci. Technol.*, vol. 38, no. 3, pp. 440–450, 2017.

[6] J. Wang, C. Li, L. Zhang, G. Que, and Z. Li, "The properties of asphaltenes and their interaction with amphiphiles," *Energy Fuels*, vol. 23, no. 7, pp. 3625–3631, 2009.

[7] T. J. Kaminski, H. S. Fogler, N. Wolf, P. Wattana, and A. Mairal, "Classification of asphaltenes via fractionation and the effect of heteroatom content on dissolution kinetics," *Energy Fuels*, vol. 14, no. 1, pp. 25–30, 2000.

[8] F. J. Ortega, F. J. Navarro, and M. García-Morales, "Dodecylbenzenesulfonic Acid as a Bitumen Modifier: A Novel Approach to Enhance Rheological Properties of Bitumen," *Energy Fuels*, vol. 31, no. 5, pp. 5003–5010, 2017.

[9] C. Vilas Bôas Fávero, T. Maqbool, M. Hoepfner, N. Haji-Akbari, and H. S. Fogler, "Revisiting the flocculation kinetics of destabilized asphaltenes," *Adv. Colloid Interface*

Sci., 2016.

[10] C. Vilas Bôas Fávero, A. Hanpan, P. Phichphimok, K. Binabdullah, and H. S. Fogler, "Mechanistic Investigation of Asphaltene Deposition," *Energy Fuels*, vol. 30, no. 11, pp. 8915–8921, Nov. 2016.

[11] E. Rogel, "Effect of Inhibitors on Asphaltene Aggregation: A Theoretical Framework †," *Energy Fuels*, vol. 25, no. 2, pp. 472–481, Feb. 2011.

[12] S. M. Hashmi, K. X. Zhong, and A. Firoozabadi, "Acid–base chemistry enables reversible colloid-to-solution transition of asphaltenes in non-polar systems," *Soft Matter*, vol. 8, no. 33, p. 8778, 2012.

[13] C. L. Chang and H. S. Fogler, "Stabilization of Asphaltenes in Aliphatic Solvents Using Alkylbenzene-Derived Amphiphiles. 2. Study of the Asphaltene–Amphiphile Interactions and Structures Using Fourier Transform Infrared Spectroscopy and Small-Angle X-ray Scattering Techniques," *Langmuir*, vol. 10, no. 6, pp. 1758–1766, 1994.

CHAPTER VII

Conclusions

Asphaltenes are polyaromatic components of crude oil that undergo an aggregation process once they are destabilized by precipitants such as n-alkanes. Production of crude oil petroleum is often hindered by fouling caused by asphaltenes. The fouling can occur on any surface in contact with crude oil, from reservoir to refinery. The work presented in this dissertation was motivated by the scientifically challenging problems related to asphaltene destabilization, aggregation, and deposition. The main conclusions of the work are presented below.

Asphaltene Destabilization and Aggregation Kinetics

Asphaltenes are a class of molecules in crude oil that are soluble in aromatic solvents, such as toluene, and insoluble in n-alkanes, such as heptane. The amount of asphaltenes and the rate by which asphaltenes grow in solution depend on the crude oil and on the concentration of n-alkanes in the oil-alkane mixture. Bulk flocculation and deposition experiments have demonstrated that there is no such thing as an "onset concentration", i.e., a concentration of alkane in oil-alkane mixture below which asphaltenes are inherently stable. The kinetics of asphaltene aggregation, assessed by means of detection time measurements, can be explained by unified aggregation model. The unified aggregation model is derived from the population balance with the Smoluchoswski collision kernel, an Arrhenius type of relation between the collision efficiency and the difference of solubility parameters of the solution and the asphaltenes. The unified aggregation model successfully predicts the aggregation of asphaltenes in dozens of combinations of different crude oil, model oils, precipitants, and asphaltenes.

Fractionation and Characterization of Asphaltenes

The impact of asphaltene polydispersity on asphaltene destabilization and aggregation was investigated. Experimental results show that asphaltene fractions will interact in solution and asphaltene-asphaltene interaction must be taken in account when computing asphaltene parameters such as solubility parameter and particle sizes. It was also found that regardless of asphaltene origin, as long as they have the same solubility parameter they will have same radius of gyration when suspended in toluene. This result indicates that the grater the cohesive energy per molecular volume, the greater the association of asphaltenes are as measured by the radius of gyration. Finally, asphaltene fractions obtained at the same fractionation condition (e.g., 1 day of aging, soluble at 48% heptane and precipitated at 60% heptane) but from different asphaltenes have identical detection time curve and, consequently, same stability. Further characterization of these fraction with same stability can reveal the mechanism of asphaltene destabilization by n-alkanes.

Dissolution of Solid Asphaltenes in Solvents

An experimental methodology was developed to measure rates of asphaltene dissolution in solvents. At sufficiently high fluid flow velocities around dissolving asphaltene particle, the dissolution rate was found to be independent of the flow velocity. The specific dissolution rate of asphaltenes from different crude oils was obtained at this high fluid region. It was found that asphaltene from different origins dissolve at different rates in toluene, with rates ranging from 0.20 to 0.74 (kg/s)/kg. This difference in dissolution rate could be due to differences in the asphaltene specific surface area. Experimental results also show that the solvent plays a role in the dissolution process, and the rate of dissolution of asphaltenes in chloroform is higher than in toluene.

A Mechanistic Investigation of Asphaltene Deposition

A new apparatus to study asphaltene deposition is introduced. The apparatus consists of a packed bed of stainless steel beads over which a mixture of oil and precipitant is flown and the asphaltene deposit monitored. The asphaltene deposition rate was measured as a function of fluid flow rate for crude oils from different origins and at different heptane concentrations in oil-heptane mixtures. The asphaltene deposit profile along the packed bed was also investigated. Experimental results show three important findings. (1) It was observed that the asphaltene deposition rate increases linearly with the concentration of unstable asphaltenes. (2) The deposition rate of unstable asphaltenes scaled with the square root of the fluid flow velocity in viscous flow regime, indicating that the asphaltene deposition process can be explained by a diffusion-limited deposition of nanoparticles. And (3), the asphaltene deposition profile along the packed bed matches theoretical behavior predicted by the diffusion-limited correlations for mass-transfer deposition.

Asphaltene Destabilization, Aggregation, and Deposition in the Presence of Amphiphilic Molecules

The addition of amphiphilic molecules to crude oil can affect asphaltene destabilization, aggregation, and deposition. The functional group of the amphiphilic molecule and the type of crude oil will play a major role in how asphaltene destabilization and aggregation is affected. Treating oils H and E with dodecylphenol resulted in a decrease of the amount of asphaltenes precipitated. Elemental analysis of deposit suggests that dodecylbenzene interact with asphaltenes containing high nitrogen and sulfur content, preventing these asphaltenes from precipitating. DBSA have opposite effects in oil H and oil E. DBSA led to an increase of precipitation in oil H and a decrease in oil E.

CHAPTER VIII

Future Work

Project 1 – Effect of amphiphiles on asphaltene destabilization, aggregation, and deposition

Understanding the effect of amphiphile molecules on the asphaltene destabilization, aggregation, and deposition asphaltenes is important for two reasons. First, the amphiphiles can be used as probe molecules that will interact with asphaltenes and can help one understand the nature of asphaltenes. And second, it can provide framework for the design of molecules to be used in mitigating asphaltene deposition problems.

Project 1.1 – Hydroxyl as a functional group in amphiphiles

Hypothesis: The hydroxyl group of the amphiphile anchors on the heteroatoms an asphaltene. The alkyl chain of this amphiphile is then incorporated to the alkyl chains of the asphaltenes, resulting in an increase of the repulsion forces between asphaltenes.

Experiment: Measure the detection time of asphaltene precipitation in the presence of amphiphiles with hydroxyl as function group and alkyl chains containing 3, 6, 9, and 12 carbons. The concentration of amphiphile in oil, in moles of amphiphile per mass of oil, should be kept constant in this experiment.

Expected results: The detection time of asphaltene precipitation is expected to increase as the length of alkyl chain increases. The increase of detection time would be a result of the increase in repulsion forces between asphaltenes as the length of alkyl chain increases.

Project 1.2 – Sulfonic acid as a functional group in amphiphiles

Hypothesis: The sulfonic acid in an amphiphile increases the attraction forces between asphaltenes, resulting in an acceleration of the aggregation process.

Experiment: Measure the detection time of asphaltene precipitation in presence of two different sulfonic acid amphiphiles: one containing an alkyl chain of 3 carbons and the other containing 12 carbons.

Expected results: The detection time of precipitation is expected to remain constant as alkyl chain increases in the benzene sulfonic acid, indicating that the functional group sulfonic acid has a leading effect on the asphaltene-asphaltene interaction.

Project 1.3 – Importance of functional group in the amphiphile-asphaltene interaction

Hypothesis: The presence of a functional group in the amphiphilic molecule is necessary for the amphiphile to modify the interactions between asphaltenes.

Experiment: Perform detection time experiments in presence of amphiphile molecules with 12 carbons in the alkyl chain and three different functional groups: sulfonic acid, hydroxyl, and no functional group. The concentration of the amphiphile in oil, in moles of amphiphiles per mass of oil, must be kept constant.

Expected results: The amphiphile with a sulfonic acid is expected to decrease the detection time of precipitation. The amphiphile with hydroxyl is expected to increase the detection time. And the amphiphile with no functional group is expected to have no effect on the detection time of precipitation.

Project 2 - Asphaltene Destabilization and Aggregation in Crude Oil Blends

Two crude oils are said to be incompatible if their asphaltenes can destabilize and aggregate when these two crude oils are mixed with each other. It has been observed that the destabilization and aggregation process of asphaltenes in blends of crude oil is similar to the process observed in oil-alkane mixture as measured by detection time experiments. It is expected that the unified aggregation model, which has been developed for oil-alkane mixtures, can be extended and used to explain and predict asphaltene destabilization for blends of incompatible crude oil as well. Further investigation is necessary to extend the unified aggregation model to be used with blends of incompatible crude oils. Preliminary results as well as path forward are presented below.

In order to investigate the destabilization and aggregation of asphaltenes in blends of crude oil, three crude oils were selected, and their properties are presented in Table 8.1.

Table 8.1 - Density, Asphaltene Content, Refractive Index and Viscosity of Oils F, G, and H

Crude Oil	**F**	**G**	**H**
Density (g/mL) @ 20°C	0.884±0.005	0.891±0.005	0.805±0.005
Asphaltene Content (wt%)	4.64	0.98	0.27
Refractive Index @ 20°C	1.5071	1.4994	1.4603
Viscosity (Pa.s) @ 20°C	0.042	0.031	0.0042

Detection time experiments were performed with crude oils F, G, and H using n-heptane as precipitant. The detection time curves are presented in Figure 8.1.

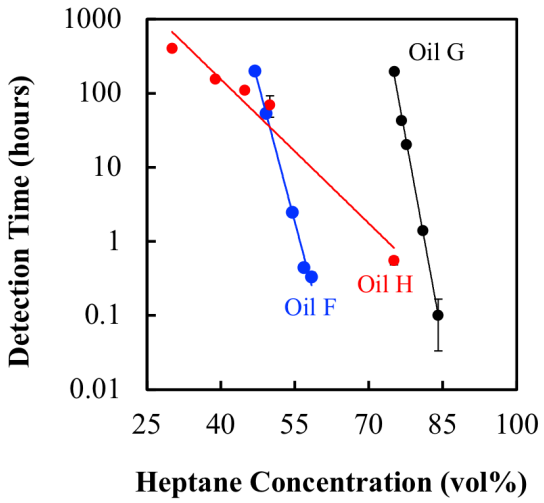

Figure 8.1 – Detection time curves of crude oils F, G and H.

In order to test for oil incompatibility, crude oils F, G, and H were blended in binary mixtures of fixed concentration of 90vol%. In these blending experiments, crude oil F is added into crude oil G as oil G is kept stirred to obtain a final mixture of 90vol of F in G. All binary blends among oils F, G, H are made and monitored under optical microscopy for 1 week as they age. Experimental results are presented in Table 8.2.

Table 8.2 – Inspection for incompatibility of binary blends of crude oils F, G, and H at a 9:1 volume ratio, i.e., a blend of oil F and G was prepared by adding oil F into oil G to obtain a final mixture containing 90vol% of oil F in the F-H blend.

90% F in G	90% G in F	90% G in H	90% H in G	90% F in H	90% H in F
No precipitation detected within one week					Precipitation detected

Experimental results from Table 8.2 shows that only the 90% blend of oil H added into oil F resulted in a detection of asphaltene precipitation within a week after the oils are blended. The detection time curve was then obtained for the blend of oil H into oil F and experimental results are presented in Figure 8.2.

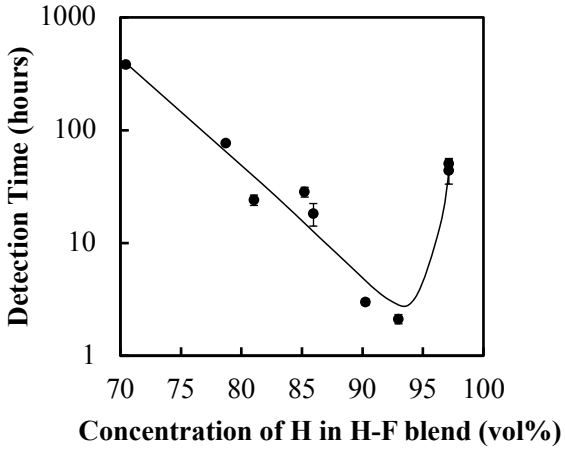

Figure 8.2 – Detection time of asphaltene precipitation when crude oil H is added into crude oil F.

It can be seen in Figure 8.2 that the detection time of asphaltene precipitation first decreases logarithmically, similar to the results in crude oil-heptane experiments, and then increases after 95% of oil H in oil F.

In detection time experiments where heptane is added to oil, there are only asphaltenes from one crude that can precipitate. However, in experiments where two incompatible crude oils are blended the precipitation of asphaltenes from either or both crude oils can precipitate. Therefore, in order to understand the kinetics of asphaltene destabilization and aggregation in blends of crude oil it is important to first understand how the blend of two asphaltenes behave. An investigation of blends of asphaltenes extracted from different crude oils and redissolved in a solvent can help understand the destabilization of asphaltenes in blend of crude oils. In addition to the asphaltene-asphaltene interaction, the asphaltene-maltene interaction also must be investigated. This investigation can be done by mixing asphaltenes from oil H with maltenes from oil F and vice versa and measuring their detection time curve.

Project 3 - Effect of Aging on the Detection Time Curve of Model Oils

Model oils consists of asphaltenes redissolved in solvents, such as toluene. It has been observed that the stability of asphaltenes in model oils decreases as the model oil ages. Understanding the aging process of asphaltene in model oil can help reveal the nature of asphaltene nanoparticle and cluster formation, and it would be an interesting project pursue. Preliminary results as well as a hypothesis to explain the aging of model oils are presented below.

In this experiment asphaltenes are dispersed in toluene at 3 and 10wt% of asphaltenes. The model oil is then split into three well bottles. The first bottle of model oil is used in the same day as it was prepared to obtain the detection time of asphaltenes. The model oil in second bottle is aged for 2 weeks, and the third bottle is aged for 4 weeks before being used for the detection time experiments. The bottles are well sealed during aging. The schematics of the experimental protocol is presented in Figure 8.3.

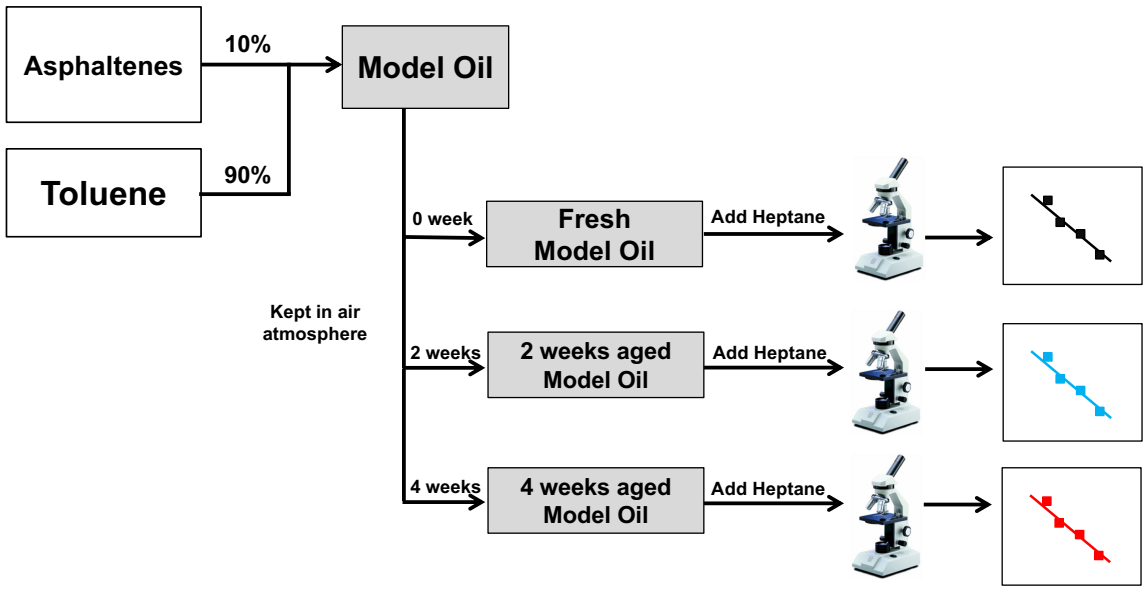

Figure 8.3 – Schematics of the experimental procedure adopted to study the aging of model oil.

The experimental results for BR asphaltenes are presented in Figure 8.4.

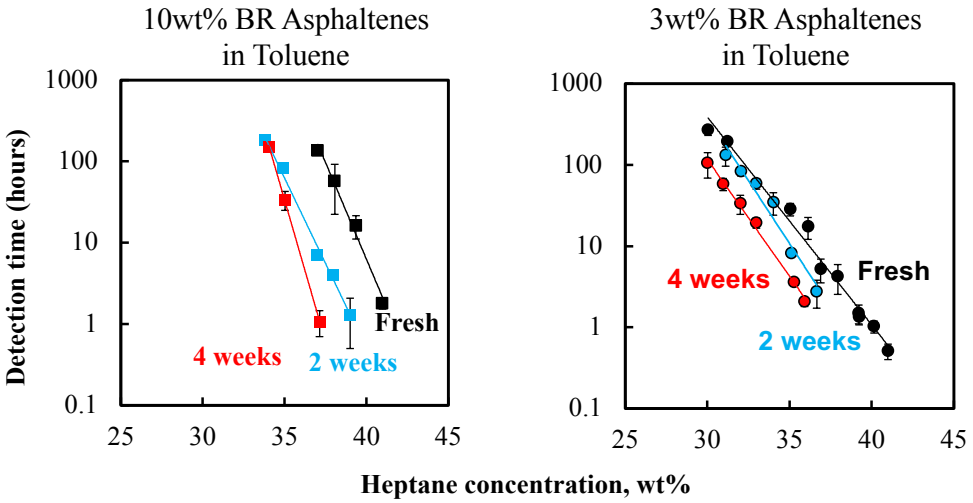

Figure 8.4 – Detection time curve of BR model oils as the model oil ages

It can be seen that at the model oil ages, the detection time curve shifts to the left as a result of less heptane being required for asphaltene precipitation to be detected. The aging is more pronounced for the model oil with 10wt% asphaltenes. Experiments were also performed with asphaltenes from different origin (GM asphaltenes). The experimental results presented in Figure 8.5 indicate the same behavior as BR asphaltenes, as the detection time curve shifts to the left as it ages.

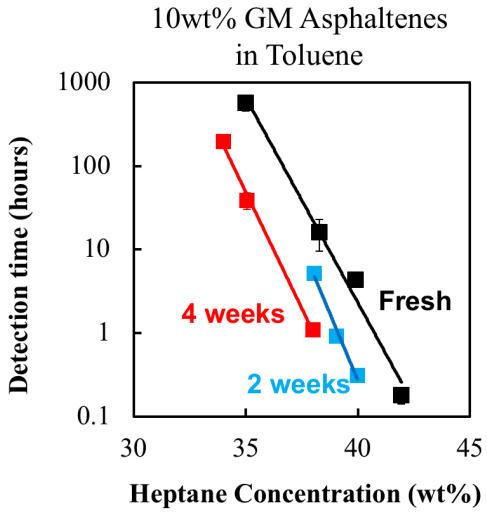

Figure 8.5 – Detection time curve of BR model oils as the model oil ages

It is hypothesized that as the model oil ages, asphaltenes clusters grow with time and when heptane is added to the aged model oil, the particles are larger to start with and will take shorter time to reach detectable size of 0.5um.

Project 4 - Effect of Water on Asphaltene Destabilization and Aggregation

It has been observed that when water is present in crude oil during production, asphaltenes deposition does not occur. However, it is not fully understood how water can prevent asphaltenes from depositing. The use of the techniques discussed in this dissertation, namely detection time experiments, centrifugation experiments, and packed bed deposition, can be used to help elucidate the mechanism by which water prevents asphaltenes from depositing. Preliminary results on the effect of water on the detection time of asphaltene precipitation as well as path forward for this project are presented below.

In these experiments, water is added to crude oil, the mixture is homogenized to form an emulsion, and then water is removed by centrifugation. The detection time curve of the

centrifugation supernatant was then obtained. This procedure of water addition-emulsification-centrifugation is repeated 4 times and the detection time curve of each supernatant is obtained. Experimental results are shown in Figure 8.6.

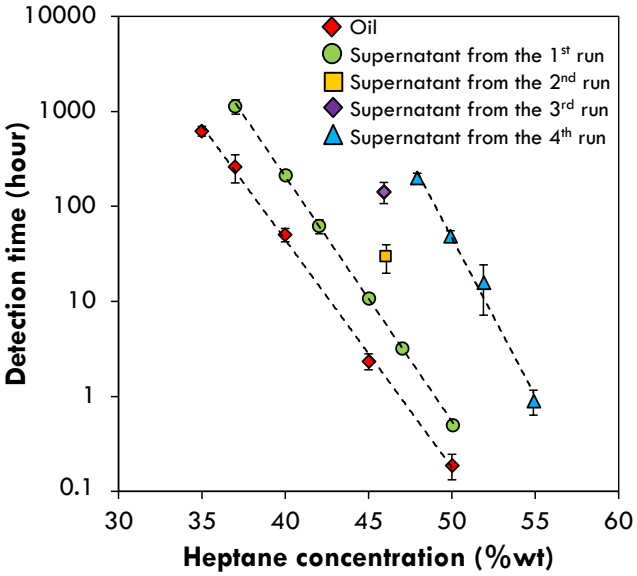

Figure 8.6 – Detection time of asphaltene precipitation for pure oil and oil washed with water to remove interfacially active asphaltenes.

It can be seen that the detection time of asphaltene precipitation increases, for a fixed heptane concentration, as the oil is "washed" with water. This result suggests that the water-oil traps asphaltenes when the emulsion is centrifuged, and as a result the oil in the centrifugation supernatant contains asphaltenes that are more stable than the original oil. In future investigation, the quantity of asphaltene left in solution as well as the asphaltene deposition rate could be obtained to further the effect of water on asphaltene deposition.

APPENDICES

APPENDIX A

Comparison of solubility parameter obtained from aggregation model and from Buckley refractive index correlation

In order to obtain the master line (Figure 2.25 in Chapter 2) the solubility parameter of asphaltene B as measured by Buckley refractive index correlation [24] was considered the benchmark. The Buckley correlation was obtained by measuring the solubility parameter and the refractive index of organic liquid compounds such as heptane, toluene and 1-methylnaphtane. A plot of the solubility parameter as a function of the refractive index function forms a straight line. The regression of this straight line provides the Buckley equation, i.e.,

$$\delta = 52.042\ \mathrm{F}_{RI} + 2.904 \tag{1}$$

Where δ is in units of $MPa^{1/2}$. F_{RI} is the refractive index function defined as

$$\mathrm{F_{RI}} = \frac{\mathrm{RI}^2 - 1}{RI^2 + 2} \tag{2}$$

In this correlation, it is assumed that the cohesive energy between asphaltene molecules is entirely given by dispersion forces. All other interactions between asphaltenes, such as hydrogen bonding and polar forces are neglected.

Next, the refractive indexes of the asphaltenes extracted from crude oil A, C, D, and E were measured and their solubility parameter was calculated using the refractive index correlation from Equation 14 and 15. Figure 2.26 shows the parity plot comparing the solubility parameters of asphaltenes obtained from the unified aggregation curve and from the Buckley refractive index correlations.

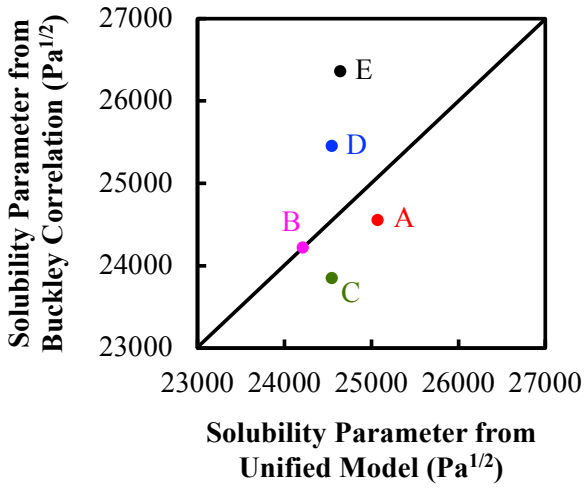

Figure A.1 – Comparison of the solubility parameter for asphaltenes A, B, C, D, E obtained with the aggregation model and with the refractive index correlation

The solubility parameter of asphaltenes B are identical for the two different methods as the solubility parameter from refractive index correlation was therefore used as the benchmark case. The deviation of the solubility parameters as measured by aggregation model and by refractive index correlation are possibly related to the uncertainty on the solubility parameter of the maltenes and also on the polydispersity of asphaltenes.

APPENDIX B

Effect of Oxygen from Air on Asphaltene Destabilization and Aggregation

B.1. Introduction

A challenge to the interpretation of the detection time and centrifugation experiments was been made by Prof. Yarranton's research group at the University of Calgary based on their bitumen experiments. Using bitumen, they have found that the oxygen from air plays a role in the kinetics of asphaltene destabilization and aggregation. Based on his results, Prof. Yarranton suggested that the long-term kinetics of asphaltene destabilization and aggregation is an experimental artifact related to oxidization of oil molecules with oxygen from air [1].

B.2. Experimental Methods

In order to learn if the oxygen from air is indeed affecting the kinetics of asphaltene destabilization and aggregation, centrifugation experiments were be performed for a given crude oil both in air and in nitrogen environments. The schematics of the experiments in nitrogen and air atmosphere are shown in Figure B.1.

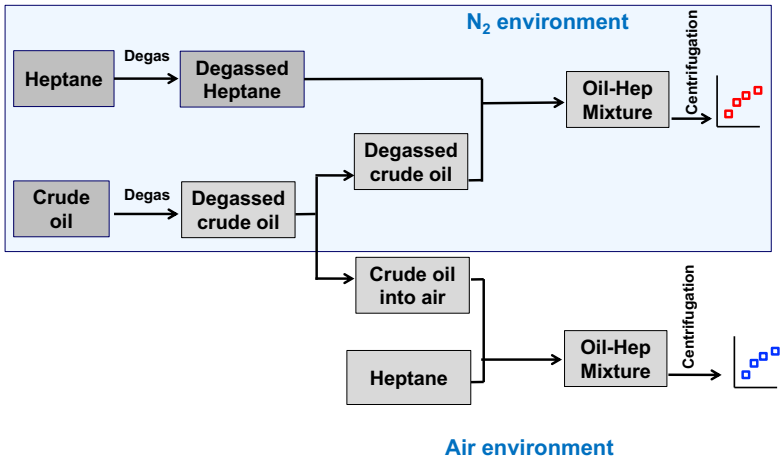

Figure B.1 – Schematics of the centrifugation experiments performed in air and in nitrogen environment.

As shown in Figure B.1, crude oil and heptane are first introduced to the nitrogen environment for degassing. The degassing process consists of blowing nitrogen through the liquid for 5 hours while keeping the liquid stirred. The goal of the degassing procedure is to displace the dissolved oxygen from heptane and crude oil for the experiments in nitrogen environment. The degassed oil is then split into two bottles, one of which will be removed from the nitrogen environment and reintroduced to air environment. Equipment, glassware, gloves, and other materials required for the centrifugation experiments were placed in the nitrogen environment as well in order to guarantee that the oil and heptane would not be in contact with air.

B.3. Experimental Results and Discussion

Centrifugation experiments were then performed for heptane concentration of 50, 60 and 70wt% both in nitrogen and air atmosphere and experimental results are presented in Figure B.2.

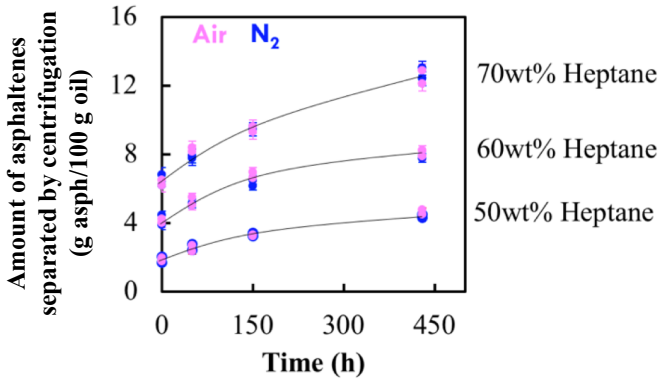

Figure B.2 –Concentration of asphaltenes that can be separated out of solution by centrifugation as a function of aging time for heptane concentration of 50, 60, and 70wt% both in nitrogen and air atmosphere.

It can be seen from Figure B.2 that amount of asphaltenes that can be removed by centrifugation is identical for the air and nitrogen environment. Therefore, experimental results do not indicate that the kinetics of destabilization and aggregation are related to oxygen from air.

The effect of oxygen from air on the detection time experiment was also investigated. In this experiment, the detection time curve of fresh asphaltenes and recovered asphaltenes is obtained for a model oil. Recovered asphaltenes consist of the asphaltenes that are obtained by evaporating the toluene and heptane from the experiments to obtain the detection time curve of the fresh. If the detection time of asphaltene precipitation is a result of oxidation of asphaltenes with oxygen from air, then the recovered asphaltenes would be chemically different than the fresh asphaltenes and, therefore, fresh and recovered asphaltenes are expected to have a different detection time curve. The schematics for this experiment is shown in Figure B.3.

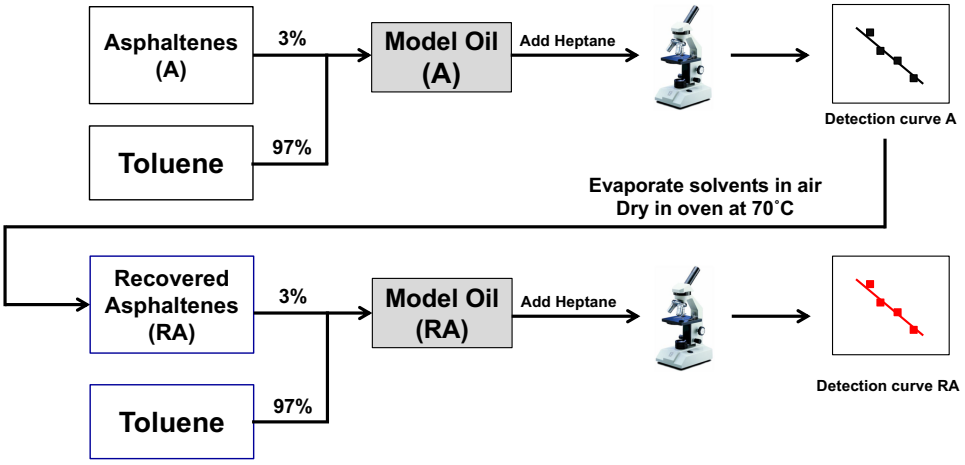

Figure B.3 – Schematics of the detection time experiment for fresh and recovered asphaltenes used to investigate effect of oxygen from air on asphaltene destabilization and aggregation kinetics.

The experimental results of detection time for fresh and recovered asphaltenes are presented in Figure B.4.

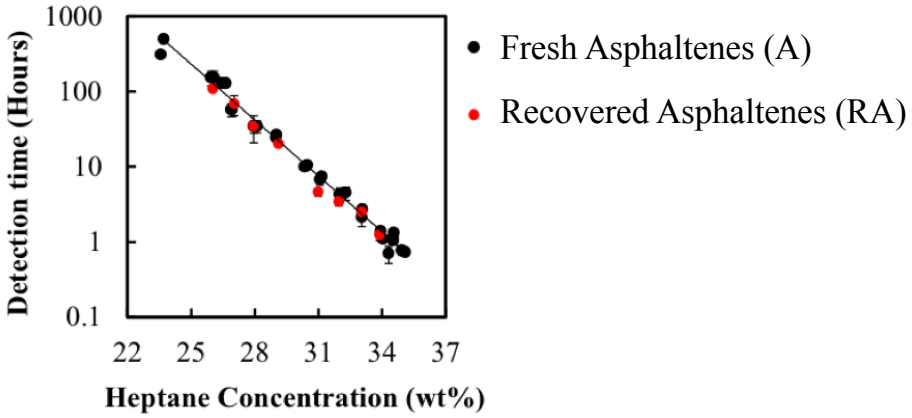

Figure B.4 – Detection time curves for fresh and recovered asphaltenes

The experimental results presented in Figure B.4 show that the detection time curve of fresh and recovered asphaltenes are undistinguishable.

B.4. Conclusions

It can be concluded that while there might be an effect of oxygen from air on the kinetics of asphaltenes destabilization and aggregation in bitumen samples, the long-term kinetics of asphaltene destabilization and aggregation in crude oil are not a result of oxidization of asphaltenes or of other crude oil molecules oxidizing turning into asphaltene-like molecules.

References

[1] J. Beck, W. Svrcek, and H. Yarranton, “Hysteresis in asphaltene precipitation and redissolution,” *Energy Fuels*, vol. 19, no. 3, pp. 944–947, 2005.

[2] T. Maqbool, S. Raha, M. P. Hoepfner, and H. S. Fogler, “Modeling the Aggregation of Asphaltene Nanoaggregates in Crude Oil−Precipitant Systems,” *Energy Fuels*, vol. 25, pp. 1585–1596, 2011.

APPENDIX C

Dissolution rate of asphaltenes B and C (whole and fractions)

The rate of dissolution of asphaltenes as a function of the squared difference of solubility parameter of asphaltenes in toluene is presented in Figure C.1.

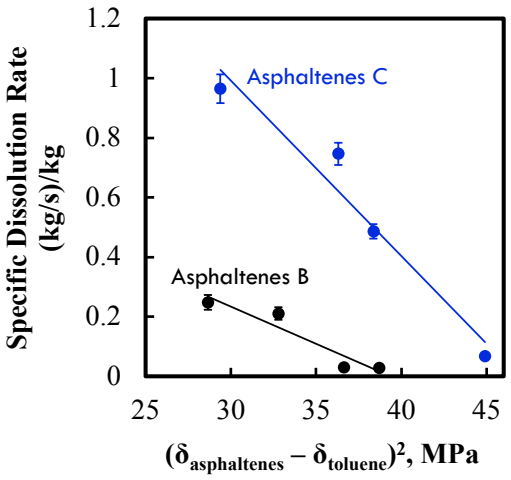

Figure C.1 – Asphaltene dissolution rate as a function of the squared difference of the solubility parameters of asphaltenes and toluene

Experimental results from Figure 3.16 show that as difference in solubility parameter of asphaltenes and toluene increases, the rate of dissolution decreases. This trend is expected, given that the solubility of asphaltenes in toluene decrease as the difference in solubility parameter increases. However, for a given of $(\delta_{asph} - \delta_{toluene})^2$, asphaltenes B and C will have different dissolution rates. This result suggests that there should be another parameter that is important for the process of dissolution and that is not captured by the solubility parameters. Further investigation is necessary to reveal the additional governing parameters of dissolution process.

APPENDIX D

Visual Inspection of Asphaltene Deposit Formation

In the deposition experiments discussed in Chapter V, oil-heptane mixture containing unstable asphaltenes are fed to the packed bed and the mass of deposit is measured at the end of the experiment. The formation of deposit can also be confirmed by visual inspection. Images of the packed bed before and after a deposition experiment are shown in Figure D.1.

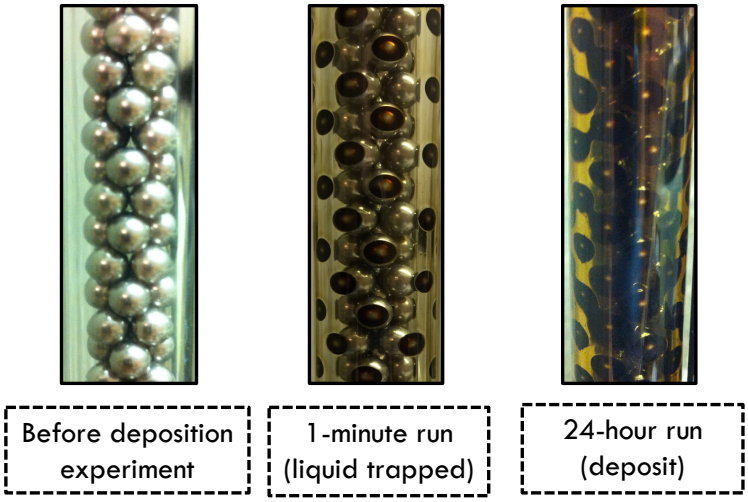

Figure D.1 – Visual inspection of deposit formation in packed bed

Figure D.1. shows three images of the packed bed. The first image is the packed bed before the deposition experiment. In the second image, oil-heptane was flown through packed bed and then drained. In this case, there is liquid trapped in the corners between glass wall and beads, but no deposit. In the third image, an oil-heptane mixture was fed to the packed bed for 24 hours and then drained. It can be seen that after 24 hours the beads are completely covered with deposits. The asphaltene content of the deposit is measured and found to be 50wt%. These images are for the deposits of Oil E, heptane concentration of 67wt, flow rate of 0.9 g/min, and 48 hours of run-time.

APPENDIX E

Effect of Asphaltene Particle Size, Bead Diameter of Packed Bed, and Bead Material of Packed Bed on the Asphaltene Deposition Rate

E.1. Effect of Asphaltene Particle Size on the Asphaltene Deposition Rate

When heptane is added to crude oil, a fraction of asphaltenes will destabilize and undergo an aggregation process. As heptane concentration increases, the fraction of asphaltenes that become unstable also increases. For a given heptane concentration in oil-heptane mixture, the asphaltene particles will grow in size as the mixture ages. Figure E.1 presents a schematic of the effect of heptane concentration and aging time on asphaltenes.

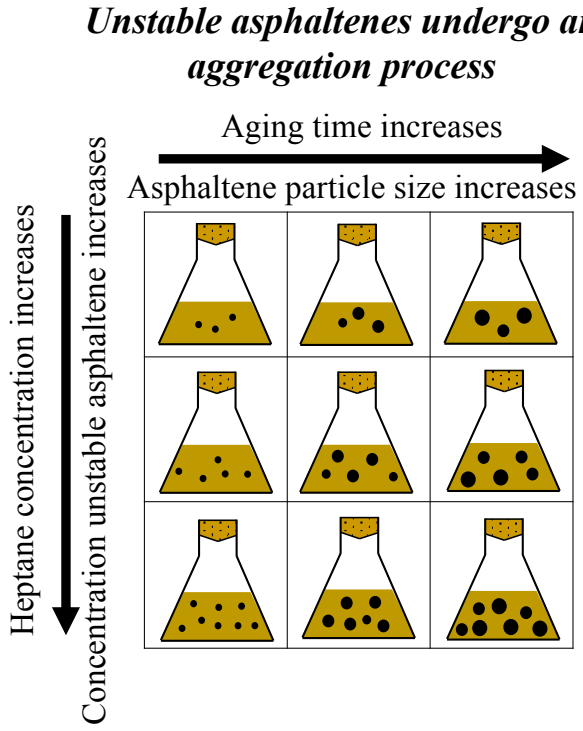

Figure E.1 – Effect of heptane concentration and aging time on the concentration and size of unstable asphaltenes in oil-heptane mixture.

The effect of aging time on asphaltene deposition was studied. For that, 37.5wt% of heptane was added to Oil G. The deposition experiments were performed at a flow rate of 0.9g/min, run-time of 8 hours, and reservoir replacement of 2 hours. Three aging times were investigated: 0, 44, and 96 hours. The concentration of asphaltenes smaller than and larger than 400nm was measured using centrifugation method. This method is described elsewhere [1]. Experimental results are presented in Figure E.2.

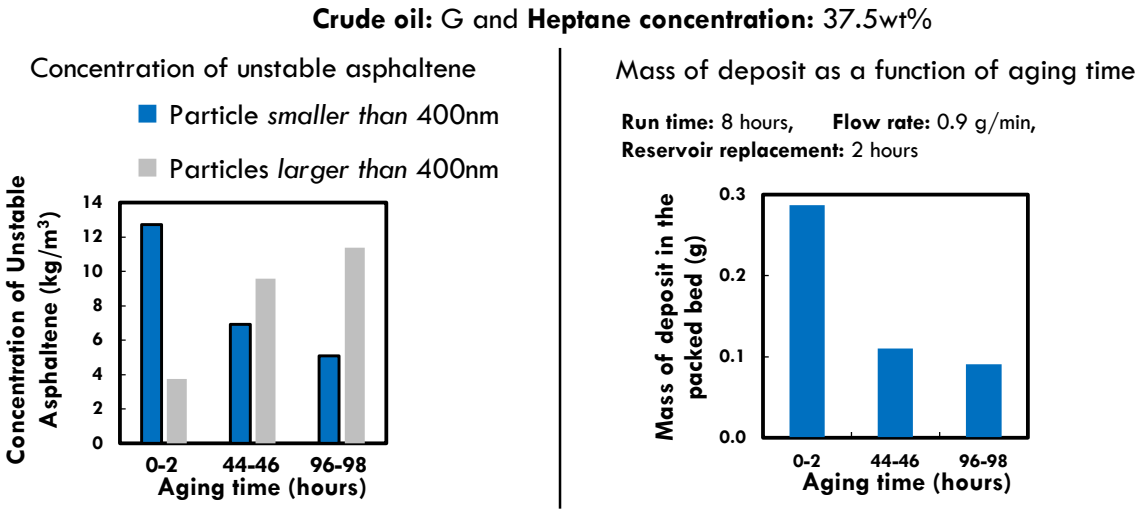

Figure E.2 – Experimental results of the effect of aging time on the asphaltene deposition rate

Experimental results presented in Figure E.2 show that both the mass concentration of nanometer-sized asphaltenes and the mass of deposit decreases the oil-heptane mixture ages. The result indicates that particle size plays an important role on the process of asphaltene deposition. In addition, results suggest that micron-meter sizes asphaltenes tend to flow through the packed bed without depositing.

E.2. Effect of Bead Diameter of Packed bed on the Asphaltene Deposition Rate

In Chapter V, a mass-transfer limited deposition model was derived to explain the process of nanometer sized asphaltenes undergoing Stokes flow in a packed bed. The simplified rate equation for a short packed bed is presented in Equation 1.

$$Rate_{dep} = 6\, A_c^{\frac{1}{2}} d_b^{-\frac{3}{2}} \frac{(1-\phi)^{\frac{3}{2}}}{\phi}\, \rho^{-\frac{1}{3}}\, \mu^{-\frac{1}{6}}\, D^{\frac{2}{3}}\, q^{\frac{1}{2}}\, L\, C_{A_0} \qquad (1)$$

In order to test the scaling relation between rates and bead size, deposition experiment with bead of different diameters were performed: 3.8, 2, and 1mm. The experiments with beads of 1mm were not successful as the packed bed could not be reproducibly drained at the end of the deposition experiment to have the mass of deposit measured. Experimental were performed with Oil H, at run-time of 8 hours, reservoir replacement of 2 hours, heptane concentration of 30.5wt, and flow rate of 0.9g/min. As the bead size changed, the porosity of the packed bed also changed. The experimental results are presented in Figure E.3 in a plot of deposition rate a function of $d_b^{-\frac{3}{2}} \frac{(1-\phi)^{\frac{3}{2}}}{\phi}$.

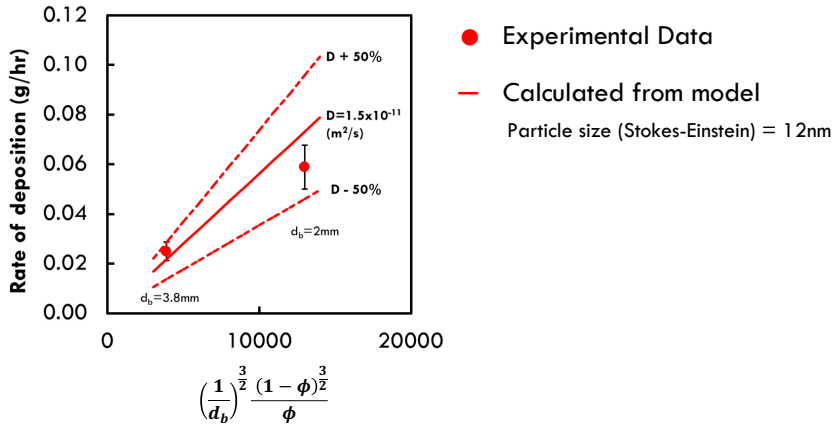

Figure E.3 – Scaling relation between deposition rate and $d_b^{-\frac{3}{2}} \frac{(1-\phi)^{\frac{3}{2}}}{\phi}$

It can be seen that as particle size decreases from 3.8 to 2mm, the value of $d_b^{-\frac{3}{2}} \frac{(1-\phi)^{\frac{3}{2}}}{\phi}$ increases and so does the deposition rate. The calculated rate based on Equation (1) is presented in red line as well as the sensitivity to the diffusivity. Good agreement is found between experimental data and model.

The experimental data from Figure E.3 is also presented in a log-log plot in Figure G.4. A black dashed line of slope 1 is also shown to compare with slope of the experimental results.

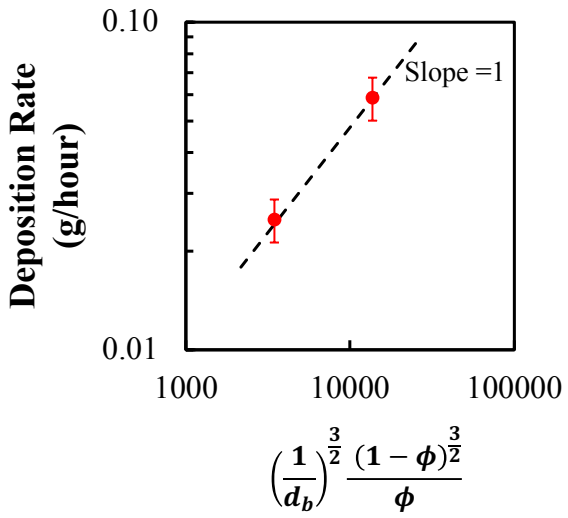

Figure E.4 – Log-log plot of scaling relation between rate and $d_b^{-\frac{3}{2}} \frac{(1-\phi)^{\frac{3}{2}}}{\phi}$

According to Equation 1, a log-log plot of rate versus should give a line of slope equal to 1. Indeed, Figure E.4 shows a close agreement between the expected and actual slope.

E.3. Effect of Bead Material on the Asphaltene Deposition Rate

The effect of bead material on the asphaltene deposition was tested. If the process of asphaltene deposition is indeed diffusion-limited, then any material that allows asphaltenes to deposit onto should present the same deposition rate. In order to test the effect of bead material on

deposition rate, the glass column as packed with beads of identical diameter but different materials: Teflon, glass and stainless steel. The packed beds with beads of different materials are shown in Figure E.5.

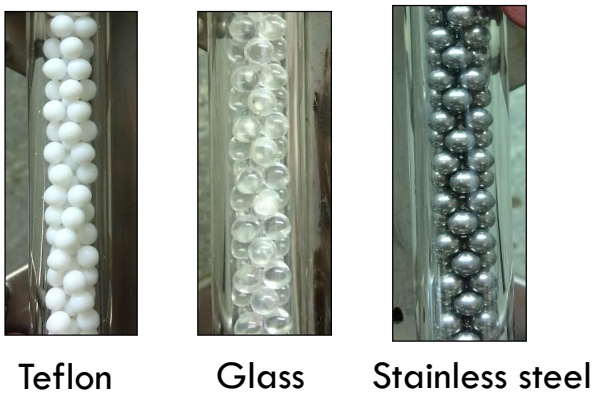

Figure E.5 – Glass column packed with three different materials: Teflon, glass, and stainless steel.

Deposition experiments were performed in the packed beds of different bead material. For that, 37wt% of heptane was added to crude oil A, the flow rate of oil-heptane mixture through the packed bed was set to 0.3g/min with a reservoir replacement of 2 hours. The experimental results for mass of deposit are presented in Figure E.6.

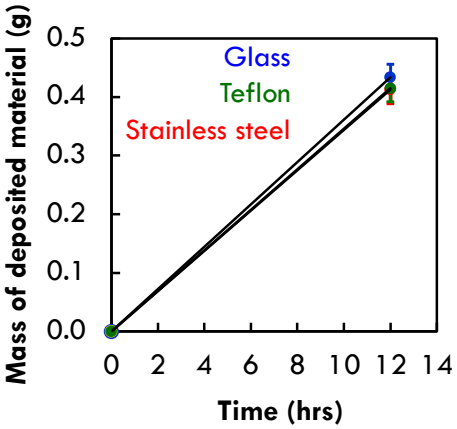

Figure E.6 – Experimental results of the deposition experiment over beads of different material

No differences in the mass of deposit is detected as the material of the beads in the packed bed changes, as shown in Figure E.6. This result is in agreement with the assumptions made on the diffusion-limited deposition model.

E.4. Nomenclature

U	$\frac{m}{s}$	Superficial Velocity
A_c	$m^2{}_{cross\ sectional}$	Cross-sectional area of empty column
C_{A_0}	$\frac{g}{m^3}$	Concentration of A at packed bed inlet
$Rate_{dep}$	$\frac{g}{s}$	Asphaltene deposition rate
L	m	Length of packed bed
D	$\frac{m^2}{s}$	Diffusion coefficient of depositing asphaltenes
ρ	$\frac{kg}{m^3}$	Density of fluid
μ	$Pa.s$	Viscosity of fluid
d_b	m	Diameter of beads
ϕ	$-$	Porosity of packed bed (void fraction)
m_{dep}	g	Mass of deposit
q	$\frac{kg}{s}$	Mass flow rate

E.5. References

[1] T. Maqbool, S. Raha, M. P. Hoepfner, and H. S. Fogler, "Modeling the Aggregation of Asphaltene Nanoaggregates in Crude Oil−Precipitant Systems," *Energy Fuels*, vol. 25, pp. 1585–1596, 2011.

APPENDIX F

Comparison of asphaltene solubility parameter obtained by different methods

The solubility parameter of fractions of asphaltenes B and C, from Chapter 3, were obtained by refractive index correlation and aggregation model. A comparison of values of solubility parameter is presented in Figure F.1.

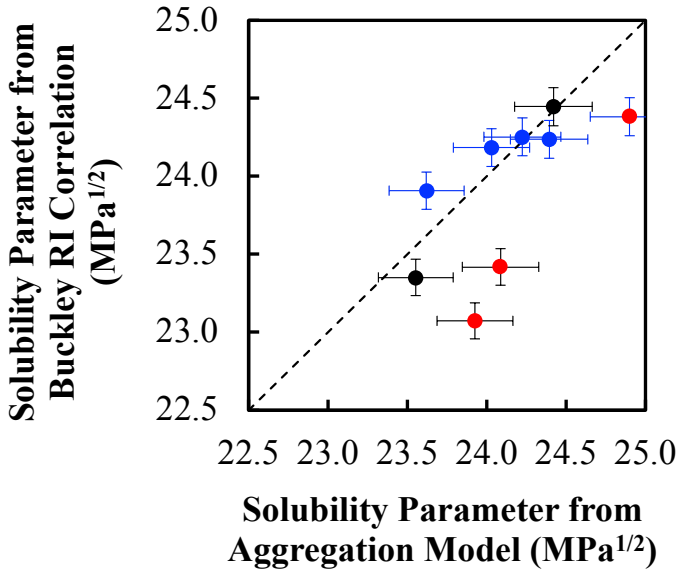

Figure F.1 - Comparison of the solubility parameter of asphaltene fractions obtained by the Buckley refractive index correlation and from the aggregation model for asphaltene fractions of B (in black) and C (in blue).

It can be seen in Figure F.1 that while there are three outliers (red dots), there is an overall agreement between the solubility parameter of fractions of asphaltenes as measured by the Buckley refractive index correlation and by aggregation model. No noticeable common characteristics for the asphaltenes in data shown in red were observed that could the explain the reason of them to outliers.